The Thesis Committee for Lokendra Jain
Certifies that this is the approved version of the following thesis:

Factors Determining Rapid and Efficient Geologic Storage of CO_2

APPROVED BY
SUPERVISING COMMITTEE:

Supervisor:

Steven L. Bryant

Larry W. Lake

Factors Determining Rapid and Efficient Geologic Storage of CO_2

by

Lokendra Jain, B.tech

Thesis

Presented to the Faculty of the Graduate School of

The University of Texas at Austin

in Partial Fulfillment

of the Requirements

for the Degree of

Master of Science in Engineering

The University of Texas at Austin

August 2011

Dedication

To my parents, teachers, sister and friends

Acknowledgements

I would like to express my gratitude to Dr. Steven Bryant for his invaluable guidance and support. Working under his supervision is a learning experience which made me think critically. I learned to look at the bigger picture while solving technical problems with him. He has helped me directly or indirectly in my academic research, professional and personal development. I am thankful for his continued support during the difficult phases of my research.

I am also thankful to Dr. Lake for his support while I was writing this thesis. I would like to thank Dr. Magsood Abbaszadeh and Bob Burruss for their timely help with my research. I would like to thank Dr. Roger Terzian and Ms. Joanna Castillo for their help with the computers and the software packages. I would also like to thank Mr. Rand Martin and Ms. Lisa Bowen for helping me in administrative matters.

I would like to extend my special thanks to my officemates Abhishek Kumar, Abhishek Gupta, Chris, Ahmed, Amir for helping me understand concepts through thoughtful discussions. I would like to thank my friends Mayank, Ankesh, Sayantan, Abhinav, Faiz, Nitish, Sahil, Vikram, Gaurav and Rahul for keeping my spirits up during the difficult times.

I would like to attribute this success to my parents and my sister in India. This would not have been possible without their continuous support and unconditional love.

I am grateful to the sponsors of Geologic CO_2 Storage Industrial Associates Project at The University of Texas at Austin: BP, Chevron, ConocoPhillips, ExxonMobil, Foundation CMG, Halliburton/Landmark Graphics, Luminant, Shell and Statoil for making this work possible.

Abstract

Factors Determining Rapid and Efficient Geologic Storage of CO_2

Lokendra Jain, M.S.E

The University of Texas at Austin, 2011

Supervisor: Steven L. Bryant

Implementing geological carbon sequestration at a scale large enough to mitigate emissions will involve the injection of supercritical CO_2 into deep saline aquifers. The principal technical risks associated with such injection are that (i) buoyant CO_2 will migrate out of the storage formation; (ii) pressure elevation during injection will limit storage rates and/or fracture the storage formation; and (iii) groundwater resources will be contaminated, directly or indirectly, by brine displaced from the storage formation. An alternative to injecting CO_2 as a buoyant phase is to dissolve it into brine extracted from the storage formation, then inject the CO_2-saturated brine into the storage formation. This "surface dissolution" strategy completely eliminates the risk of buoyant migration of stored CO_2. It greatly mitigates the extent of pressure elevation during injection. It nearly eliminates the displacement of brine. To gain these benefits, however, it is essential to

determine the costs of this method of risk reduction. This work provides a framework for optimization of the process, and hence for cost minimization.

Several investigations have tabulated the storage capacity for CO_2 in regions around the world, and it is widely accepted that sufficient pore volume exists in deep subsurface formations to permit large-scale sequestration of anthropogenic CO_2. Given the urgency of implementing geologic sequestration and other emissions-mitigating technologies (storage rates of order 1 Gt C per year are needed within a few decades), the time required to fill a target formation with CO_2 is just as important as the pore volume of that formation. To account for both these practical constraints we describe in this work a time-weighted storage capacity. This modified capacity integrates over time the maximum injection rate into a formation. The injection rate is a nonlinear function of time, formation properties and boundary conditions. The boundary conditions include the maximum allowable injection pressure and the nature of the storage formation (closed, infinite-acting, constant far-field pressure, etc.) The time-weighted storage capacity approaches the volumetric capacity as time increases. For short time intervals, however, the time-weighted storage capacity may be much less than the volumetric capacity.

This work describes a method to compute time-weighted storage capacity for a database of more than 1200 North American oil reservoirs. Because all of these reservoirs have been commercially developed, their formation properties can be regarded as representative of aquifers that would be attractive targets for CO_2 storage. We take the product of permeability and thickness as a measure of injectivity for a reservoir, and the product of average areal extent, net thickness and porosity as a measure of pore volume available for storage. We find that injectivity is not distributed uniformly with volume: the set of reservoirs with better than average injectivity comprises only 10% of the total volumetric storage capacity. Consequently, time weighted capacity on time scale of a few

decades is 10% to 20% of the nominal volumetric capacity. The non-uniform distribution of injectivity and pore volume in the database coupled with multiphase flow effects yields a wide distribution of "filling times", i.e. the time required to place CO_2 up to the boundaries of the formation. We define two limiting strategies based on fill times of the storage structures in the database and use them to calculate resource usage for a target storage rate. Since fill times are directly proportional to injectivity, smallest fill time corresponds to best injectivity and largest fill time corresponds to smallest injectivity. If best injectivity structures are used first, then the rate at which new structures would be needed is greater than if worst injectivity structures are used first. A target overall storage rate could be maintained for longer period of time when worst injectivity structures are used first.

Because of the *kh* vs PV correlation, most of the pore volume remains unused when no extraction wells are used. Extraction wells require disposal of produced brine, which is a significant challenge, or beneficial use of the brine. An example of the latter is the surface dissolution process described in this thesis, which would enable use of a much greater fraction of the untouched pore volume.

Table of Contents

List of Tables

List of Figures

Chapter 1: Key Issues with CO_2 Storage in Saline Aquifers and Objective of this Study

The present generation is faced with the task of preventing the world to go over the tipping point beyond which irreversible climate change would occur. The greenhouse gases like carbon dioxide, carbon monoxide, chloro-fluoro-carbons, methane etc when released into the atmosphere cause the trapping of infrared rays leading to increase in the ambient temperatures. The anthropogenic emissions constitute all the above mentioned components while natural emissions exclude chloro-fluoro-carbons. This is due to the fact that carbon dioxide is the by product of combustion of fossil fuels, which make up the vast majority of the world's fuel supply, and with the increase in world's energy demand and rapid deforestation the rate of increase of atmospheric carbon dioxide levels has gone up.

Geological sequestration of carbon dioxide is projected as one of the several effective ways needed to mitigate the problem within the rather short time frame (a few decades to one century) to avoid much greater temperature increase. This mitigation would allow the world to build cleaner and green technologies. Geological sequestration involves capture at the source and injection of carbon dioxide into an underground aquifer or a depleted oil or gas reservoir.

1.1 ISSUES

In a general sense, carbon storage will only be favorable if high capacity storage sites are confirmed and permanent and cost-effective storage is promised. Site assessment includes selection of an appropriate reservoir based on geologic understanding and features suitable for efficient CO_2 injection. Another important attribute is that after injection operations end, injected CO_2 should be trapped via mechanisms such as

capillary trapping, dissolution and mineralization which make the storage scheme safe and ensure permanence. The ways CO_2 migrates in the storage structures can be controlled by suitable injection strategies (like well placement relative to upper or lower portions of the formation and relative to heterogeneity distribution). Modeling CO_2 storage also poses a significant challenge because it requires coupled fluid flow – phase – geochemical – geomechanical simulations. This is because capillary trapping is considered as the major permanent CO_2 storage mechanism yet only a few experimental relative permeability measurements for both drainage and imbibition cycles are available. Mineralization is cited as a long term, permanent storage mechanism but chemical kinetics of mineral precipitation is poorly known.

These issues become more important for storage in saline aquifers because of lack of data due to no economic incentive behind data gathering. This limits our ability to assess the storage capacity accurately in advance of deploying projects. Knowing the capacity is very important because storage in saline formations is being counted upon to contribute substantially to global reductions in atmospheric CO_2. The relative lack of information on hydrogeology, water/rock interactions and extent of CO_2 migration in formations lacking well defined structural closure are principal issues surrounding CO_2 storage in saline formations (Imbus and Orr , 2006).

The large scale implementation of carbon capture and storage (CCS) faces its greatest challenge in economics of CO_2 transportation and capture costs along with establishment of legal and regulatory framework for storage. The development of businesses and regional infrastructure needed to realize large scale CCS will require long term predictability of CO_2 storage value (price and regulatory issues) (Imbus and Orr , 2006).

1.1.1 Key Questions related to subsurface storage

Hundreds or thousands of large capacity saline aquifer storage projects would be required worldwide if CO_2 storage is to be implemented at the scale necessary (of the order of $GtCO_2$/year) to mitigate the atmospheric CO_2 emissions for a significant duration of time. The feasibility of the implementation depends on the answer to certain questions:

- How is CO_2 stored underground? How does it get trapped in the formation after injection? The injection rate into saline formation depends on the pressure build up, permeability and thickness of the formation, and the presence or absence of permeability barriers within it. The spread of CO_2 within or from the formation post injection depends upon several factors: the pressure regime established during injection; redistribution of the fluids due to hydraulic gradients and density difference between the formation fluids; and dispersion caused by heterogeneities and the mobility contrast between CO_2 and the formation brine (Celia et al., 2005, van der Meer, 1995; Flett et al., 2005). These factors along with the hydrodynamic regime cause the CO_2 to get trapped (capillary, dissolution, and mineralization). The knowledge about these factors is essential for understanding the permanent storage of CO_2. There are a lot of uncertainties associated with how CO_2 gets trapped post injection because of the uncertainties in geology and ground water flow systems.

How long can CO_2 stay in the ground? This question is generally answered by citing the analogy with oil and gas fields which indicate that hydrocarbons can remain trapped for millions of years (Magoon and Dow, 1994). This can only happen given the right trapping conditions like structural traps with non-leaking cap rocks. There are documented geologic formations from which oil leaks can be seen at the surface. For

example, at Coal Oil Point, estimated seepage rate of oil ranges from 500 to 8000 t/year (Wilkinson, 1971). In Santa Monica bay, seep estimates by Wilkinson (1971) range from 100 to 1000 t/year. Thus the issue here is proper site assessment and selection. Given the right conditions CO_2 could stay trapped for thousands of years as has been the case for natural thermogenic CO_2 accumulations like Bravo Dome in New Mexico.

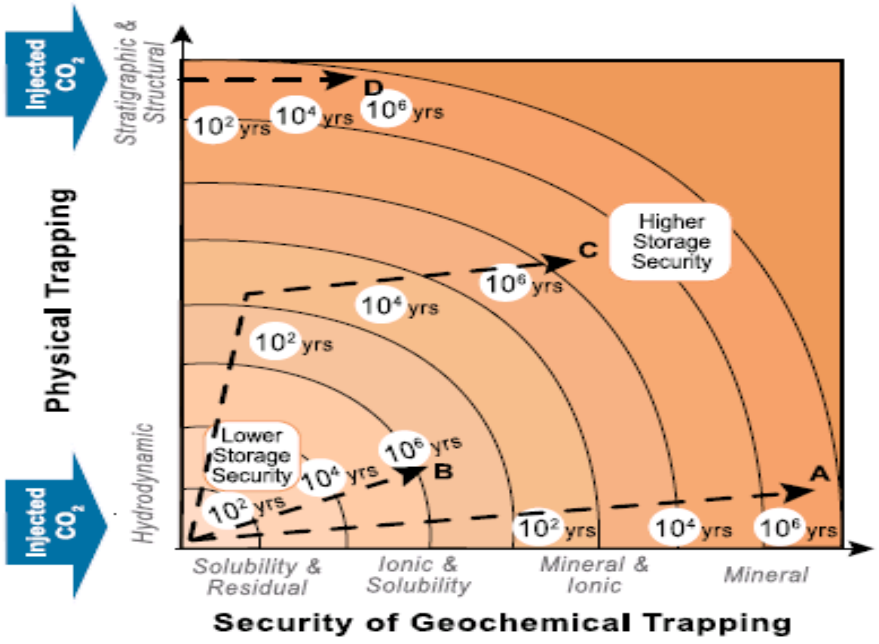

Figure 1-1 Physical and geochemical trapping govern the security and how long will injected CO_2 will stay in the ground (IPCC, 2007).

The time scales associated with the different trapping mechanisms which ensure complete security are of the orders of tens of thousands of years (Figure 1-1). This time scale is very long and thus creates uncertainties associated with the subsurface tectonic activities which might lead to leakage. Thus there is considerable incentive to investigate how to achieve accelerated trapping of CO_2 in saline aquifers.

- Is sufficient storage volume available to contain large proportion of CO_2 emitted into atmosphere currently? The difference between the way

various mechanisms help trap CO_2 in saline formations can be used to estimate the storage capacity. The volumetric capacity depends on two factors: the fraction of pore volume that injected CO_2 can occupy, and the pressure and temperature of the storage aquifer. Pressure and temperature govern the density of injected CO_2. The higher the density, the higher is the storage capacity. For solubility trapping, capacity is the amount of CO_2 that can be dissolved in the formation brine. For mineral trapping, capacity is dependent on the presence of minerals containing divalent cations which would lead to carbonate precipitation. The drawbacks with these simple methods to calculate capacity in a geological formation are lack of data, uncertainty and the fact that different trapping mechanisms work together and at different time scales. So the time frame of CO_2 storage affects the capacity estimates. The interactions between the different storage mechanisms evolve with time (Figure 1-2) and are dependent on local conditions. Thus global capacity estimates calculated with these simplifying assumptions may not be reliable. The local and regional capacity estimates are more reliable but they are also incorrect due to the lack of data. The other issue is that the basin specific capacity estimates are only available for countries in North America, Western Europe, Australia and Japan.

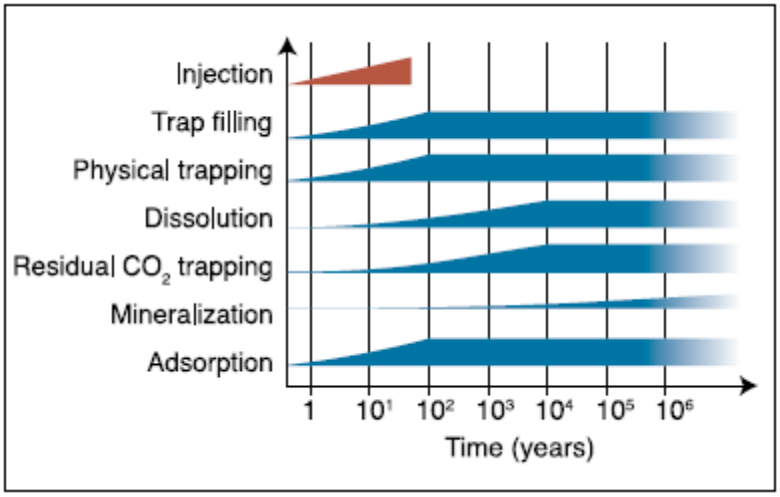

Figure 1-2 Time evolution of different CO_2 storage mechanisms operating in deep saline aquifers during and after injection (IPCC, 2007).

- Can the injected CO_2 be monitored post injection to ensure that it stays in place? In other words, is there sufficient level of technological knowhow to monitor post injection movement of CO_2 sub-surface? How long the monitoring is required before it is determined that CO_2 is trapped permanently? Monitoring is required for wide variety of purposes. The most significant risk of leakage lies in the failure of completion of the injection wells (Perry, 2005). Thus efficient injection well pressure monitoring (wellhead and downhole) has to be ensured. Monitoring during injection is also required so that the injection strategy could be changed with time to ensure maximum storage efficiency. Monitoring is also required to enable detect early signs of possible leakage so that remedial action could be taken in time. Monitoring technologies developed for natural gas storage in saline aquifers could be a useful industrial analogue, but the uncertainties associated with sub-surface may still limit the

accurate prediction and monitoring strategy. The distribution of CO_2 in the sub-surface could be monitored based on the data gathered at the wells, which is precisely what is done for EOR projects. Other alternatives include tracer injection and analysis along with time-lapse seismic analysis.

- What are the chances that the storage site will leak and what would be the consequences? Storage of CO_2 is engineered and with the level of uncertainty associated, there is some probability that leakage of CO_2 will take place from some of the injection sites. So far no study has been done to carefully assess the probability and the magnitude of leakage across potentially viable brine storage systems. To date the conclusions in all the studies done on leakage risk analysis take natural gas storage as the industrial analogue. The problem with this analogy is that gas storage engineered systems are designed to work for small time scales, but the stored CO_2 for sequestration purposes has to stay in place for geological time scales. There are a few studies done on the current demonstration and commercial injection projects like Sleipner. Lindberg (2003) found from simulation that the injected CO_2 would not migrate into the North Sea for about 100,000 years and after hundreds of thousands of years the rate of leakage would be very low. The probabilistic leakage studies on Weyburn also suggest that there is 95% probability that less than 1% of the stored CO_2 would be released (Walton et. al, 2005). The issue with these leakage studies is that they do not account for all the factors which might lead to leakage like abandoned wells and other disturbances like tectonic activities. The consequences of leakage on human health and safety are of

prime importance. The challenge in estimating the risk posed by CO_2 leakage is to estimate the spatial and temporal distribution of CO_2 fluxes reaching the shallow subsurface and prediction of ambient CO_2 concentration resulting from the given flux. CO_2 concentration in air is strongly affected by surface topology and the atmospheric conditions. Since CO_2 is denser than the air it tends to flow along the surface and tend to accumulate in low lying areas. The upward migration of CO_2 also poses a risk to the potable water resources. The impact of CO_2 dissolution and possible geochemical reactions which might cause toxicity in the drinking water has not been carefully studied at the regional level.

- Can something be done if leakage occurs? Geological storage projects have to be selected and operated in such a manner that the risk of leakage is minimized. However if leakage happens than the remediation has to be done either by stopping the leak or by minimizing the human impact. A very little effort has been placed in the study of remediation options. A survey of the current remediation practices for natural gas storage, underground waste and soil contamination, waste disposal in deep formations could provide us with some insight.
- What are the social, legal and regulatory issues surrounding CO_2 sequestration? According to the principles of international law sovereign states can engage in storage activities in the onshore and offshore areas under their jurisdiction. However if the storage activities cross the international boundaries then states are responsible to avoid environmental damage to other states. There are number of global and regional environmental treaties on climate change like Kyoto protocol and law of

the sea and marine environment which as presently drafted could be interpreted as relevant to permissibility for sequestration, particularly in the saline aquifers offshore. But as currently framed, these treaties do not put states under any legal obligation to reduce emissions or implement mitigating technologies like sequestration in saline aquifers. The key issue with implementation of sequestration is policy. This has been witnessed most recently by the debacle of climate change meeting in Copenhagen 2010 where responsible parties failed to reach at any conclusive plan. Previous treaties like Kyoto protocol are in the danger of being shelved. There are issues with further amendment of treaties, which might require more negotiations, a minimum level of support for their adoption and subsequent entry into force. When interpreting the existing treaties for the purposes of CO_2 storage especially in offshore saline aquifers, it should be kept in mind that they were meant to prohibit marine dumping and not support CO_2 storage (IPCC, 2007).

- Storage sub-surface also raises questions about the ownership of pore space and can the ownership rights be transferred? Who owns the stored CO_2 and how can the storage be managed so that there is minimal damage to other mineral resources or water rights? Right to pore space is an issue because unlike most of European countries and Canada, in United States the right to pore space lies with the surface owner, not to the government.
- Scale at which CO_2 plume migrates is very large. It has been shown by Rutqvist (2002) that for a 1 GW power plant the CO_2 injection into 100 m thick saline aquifer for 30 years would cause the plume to range over 100 square km. 100 square km is large area and to get the property rights over

such a big area especially in United states would pose legal challenges. This also poses social challenges. The public perception about CO_2 sequestration also has to be favorable. There is insufficient public knowledge about the impact climate change has on environment, ecosystems and human health, and of available mitigation technologies. From Netherlands to U.S public opposition can and has proven to be an obstacle for carbon capture and storage projects around the world. Shell's project in Barendrecht has been delayed by three years because of public opposition (Kuijper, 2010). The reasons for this are the distrust in the developers and the risks associated with injection. There is public opposition over plans to sequester CO_2 beneath Greenville , Ohio. There are similar examples across the world where CCS projects are facing public opposition. Comparisons show that while issue of trust is important, in many cases public mood is more affected by local socio-economic conditions (Carbon Capture Journal, Aug 11, 2010). Opposition to CCS projects has shown that there is a need to better understand local beliefs and to situate plans in local context. Public attention has to be drawn to the benefits of the remedial measures like sequestration in saline aquifers. Thus at the end there are three points which would led to successful implementation to sequestration; a) anthropogenic climate change has to be recognized as a potential danger for future generations globally, b) there has to be acceptance to the need of global CO_2 emissions reduction very quickly and c) public has to accept sequestration as a harmless technology which can provide resolution to this problem.

- What is the likely cost of geological storage of CO_2 in saline aquifers? The major cost components to sequestration in saline aquifer include well costs, infrastructure and project management costs. Operating costs include maintenance, monitoring, manpower and fuel costs. Monitoring costs are going to be sensitive to regulatory requirements and duration. Over long term remediation costs along with the liability costs might be added to the total costs. The liability costs are still a policy matter as to who will be responsible if a potential leak appears and harms human civilization in any way. The cost of sequestration is site specific. The detailed review of costs for about 50 project sites around Australia by Allinson et. al (2003) suggests that the median cost onshore is at about 0.5US$/t$CO_2$ and the offshore median cost is at about 3.4US$/t$CO_2$. These cost estimates like most other are very old and the revised estimates are much higher at 67 US$/t$CO_2$ (Fisher et al, 2005). Other than EOR projects, there are a very few experience based cost estimates for CO_2 injection and storage. Currently there is inadequate information on monitoring requirements which affect cost estimates. This is required for the policy makers to give incentives for the storage industry to gain pace.

1.2 OBJECTIVE

Two questions can be synthesized which address several topics in the preceding list of challenges:

- Given a set of available storage structures, what is the optimal way to use them? What parameters govern the optimal deployment of these resources?

- What safe technologies are currently available for CO_2 storage in saline aquifers?

Above challenges are the drivers behind this research work because the resources available to us in terms of potential sites for storage are limited. This problem has to be addressed at two scales. At the individual project scale the injection strategy has to be such that the maximum storage efficiency is achieved. There are several ways this could be done using the current state of technology but for large scale sequestration site selection is another challenge. Once it is proven that the site is suitable for sequestration, the way the available sites are used to achieve total injection targets (regional, national or global) is a very important question. For individual sites the detailed modeling allows site specific storage capacity estimates, but at the large scale these are of no use unless they are integrated with the long term requirements. This is because multiple projects running simultaneously are the only way to achieve meaningful mitigation of emissions. In the time frame in which new cleaner energy alternatives are developed (several decades), a large amount of CO_2 must be sequestered. For large amount of CO_2 to be sequestered, efficient use of all the available storage sites is a must. We address all the factors which govern efficient use of the resources. We also suggest a way to deal with the issue of optimal use of resources by highlighting limiting cases along with their advantages and disadvantages. We also bring to light the limitation which infinite acting boundary condition poses to the injection rates and the advantages of relief wells for large scale sequestration and their impact on resource usage.

The second objective of this research is to analyze an alternate sequestration technology proposed by Burton et al. (2008) called surface dissolution and suggest design parameters which would minimize the total cost of sequestration. While trying to minimize the cost we never compromise the integrity of the whole scheme which

promises permanent and safe disposal of CO_2, eliminating the extensive monitoring costs which are associated with the standard injection strategy. The focus of this study is to analyze the impact pressure field has on the strategy and use it for our benefit to achieve the minimum cost operating project.

Chapter 2: Literature review

"Annual total greenhouse gas emissions (GHG) arising from the global energy supply sector continue to increase" (IPCC 2007; IEA 2006b) (see Figure 2-1). The major contributor towards the GHG emissions is combustion of fossil fuel. The near-term non-cooperation between the governments on implementation of effective GHG emissions reduction policies has led to projected rise of GHG emissions over 50% from 26.1Gt CO_2 in 2004 to 37-40 $GtCO_2$ by 2030 (IEA, 2006b; Price and de la Rue du Can, 2006). With rising GHG emissions and no proven technology to curb the rising GHG levels in atmosphere, mitigation has therefore become more challenging. Industrial revolution has led to emission of 100 $GtCO_2$ into the atmosphere since the mid -19th century.

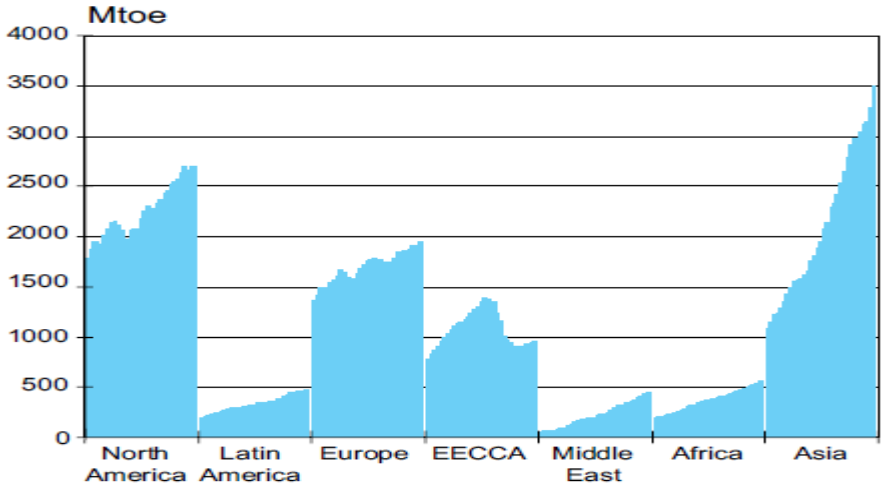

Figure 2-1 Global annual primary energy demand (including traditional biomass), 1971-2003 by region, Source IEA, 2004a. Note: EECCA = countries of Eastern Europe, the Caucasus and Central Asia.

The current energy usage trends predict huge consumption of fossil fuels, thus the storage capacity for CO_2 should be large to keep atmospheric CO_2 levels below the tipping point.

Avoidance of climate change calls for stabilization of atmospheric concentrations of greenhouse gas at some relevant specific level (like 450 ppm). Stabilization can only occur when the rate of addition of GHGs to the atmosphere equals the rate at which natural systems remove them (transfer to oceans, uptake by atmospheric reactions and biosphere). At the current rate of emissions the removal by natural systems is not sufficient to achieve stabilization.

Kaya, 1995 proposed simple identity to consider the major factors influencing CO_2 emissions from the supply and the use of energy.

$$CO_2 \text{ emissions} = \text{Population} * \left(\frac{\text{GDP}}{\text{Population}} \right) * \left(\frac{\text{Energy}}{\text{GDP}} \right) * \left(\frac{\text{Emissions}}{\text{Energy}} \right)$$

It shows that the level of CO_2 emissions can be interpreted to depend upon size of the human population, on the level of global wealth, energy intensity of the global economy, and emissions as a result of production and use of energy. With rise in population energy use is going up but in some countries energy intensity is going down. This decrease in energy intensity is very slow though and deep cuts in emissions would required major changes in third and fourth factor in the above equation. A wide variety of technical options have the potential to reduce net CO_2 emissions. A host of available techniques are described in next paragraphs. The targets of emission reduction will influence the extent to which each technique will be put to use.

CO_2 mineralization is a novel technique for binding CO_2 in solid form which was first proposed by Seifritz (1990). Mineral carbonation is the process where CO_2 from capture step is brought into contact with metal oxides with the purpose of fixing CO_2 as carbonates (Dunsmore, 1992; Lackner, 1995). Interest in the mineralization stems from two unique features namely the abundance of metal oxide bearing minerals, particularly of natural silicates and the permanence of storage of CO_2 in stable solid form which

ensures storage for millions of years. The challenge with mineralization is to find ways to accelerate carbonation (Butt et al. 1996).

Another way of getting rid of anthropogenic CO_2 is burying it deliberately into deeper ocean where it could remain stored for centuries. There are many ways of releasing CO_2 into ocean. First of the approaches is to transport the compressed CO_2 into deep sea and release it at or above the sea floor where it stays isolated from the atmosphere for a very long time. Marchetti (1977) proposed injection of liquefied CO_2 into waters flowing over Mediterranean sill into the mid depth North Atlantic. Kheshgi (1995) and Rau and Calderia (1999) proposed CO_2 storage by carbonate minerals in deep ocean environment. Over thousands of years, the increased sea water acidity due to dissolved CO_2 from atmosphere will be neutralized by slow natural dissolution of carbonate minerals in sea floor sediments. This process allows the ocean to absorb more CO_2 without significant change in the pH of sea water (Archer et al. 1997, 1998). Loken and Austvik (1993) and Holdren and Baldwin (2001) showed that concentrated CO_2 and water react under typical ocean conditions at modest depths to form hydrates. The density of pure CO_2 hydrate is more than the ocean water. This is a very critical property which could be used to store CO_2 in deep ocean. There are other methods for deep sea CO_2 storage like water-$CaCO_3$-CO_2 emulsion (Swett et al, 2005), emplacement in carbonate sediments (Murray, 1997), dry ice torpedos (Steinberg, 1985) and direct flue gas injection. This is potentially a very good way to mitigate the rising CO_2 levels. Relative to the amount of fossil fuel reserves, oceans have a large physical capacity for CO_2 storage. The degree to which the existing capacity could be utilized depends on the costs, energy penalty incurred on compression and transportation of CO_2, and extent of knowledge about the environmental impact.

Though mineralization and CO_2 storage in deep ocean are very promising techniques, they have not been implemented due to lack of technical knowhow and understudied economics. If the carbon mitigating techniques have to be implemented in near future, geological sequestration is the answer due to the technical efficiency level of oil and gas industry. Geological sequestration of CO_2 can be undertaken in a variety of geological settings in sedimentary basins. Within these basins, oil fields, depleted gas fields, deep coal seams, and saline formations are all possible storage prospects (see Figure 2-2).

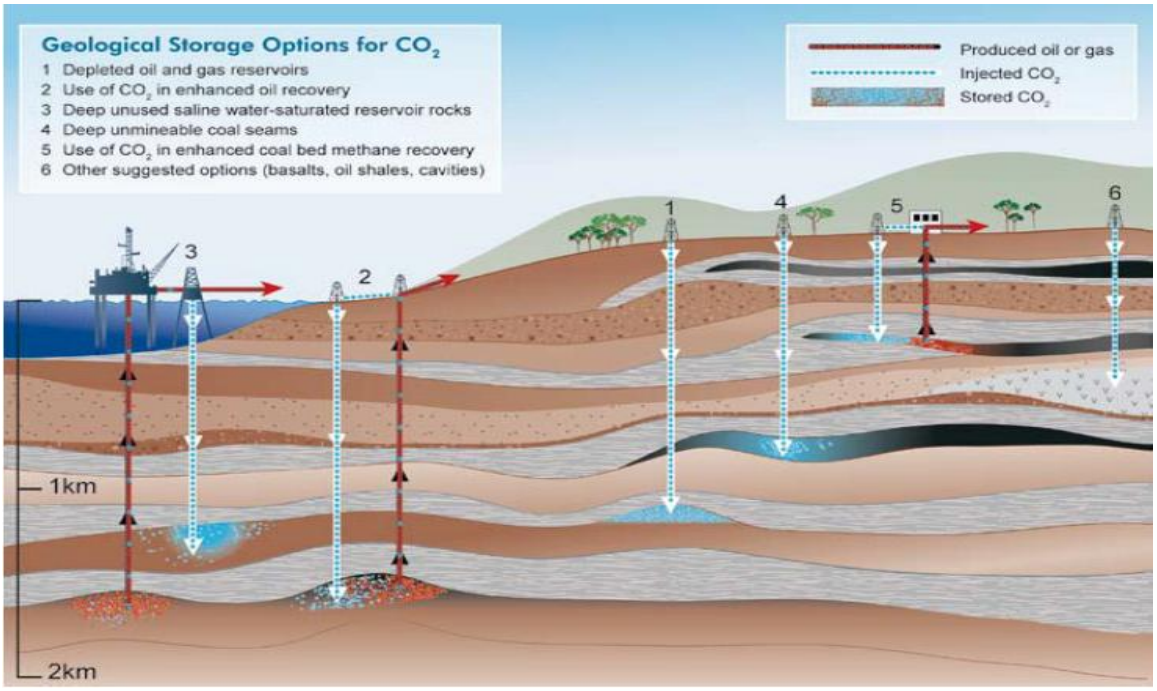

Figure 2-2 Diagram showings various options available for geological sequestration (courtesy Cook, 1999)

Reservoir type	Lower estimate of storage capacity ($GtCO_2$)	Upper estimate of storage capacity ($GtCO_2$)
Oil and gas fields	675[a]	900[a]
Unminable coal seams (ECBM)	3-15	200
Deep saline formations	1000	Uncertain, but possibly 10[4]

[a] These numbers would increase by 25% if "undiscovered" oil and gas fields were included in this assessment.

Table 2-1 Capacity estimates predictions for geological sequestration, (IPCC 2007)

Table 2-1 shows the storage capacity estimates for different options in geological sequestration. With the predicted increase in energy demand i.e. fossil fuel combustion (see Figure 2-1) deep saline aquifers seem to be a suitable choice for geological sequestration. More than 14 global capacity estimates have been made for saline formations and they range from 200-56000 $GtCO_2$ (IEA-GHG 2004).

2.1 CO_2 SEQUESTRATION IN DEEP SALINE AQUIFERS

CO_2 sequestration in deep saline aquifers entails injection of super critical CO_2 into aquifers below the depth of 800 m where the temperature and pressure are suitable to allow CO_2 to remain supercritical. The general site selection criteria for sequestration in deep saline aquifers depends on

- Adequate capacity and injectivity
- A satisfactory sealing caprock or confining unit
- A sufficiently stable geologic environment to avoid compromising the integrity of storage aquifer

Bachu (2000, 2003) and Bradshaw et al (2002) suggested that along with the site selection, the basin selection is also important for sequestration. The other important criteria according to them should be:

- Basin characteristics (tectonic activity, sediment type, geothermal and hydrodynamic regimes)
- Industry maturity and infrastructure

- Societal issues such as level of development, public education and attitude, economy and environmental concerns

The effectiveness of geological storage in deep saline aquifers depends on the level of security associated with different storage mechanisms in play (see Figure 2-4).

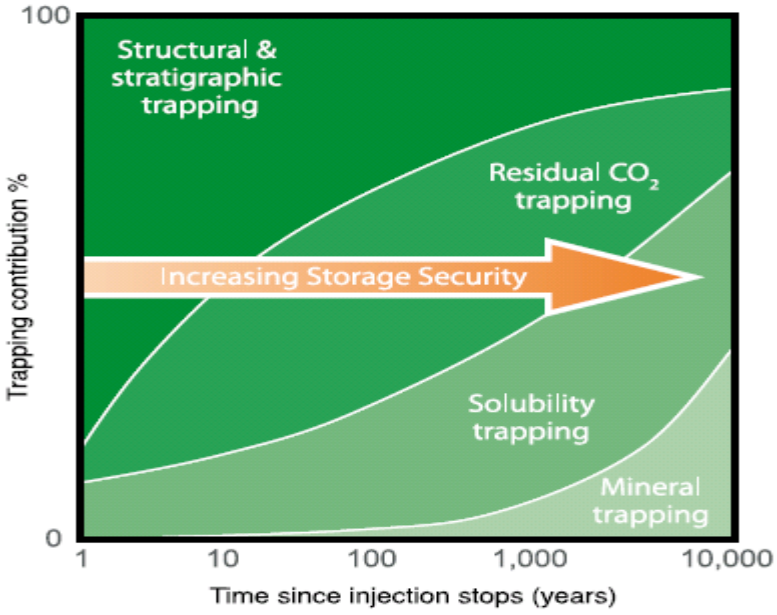

Figure 2-4 Security of storage depends on a combination of physical and geochemical trappings (courtesy, IPCC 2007)

2.1.1 Physical trapping: structural and stratigraphic

Physical trapping can occur in stratigraphic and structural traps which are occupied by saline water. Structural traps include those formed by folds or faults. Faults can act as permeability barriers or capillary barriers (Salvi et al 2000) for trapping of injected CO_2. Stratigraphic traps are formed by changes in rock type caused by variation in the settings where the rocks have been deposited. With these types of traps, care has to

be taken to not exceed the allowable over pressure to maintain safe disposal of CO_2 (Streit et al. 2005).

2.1.2 Physical trapping: hydrodynamic trapping

Hydrodynamic trapping occurs in saline formations when the injected CO_2 moves upward due to buoyancy and travels ahead leading to residual trapping (Juanes, 2008). This kind of trapping can occur in the saline formations which do not have a closed trap. In the case where the distance between the deep injection site to the surface outcrop is hundreds of kilometers, the time scale for CO_2 to reach surface from the deep basin can be millions of years (Bachu et al. 1994).

2.1.3 Geochemical trapping

CO_2 injected in the sub-surface can undergo some geochemical interactions like dissolution and mineral trapping. Injected CO_2 dissolves into the formation brine to a concentration that depends on the formation pressure, temperature and salinity. Once CO_2 is dissolved it no longer exists as a separate phase leading to safe storage. Next is the formation of ionic species as the rock dissolves, which is accompanied by the increase in pH. Some of these ionic species may convert to carbonates, which is called mineral trapping (Gunter et al. 1993). Geochemical trapping is the most permanent form of storage possible.

With all the trapping mechanisms in place Figure 2-3 shows that the geochemical trapping occurs over very large time scales. In a saline formation as CO_2 is injected and as it migrates, some of it will dissolve in the brine. In systems with slowly flowing ground water, over 30% of the injected CO_2 is predicted to dissolve in the formation brine over tens of years (Doughty et al. 2001). Similarly McPherson and Cole (2000) and Ennis-King et al. (2003) predict that on basin scale all injected CO_2 would dissolve in

formation brine. When CO_2 is dissolved in the formation brine the migration rate of saturated brine is very slow in comparison to the bulk phase CO_2 on account of very slow groundwater flow velocities, typically on the order of millimeters to centimeters per year (Bachu et al. 1994). Water saturated with CO_2 is slightly denser than the normal formation brine (Bachu and Adams 2003) which may lead to free convection if the formation has large permeability. The free convection leads to replacement of pure formation water and speeds up the dissolution of CO_2 (Lindeberg and Wessel-berg, 1997 and Ennis-King and Paterson, 2003) though the complete dissolution would still take thousands of years.

Residual trapping along with the geochemical trapping ensures permanent storage but the time scales associated with all of these are long. Thus alternative injection approaches have been suggested to ensure complete and permanent storage. Co-injection of supercritical CO_2 and brine could speed the dissolution trapping (Georgescu et al.2006). Noh et al. (2007) have suggested chasing the injected CO_2 with brine to increase residual trapping. Bryant et al. (2006) suggested another strategy of injecting deep and allowing buoyancy to work and increase residual trapping. With all the uncertainties arising from geological heterogeneity associated with the above strategies, leakage of CO_2 from the formation is a risk so Burton et al. (2008) proposed "surface dissolution" as an alternate approach for sequestration which depends on CO_2 solubility in brine. CO_2 solubility depends on pressure, temperature and salinity of brine. The impact of pressure, temperature and brine salinity on CO_2 solubility along with the density of saturated brine was studied by Kumar (2004). He developed solubility, saturated brine density and viscosity models and calibrated them with the experimental data, as in Figure 2-5. The solubility of CO_2 in brine increases with increase in pressure and decrease in temperature and salinity.

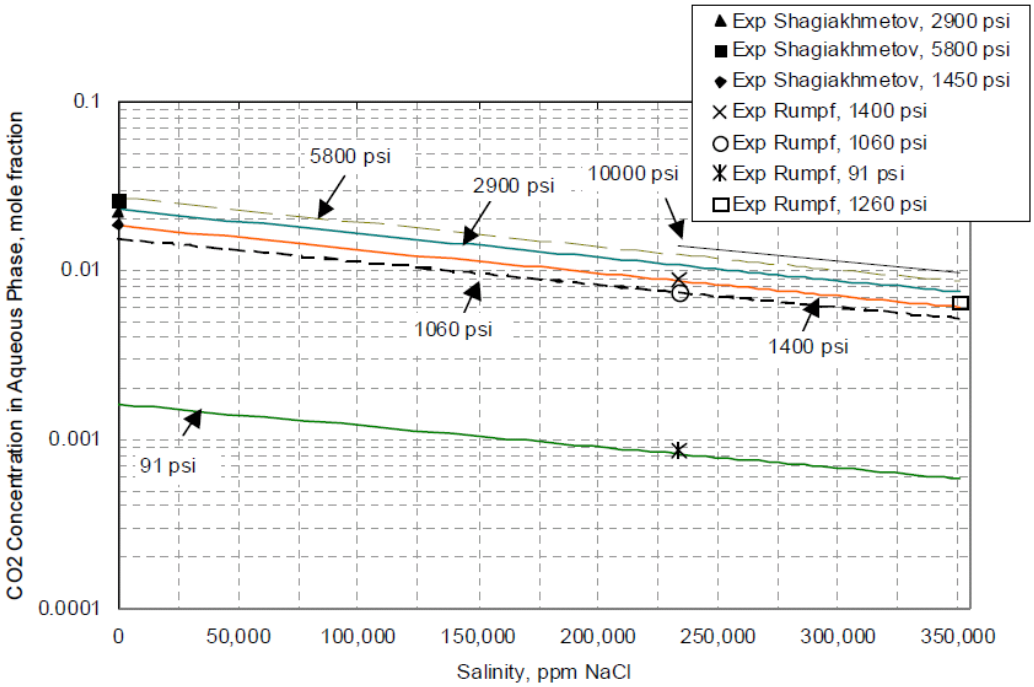

Figure 2-5 Effects of brine salinity and pressure on CO_2 solubility in aqueous phase at T = 140 F. (Kumar, 2004)

Figure 2-5 shows that solubility of CO_2 in brine is rather small so the amount of brine required would be very large. Burton (2008) also report that the amount of brine required can be handled with the current pumping capacity. Burton (2008) also shows that the total costs are not prohibitively higher for surface dissolution in comparison to standard bulk phase CO_2 injection (see Figure 2-6).

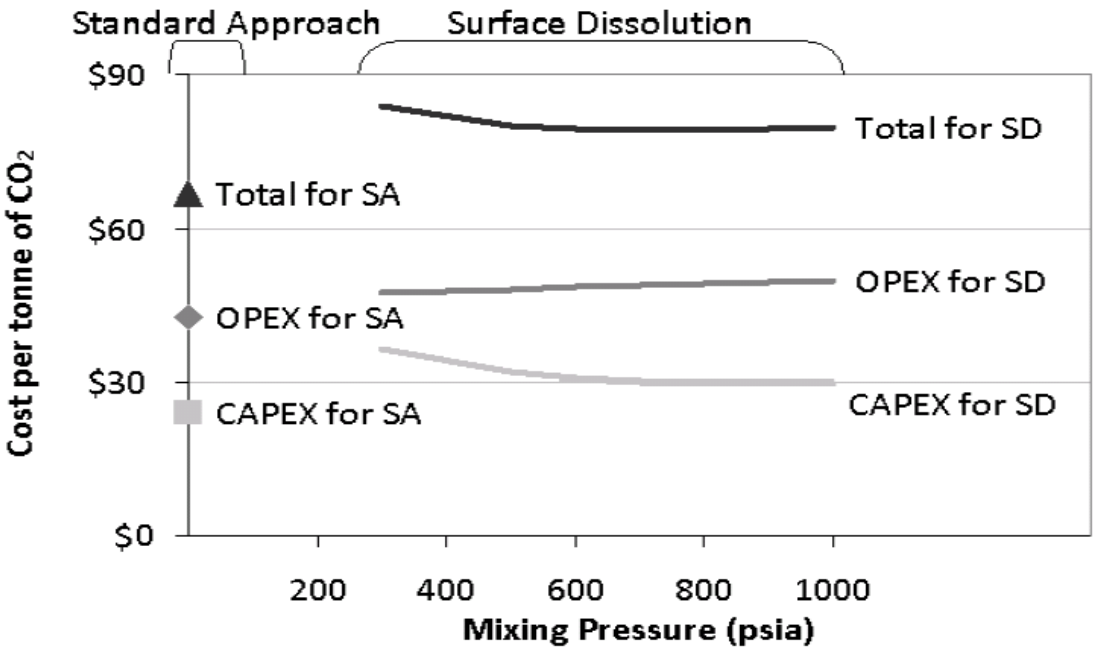

Figure 2-6 The optimum for surface dissolution lies between 600-1000 psi mixing pressure. In other words, it means surface dissolution would cost \$79/t-CO_2 in comparison to \$67/t-CO_2 for standard approach. Thus surface dissolution would cost 19% more than standard approach. (Burton, 2008)

Chapter 3: Surface Dissolution: Model and Design

3.1 INTRODUCTION

Large scale implementation of geological sequestration enough to mitigate anthropogenic emissions will involve the injection of supercritical CO_2 into deep saline aquifers as these structures are more widely available than hydrocarbon reservoirs. This method of sequestration is referred to as "standard approach" in this thesis (Figure 3-1a). The principal technical risks associated with the standard approach are:

a) Buoyant CO_2 migration out of the formation: Safe storage of CO_2 in a saline formation is attributed to dissolution, structural and capillary trapping. Trapping efficiency defines the fraction of stored CO_2 under the influence of any of the three trapping mechanisms. The buoyant movement of CO_2 undermines trapping efficiency. Small trapping efficiency allows more post injection CO_2 movement and greater leakage risks posed by geological and human introduced uncertainties, such as leaky wellbores

b) Pressure elevation during injection: The pressure elevation in the formation due to injection of CO_2 limits storage rates and may induce fracturing of the storage formation and possibly even seismic activity.

c) Contamination of ground water resources: Direct contamination of ground water resources might occur due to CO_2 migration. Indirect contamination might also be a consequence of brine displacement from storage formation.

These risks directly result in higher monitoring and insurance costs. An alternative to injecting CO_2 as a buoyant phase is to dissolve it into brine extracted from the storage formation, then inject the CO_2-saturated brine into the storage formation (Burton, 2008). This "surface dissolution" strategy completely eliminates the risk of

buoyant migration of stored CO_2. It greatly mitigates the extent of pressure elevation during injection. It nearly eliminates the displacement of brine.

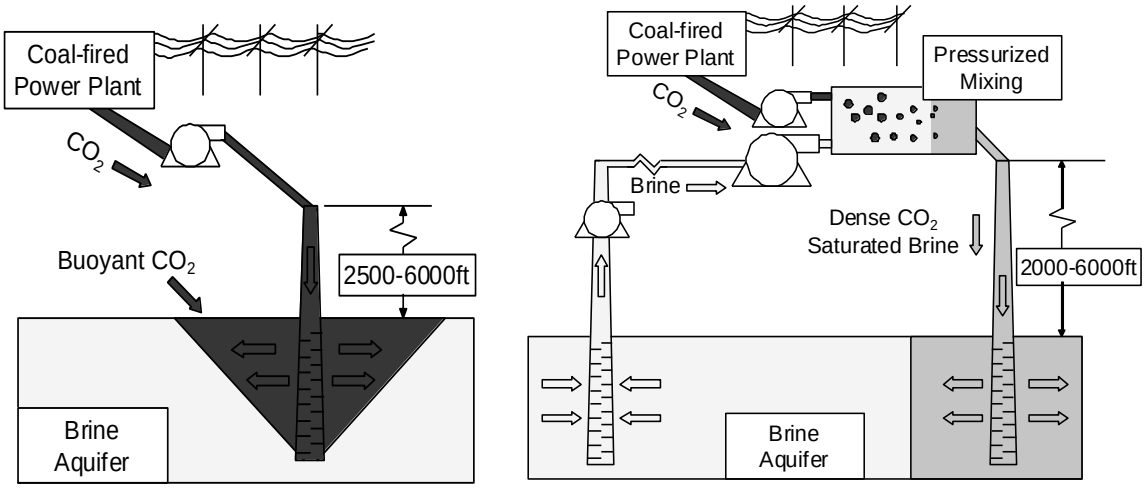

Figure 3-1 a) Schematic of the standard approach for carbon capture and sequestration (CO_2 bulk phase) includes the captured stream which is compressed to an appropriate pressure and injected into a brine aquifer. b) Schematic of the brine dissolution strategy includes pumps for the brine extraction, brine injection, and compression of the captured CO_2 stream. The two fluids are mixed until the CO_2 dissolves, and then the saturated brine is re-injected.

Extraction of CO_2 from flue gases, mixing of CO_2 in brine extracted from the saline aquifer and reinjection of that CO_2 saturated brine is referred to as surface dissolution approach (Figure 3-1b). The CO_2 saturated brine is slightly denser than resident brine which eliminates the risk of buoyant movement and meets all the concerns of safe storage. This process largely depends on solubility of CO_2 in brine which is a function of temperature, pressure and salinity (Figure 3-2). Previous study (Burton et al., 2008) on this subject has concluded that power requirement for pumping and mixing is manageable. Here we extend that study and identify the constraint imposed by the pressure field in the storage formation during injection period as a main parameter controlling the design. We describe a framework in which this parameter determines well

count, required formation volume and storage footprint (areal extent of CO_2) for ideal aquifers. This allows optimization with respect to the costs of implementing surface dissolution.

Implementation of geological carbon storage (GCS) at a scale sufficient to mitigate CO_2 emissions will require large areas and volumes of subsurface formations. Thus another important point of comparison for different storage strategies is storage efficiency. Here we define storage efficiency as the fraction of total pore volume occupied by CO_2 molecules regardless of concentration. The storage efficiency is defined this way because pore space rights will be acquired on a volumetric basis for the entire thickness of the storage formation. Estimates of the storage efficiency for standard approach range between 1 to 4% [3, 4]. These efficiencies are small because of gravity override during injection and post-injection buoyant movement of CO_2 plume. As shown below, the storage efficiency for surface dissolution ranges between 30 to 60%. The storage efficiency for surface dissolution is a much larger than the standard approach because in effect surface dissolution is a unit mobility ratio displacement, and for such displacements volumetric sweep efficiencies are very high. For surface dissolution there is no residual saturation which also leads to higher storage efficiency.

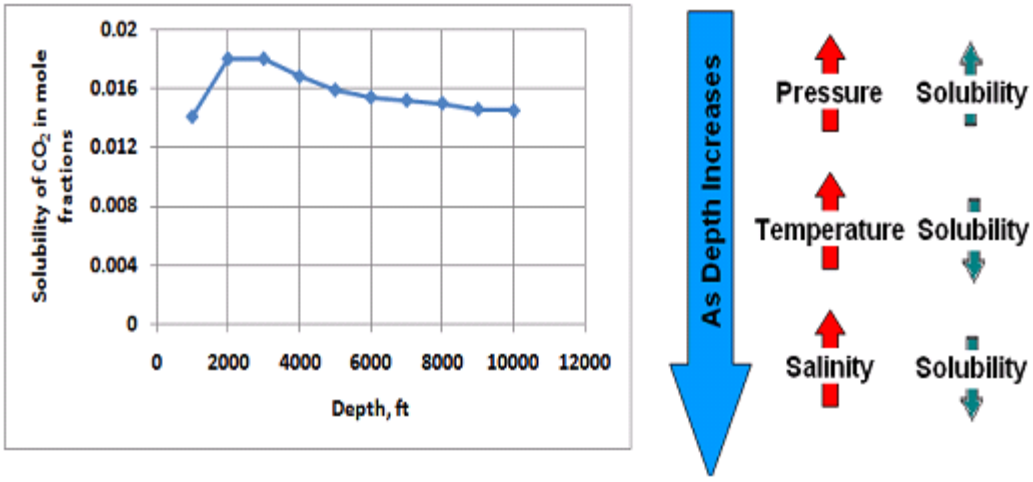

Figure 3-2 Solubility of CO_2 in brine increases as depth increases to 2000 ft, then decreases slowly. The solubility trend shown is based on gradients of pressure (0.433 psi/ft), temperature (1.6 F/100 ft) and salinity (15 ppm/ft). The nonlinear behavior is the result of counteracting influences of these parameters on solubility. The data for this graph comes from the code developed by Burton, (2008).

3.2 SURFACE DISSOLUTION: THE DESIGN

Dissolution of CO_2 in brine changes the nature of flow in the subsurface compared to standard approach. All the calculations for design assume no difference between the properties of resident brine and CO_2-saturated brine. In other words we assume that the mobilities of resident brine and CO_2 saturated brine are the same for practical purposes and flow in storage formation stays single phase. In contrast the standard approach involves multiphase flow with interphase mass transfer (Noh et al., 2007; Burton et al., 2008). The reasonable assumption of single phase flow allows us to use simple analytical tools. We demonstrate the calculation procedure by choosing line drive injection pattern as a base scenario.

The surface dissolution approach needs injection and extraction wells operating in essentially a balanced condition. A difference of about 5% in injection and extraction

rates exists because the mass of CO_2-saturated brine exceeds the mass of extracted brine by about 5% (Burton and Bryant, 2009). The balance of injection and extraction leads to an important conclusion: during post-injection period pressure in the aquifer will equilibrate to the pre-injection value, which we presume to be hydrostatic. Thus initial hydrostatic pressure sets an upper bound on the bubble point pressure (P_b) for the CO_2-saturated brine. The CO_2 solubility at P_b equal to hydrostatic pressure is thus the maximum useful solubility to be obtained in the surface mixing process. This constrains the extent of dissolution achieved in the mixing tank. Dissolving more CO_2 could lead to evolution of second phase in the aquifer after injection ends because P_b would exceed the equilibrated aquifer pressure. Dissolving less than the maximum would reduce storage efficiency.

The obvious limit on the process is that extraction would stop when CO_2-saturated brine breaks through at an extraction well. The overall injection rate would be reduced correspondingly. The more severe constraint is the location of the contour of bubble-point pressure during injection. This depends on the pressure field established in the aquifer during injection period. During injection, the pressure anywhere in the aquifer containing CO_2-saturated brine should not fall below bubble point pressure to avoid formation of a buoyant CO_2 rich phase.

3.2.1 Pressure Field during injection: Line drive injection pattern

We illustrate the optimization using a line drive pattern, Figure 3-3a. We assume homogeneous aquifer properties. This assumption would yield optimistic design because with heterogeneity the aquifer utilization efficiency (next section) decreases. We also assume that the CO_2-saturated brine and resident brine have same flow properties. The pressure field depends on the flow profile along the streamlines joining injector and

producer. For this pattern radial flow exists near injectors and producers and linear flow in the regions far from both lines of wells. This knowledge of flow patterns along with an assumption that mobilities of resident brine and CO_2 saturated brine are equal, defines injectivity equation as:

$$P_i - P_p = \frac{q\mu}{2kh}\left[\frac{2}{\pi}\ln\left(\frac{H}{2r_w}\right)+\frac{D}{H}-\frac{\pi}{4}\right] \quad , \quad H < D \tag{3.1}$$

See Appendix A for the derivation of the above equation. This equation will be used to estimate the approximate flow rate for a line drive pattern with unit mobility ratio flow when the pattern *H/D* ratio is less than unity. For *H/D* ratios more than unity, we used an alternate method to relate flowrates with drawdown ($P_i - P_p$). This method based on streamlines is described in Appendix B. The dimensionless form of Eq. 3.1 is

$$P_D = \frac{2}{\pi}\ln\left(\frac{H_D}{2}\right)+D_D-\frac{\pi}{4} \tag{3.2}$$

where equation 3.2 is the dimensionless form of the injectivity equation 3.1. P_d is dimensionless pressure:

$$P_D = \frac{P_i - P_p}{\frac{q\mu}{2kh}} \tag{3.3}$$

Dimensionless injector-injector spacing is

$$H_D = \frac{H}{r_w} \tag{3.4}$$

Dimensionless injector-producer spacing is

$$D_D = \frac{D}{H} \tag{3.5}$$

This injectivity equation can be used to predict pressure field in the aquifer at a certain flow rate. This injectivity equation assumes steady incompressible flow. The

pressure profile can be used to determine available aquifer volume for safe storage of CO_2 (see Figures 3-3a and 3-3b). For convenience we refer to the left hand side of Eq. 3.1 as "drawdown".

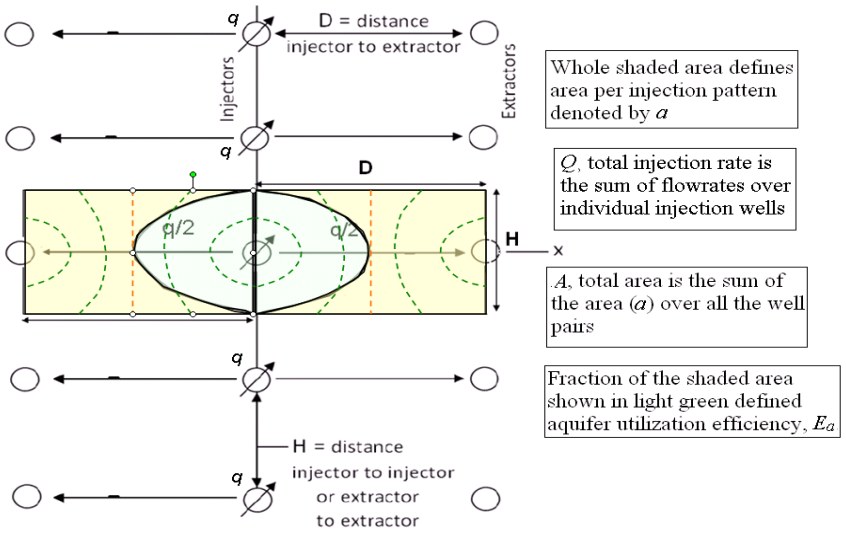

a)

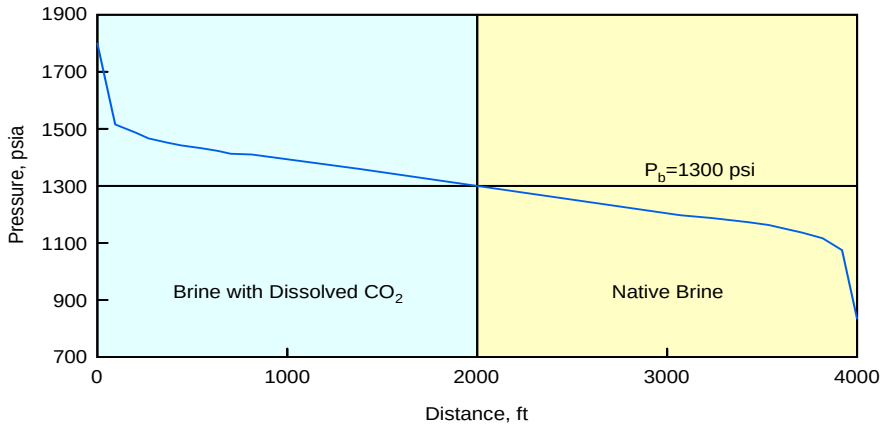

b)

Figure 3-3 (a) Schematic shows the layout of line drive pattern along with the pressure contours and injected fluid front shape when it reaches the bubble point pressure contour (Shown in orange). (b) Example pressure profile along the line joining injector/producer pair in (a) for extraction at 500 psi below hydrostatic and injection at 500 psi above hydrostatic, which is 1300 psia. The radial flow near wells and linear flow regime far from wells is evident. If CO_2 saturated brine having bubble point pressure of 1300 psia is injected, the green colored area marks the region where CO_2 stays in the solution.

The flow rate in Eq. 3.1 depends on the pressure difference between extraction and injection wells ($P_i - P_p$) and the pattern configuration (H and D). The flow rate increases with the increase in (H/D) ratio but varies only slightly with H. This also stays true for the cases where (H/D) is greater than unity (cf. Appendix B). The streamlines in the line drive pattern are used to determine the fluid front shape when it reaches the saturation pressure contour; this is light green region in Figure 3-3a. The fluid front shape is shown in Figure 3-3a in black line. It is elliptical because the streamline in the centre is the fastest while the streamline which originates in the direction perpendicular to the fastest line travels very slowly. Thus in the same amount of time a particle on each of these streamlines travels different distances and hence the shape. Continued injection would cause a gas phase to form downstream of this contour. Thus the area within the light green region determines the aquifer utilization efficiency (E_a) described in the next section.

An upper bound on the bottomhole pressure at extraction wells is the bubble point pressure of the CO_2-saturated brine. The lower bound is atmospheric pressure. Operation at the upper bound would achieve maximum possible storage efficiency, but the flowrates would be small. Operation at the lower bound would enable maximum possible flowrates, but storage efficiency would be small. Thus the optimum extraction pressure is likely to lie somewhere between these limiting cases.

3.2.2 Aquifer Utilization Efficiency

Aquifer utilization efficiency is the definition of storage efficiency for surface dissolution process. It is defined as the fraction of pore volume swept when the CO_2 saturated brine reaches the bubble point pressure contour in the aquifer. It is apparent that E_a is closely related to areal sweep efficiency.

$$E_a = \frac{\text{Volume occupied by } CO_2 \text{ saturated brine upstream of bubble point pressure contour}}{\text{Total pore volume between injectors and producers}} \quad (3.6)$$

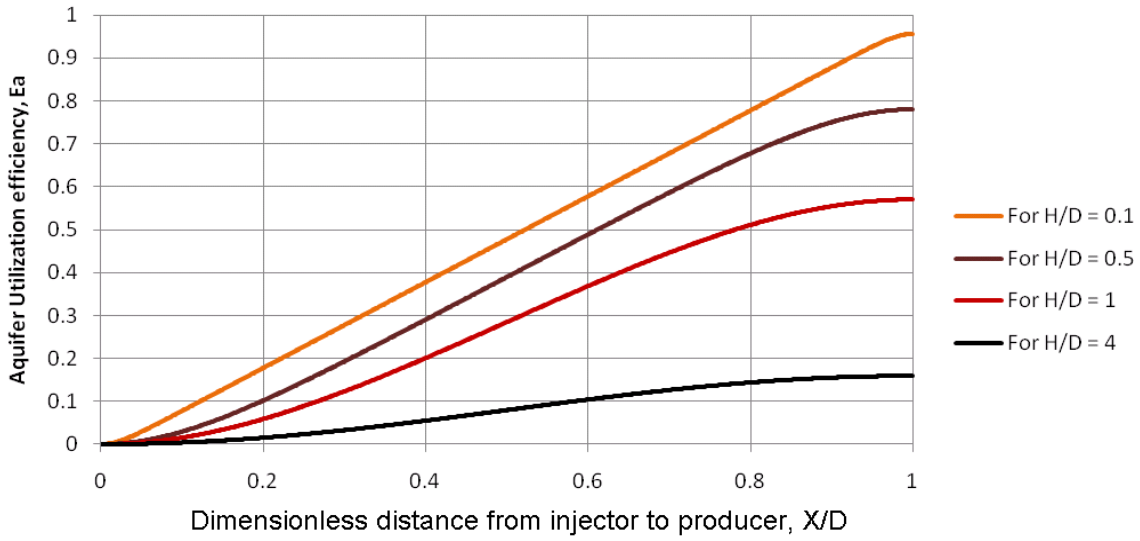

Figure 3-4 Variation of aquifer utilization efficiency for a homogeneous aquifer with CO_2 saturated brine displacing resident brine (mobility ratio of unity) and different line well spacings.

In Figure 3-4, *x* is the distance from injector to any point along the line joining injector extractor pair. The dimensionless distance (*x/D*) is the ratio which would lie between 0 (at the injector) and 1 (at the extractor). In a line drive injection scheme the aquifer utilization efficiency is a function of the dimensionless position (*x/D*) of the leading edge of the CO_2-saturated brine from the injector (Figure 3-3a). This is due to the fact that the fastest streamline in a line drive pattern travels along the line joining injectors and extractors (see Appendix B). The CO_2 saturated brine reaches the location of bubble point pressure along this line earlier than anywhere in the storage formation. Since our design goal is to avoid any CO_2 gas phase in the storage formation, the volume injected at this time of arrival determines aquifer utilization efficiency. Aquifer utilization efficiency increases as the CO_2 saturated brine moves towards extraction wells because

the closer the injection front approaches the extraction wells, the more fluid has been automatically injected. For a given *H/D* ratio the slopes of the curves in Figure 3-4 near *x/D* = 0 and *x/D* = 1 are smaller. This is because the flow field near the injection and extraction wells is radial. Aquifer utilization efficiency also increases as the *H/D* ratios decrease. This is due to the fact that as *H/D* ratio decreases, the flow field becomes more linear for greater distance and thus sweep becomes more uniform.

3.2.3 Risk

Surface dissolution scheme involves extractors and injectors. To allow injection the bottomhole pressure of the injectors always is higher than the initial hydrostatic pressure. Similarly the bottomhole pressure of the extractors is less than or equal to saturation pressure which is limited by initial hydrostatic pressure. With these boundary conditions, hydrostatic pressure contour has to lie between injection and extraction lines. The area lying between injection line and the hydrostatic pressure contour is called the overpressure region. This over pressured region poses geomechanical failure risk which has potential to contaminate overlying aquifer systems. This risk has associated costs just like well costs and pore volume costs so it is included in the design. We define a proxy for the risk to be the fraction of the total volume in the region of elevated pressure. This could be factored into the design by assigning some cost associated with this risk.

Risk = Volume associated with the over pressured region/Pattern volume

3.3 OPTIMIZATION REQUIREMENTS FOR THE DESIGN

Any sequestration project is likely to operate at the maximum safe rate of injection. The maximum safe rate would ensure minimum number of wells for the whole project, thereby reducing the total capital cost. To satisfy this requirement the bottomhole pressure of all the injectors could be set at fracture pressure. Similarly, extractor

bottomhole pressure could be set to saturation pressure to achieve maximum aquifer utilization efficiency. The question arises whether these boundary conditions give us minimal cost. We optimize the well pattern with respect to three contributions to the cost: the volume of rock required, number of wells required and the risk associated with injection.

$$\textit{Total Capital Cost} = X*\textit{Well Count}*\textit{Depth} + Y*\textit{Total Area} + Z*\textit{Risk} \quad (3.7)$$

Here X is the cost of well construction in dollars per foot, Y is the cost of acquiring land in dollars per acre and Z is the cost associated with mitigating or averting risk due to overpressure in dollars per acre. Three quantities turn out to drive the cost optimization i) flow rate in the line drive pattern design, ii) fluid front movement and iii) pressure profile inside the aquifer. The pattern flow rate determines the number of well pairs needed for a target sequestration rate. Aquifer utilization efficiency determines the rock volume needed. The areal extent of pressure elevation within the aquifer is assumed to determine risk. We treat as independent parameters the injection pressure (P_i), extraction pressure (P_p), bubble point or saturation pressure (P_b), and the pattern design parameter injector-injector spacing (H). The desired CO_2 storage rate and the aquifer properties are assumed fixed. That is, the optimization does not examine whether a given aquifer could be better utilized at a different storage rate. Nor does it examine the optimal aquifer properties for a given storage rate.

$$\textit{Total Capital Cost} = f(P_i, P_p, H, P_b, \text{Aquifer and } CO_2 \text{ storage rate}) \quad (3.8)$$

Let us consider how the independent parameters determine the other operating parameters. For a given storage rate and bubble point pressure (P_b), the total brine injection rate is readily determined. From the storage rate and for a given aquifer, with project life known, total area required can be calculated. The flowrate is a function of drawdown ($P_i - P_p$), pattern parameters (injector-injector spacing (H) and injector-

extractor spacing (D)) and aquifer petrophysical properties (k, h). The saturation pressure is also treated as an independent parameter because it governs the aquifer utilization efficiency. This is further explained in the next section on operating point determination.

The injector-extractor spacing D is not one of the independent parameters. To see this, recall from Eq. 3.1 that for a set of parameters (P_i, P_p, and H) the injection rate varies with H/D. As H/D varies, the location of the contour of saturation pressure (P_b) also varies. That is, aquifer utilization efficiency varies with H/D. As H/D ratio increases, injection rate increases (Eq. 3.1) and aquifer utilization efficiency goes down (Figure 3-4). For the project life, total amount of CO_2 injected into the formation has to be equal to the volume occupied based on aquifer utilization efficiency. With all the independent parameters fixed the above mentioned condition could only be satisfied at only one value of D.

3.4 OPERATING POINT DETERMINATION FOR A SET OF INDEPENDENT PARAMETERS

The identification of optimum drawdown along with the information on ratio of pattern area occupied by CO_2 to the total area play a very important role in design of the injection pattern and number of wells needed. For the design and operating point determination we assume that the CO_2 storage rate, the project life and the aquifer properties are fixed. The total pore space required for the project depends on bubble point pressure solubility value (S), average porosity of the aquifer (ϕ), the total life period of the project (T), the target sequestration rate ($\dot{m}_{CO_2}$) and the aquifer utilization efficiency. For the design purpose, aquifer is assumed to be homogeneous and isotropic. In a homogeneous aquifer injecting CO_2 saturated brine will exhibit 100% vertical sweep efficiency. The areal sweep efficiency is less than 100% because of the non uniform displacement front shapes in the line drive pattern or (any injection/extraction pattern).

The value of E_a is bounded above by the areal sweep efficiency at breakthrough for the line drive pattern. Total area (A) required will be given by:

$$A = \frac{(1-S)}{S} \frac{M_{H2O}}{M_{CO2}} \frac{\dot{m}_{CO2} T}{\rho_{H2O} h \phi E_a} \tag{3.9}$$

where S is expressed as mole fraction, M_{H2O} is molecular weight of water and M_{CO2} is molecular weight of CO_2, ρ_{H2O} is brine density and h is aquifer thickness. Each element of the well pattern has area a given by $a = HD$. Thus the ratio A/a determines the number of well pairs; we refer to this as the "area basis" constraint.

$$\text{Wellpairs on area basis, } Wp = \frac{A}{a} \tag{3.10}$$

For a given aquifer depth (d), thickness (h), permeability (k), brine viscosity (μ), and a set of values of independent parameters the flow rates per well pair are calculated using methods described in Appendix A and B. For a sequestration project, the total amount of CO_2 disposed per day is known. This fixes the required brine flow rate Q, once the target solubility S has been chosen:

$$Q = \frac{(1-S)}{S} \frac{M_{H2O}}{M_{CO2}} \frac{\dot{m}_{CO2}}{\rho_{H2O}} \tag{3.11}$$

Each well pair has a flow rate $q/2$ because each injection well has a flowrate of q and with each injection well two well pairs are associated so flow divides itself into half see Figure 3-3a). So the ratio $Q/(q/2)$ provides an independent constraint on the number of well pairs, which we term the "flow rate basis" constraint.

$$\text{Wellpairs on flowrate basis, } Wp = \frac{2Q}{q} \tag{3.12}$$

The solution approach solves the "area basis" and "flow rate basis" constraints simultaneously. For a given set of values for the independent parameters (P_i,P_p,P_b,H), we determine the operating point at which the line drive pattern configuration has unique dimensions H and D. We compute flow rate per injection well (q) for several values of H/D (Appendix A and B). From the pressure contours computed at each value of H/D ratios, we calculate aquifer utilization efficiency (E_a). From the values of q and E_a, we calculate A/a and Q/q, and then the area basis and flow rate basis well pair requirement can be determined as a function of H/D. The operating point is the intersection of Eqs. (3.11) and (3.12). A graphical solution is illustrated in Figure 3-5 for the example parameters of Table 3.1, for which the solution is D = 4100 ft, number of well pairs is 168, the injection rate per well is q =7358 b/d, and the total area required is A = 16215 acres.

The operating point is the heart of all the calculations leading to optimization. The well pairs required, pore volume required and total area in the region of overpressure is function of the operating point for a given set of independent parameters.

Storage rate	Project life	k	H	Porosity	T	Depth	P_i	P_p	P_b	H
10^7 kg/day	30 years	100 md	1000 ft	0.12	80 F	2000 ft	1400 psi	800 psi	860 psi	1000 ft

Table 3-1 Parameters for example operating point determination

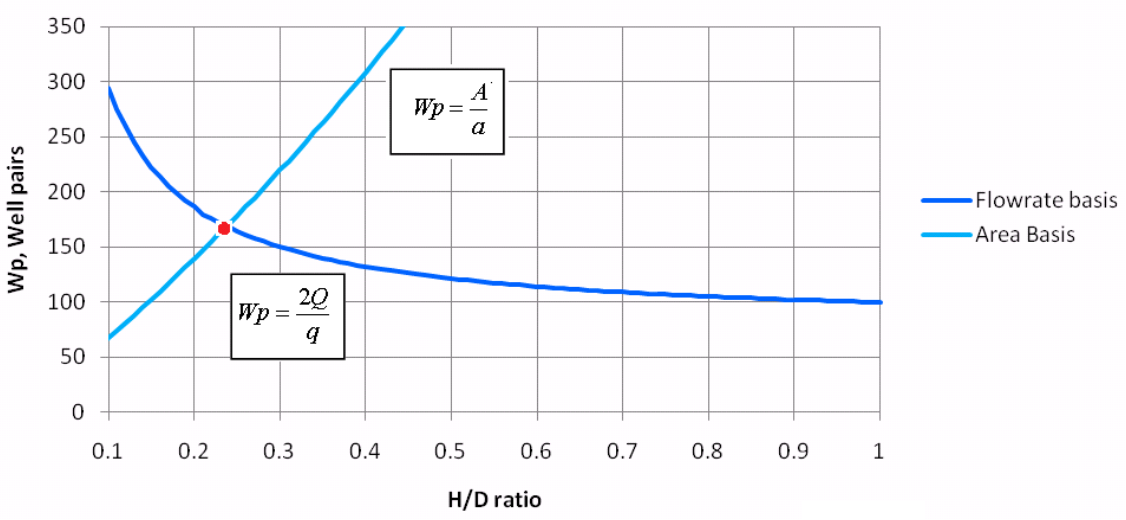

Figure 3-5 Schematic showing the intersection of the well pair curves based on flowrate basis and area basis. This intersection is the operating point for the given independent parameters in table 3-1

3.4.1 Impact of variation of independent parameters on operating point

The operating points for two values of injector-injector spacing H at fixed P_i (1400 psi), P_p (800 psi) and P_b (860 psi) are shown in Figure 3-6. The pattern area has a direct dependence on H, hence change in H leads to the large shift in the "area basis" curve in Figure 3-6. In contrast, the flow rate per well pair depends weakly on H and the "flow rate basis" curve shifts slightly upward. For H/D larger than 0.25 the number of well pairs required on area basis decreases slowly with H/D. Hence number of well pairs decreases slowly while the ratio H/D increases rapidly as H increases, that is, the operating point moves towards right and downwards.

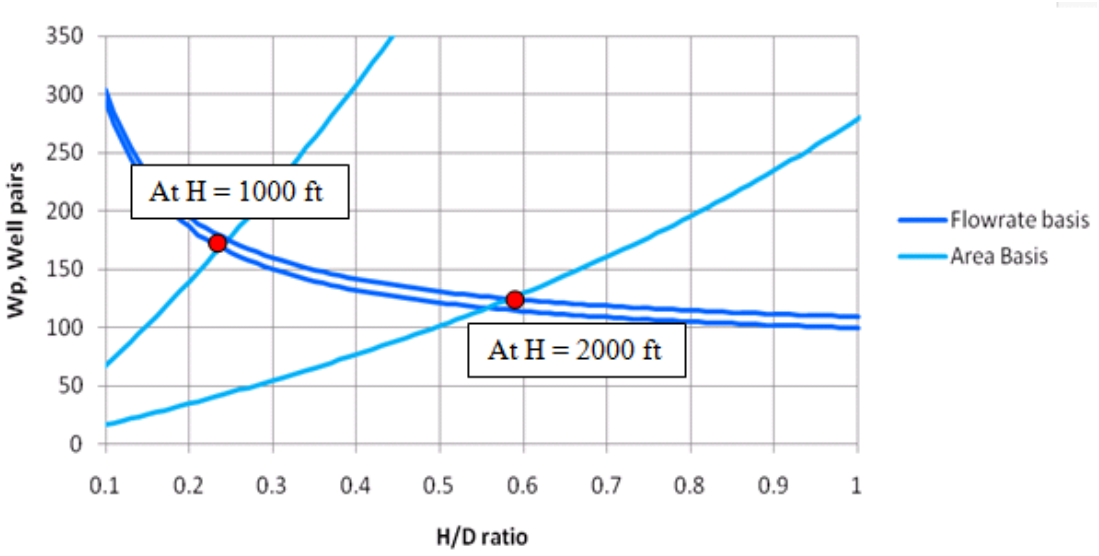

Figure 3-6 Effect of H on the operating point and thus on the well pairs required at P_i = 1400 psi, P_p = 800 psi and P_b = 860 psi

This leads to decrease in the well pairs required at the operating point for higher H but since the operating point moves towards right i.e. at higher H/D ratio, the aquifer utilization efficiency decreases. A decrease in well pairs reduces cost while decrease in aquifer utilization efficiency increases cost. Thus the optimum will depend on relative costs.

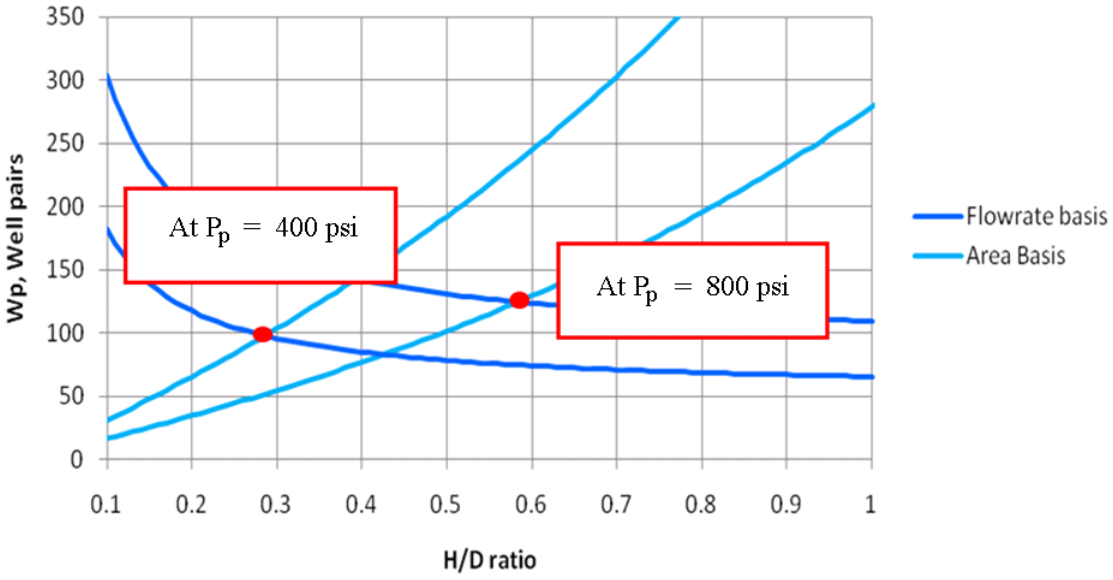

Figure 3-7 Effect of extraction well bottomhole pressure P_p on the operating point and its effect on the number of well pairs required at P_i = 1400 psi, P_b = 860 psi and H = 2000 ft.

The variation of operating point with change in producer pressure (P_p) at fixed P_i (1400 psi), P_b (860 psi) and H (2000 ft) is illustrated in Figure 3-7. With increase in drawdown, here achieved by decreasing P_p, flow rate increases and the well pair requirement decreases causing the curve based on flow rate to shift down. Decreasing P_p also causes the contour of saturation pressure to move toward the injectors, reducing the area that can be occupied by saturated brine. This decreases the aquifer utilization efficiency which leads to higher total area requirement. For a given pattern area (a), more well pairs are needed to satisfy the total area requirement. Thus the "area basis" curve shifts upward in Figure 3-7. The combined effect is to reduce the number of well pairs and the ratio of H/D when the drawdown increases. Thus increase in drawdown leads to decrease in number of well pairs required but leads to increase in total area required. The effect is similar to the effect of increasing H.

3.5 DESIGN AND INTEGRATION

All the four design variables (bubble point pressure, P_p, P_i, and H) are now varied independently. To begin the process we pick a pair of values of injection pressure (P_i) and saturation pressure (P_b). We then vary extraction pressure (P_p) and injector-injector spacing (H) systematically. For each combination of P_p and H, we find the location of the bubble point contour (and hence the aquifer utilization efficiency), the contour of hydrostatic pressure, and an operating point as described above. The operating point determines the number of well pairs. The location of hydrostatic pressure contour determines the fraction of the formation that experiences over-pressure during injection. This is taken to be directly proportional to the risk. At this point, we have sets of values of well pairs, aquifer utilization efficiency and risk for a range of values of P_p and H at given P_i and P_b. This gives us a set of 2-D matrices for well pairs, aquifer utilization efficiency and area of over pressured region. This process is repeated for several bubble point pressures. At this point, variation in three independent parameters (P_p, P_b, H) gives 3-D matrices for well pairs, aquifer utilization efficiency and area of over pressured region. These matrices are multiplied by corresponding cost parameters (X, Y, Z) to obtain well costs, area costs and risk costs. The total cost is determined by summing up the well costs, area costs and risk costs. The variation of total cost with respect to P_b, P_p and H determines the minimum cost point for a given injection pressure. The steps defined above are outlined in a flowchart below. When this is repeated for multiple injection pressures the optimum combination of P_i, P_p, H and P_b is the point with the least total cost.

This flowchart outlines the design steps when aquifer properties, CO_2 storage rate and project life are given

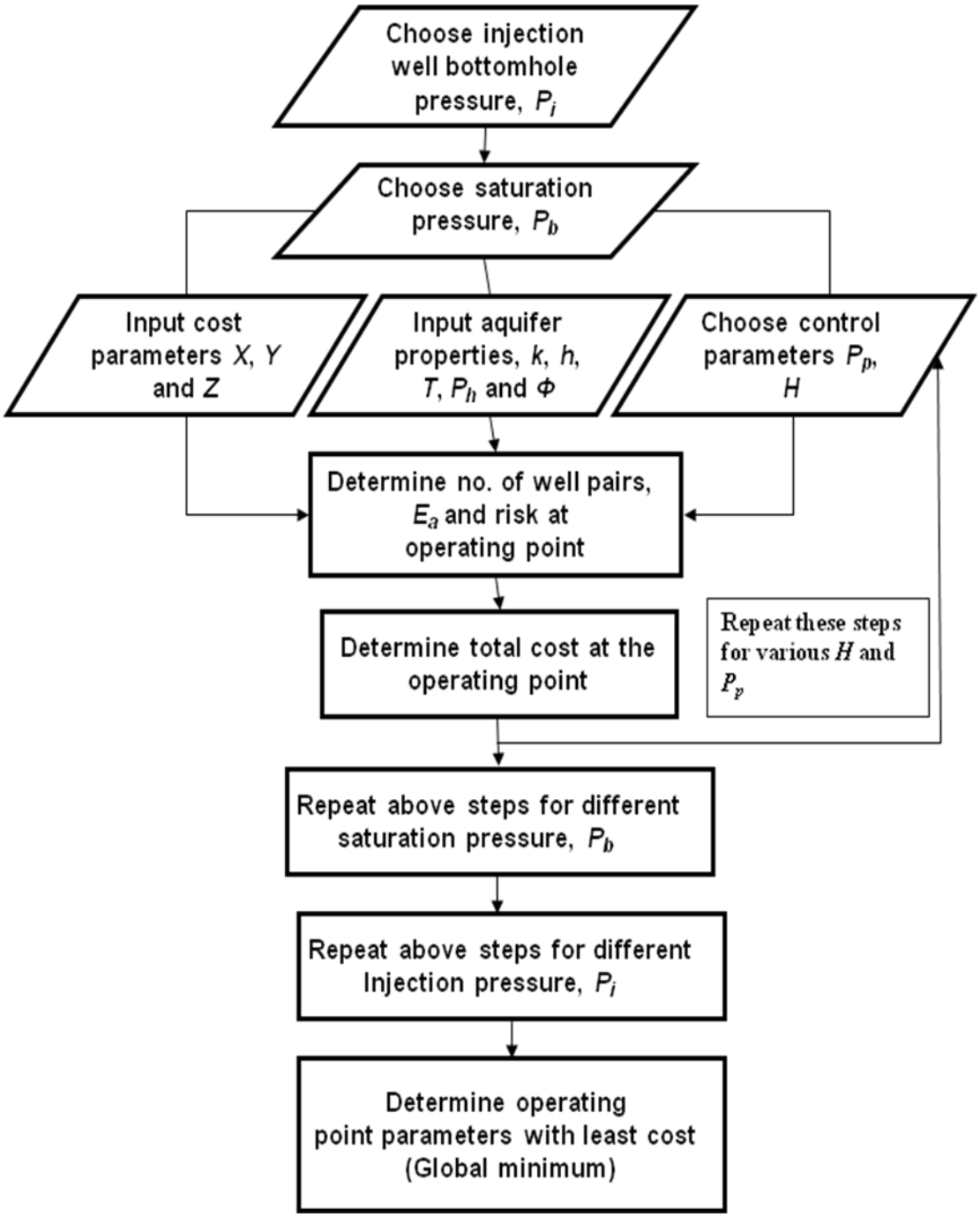

The impact of various independent parameters on design and their integration for an optimal design is now illustrated. Consider a 500 MW coal fired power plant which

emits 10 million kilograms/day of CO_2. The properties of the aquifer in which the injection takes place are given in Table 3-2. We choose the target solubility to be the value at aquifer conditions, which is $S = 0.021$ (mole fraction). The required brine flow rate is thus 1.4 million barrels/day at the target solubility. Maximum allowable injection pressure is equal to 1400 psi, based on a typical fracture gradient of 0.7 psi/ft and an aquifer depth of 2000 ft. The duration of the sequestration project is 30 years. Costs are taken as $X = 600$ $/ft for well construction, $Y = 4000$ $/acre for land, and $Z = 1000$ $/acre for risk.

Petrophysical and fluid properties required for the example design

Aquifer Description	
Injection Depth (d)	2000 ft (600 m)
Permeability (k)	100 md
Porosity	12%
Salinity	75,000 ppm
Initial Temperature	80 °F
Initial Pressure	866 psig (9 MPa)
Dip Angle	0°
Frac gradient (F_d)	0.7 psi/ft
Pore pressure gradient (P_p)	0.43 psi/ft
Thickness (h)	1000 ft
Fluid Properties	
Brine viscosity	1 cp
CO_2 solubility (S)	0.021 mole fraction
Saturation pressure P_b	860 psi
Well Properties	
Skin	0
Well radius (r_w)	0.5 ft

Table 3-2 Petrophysical and fluid properties for the example design

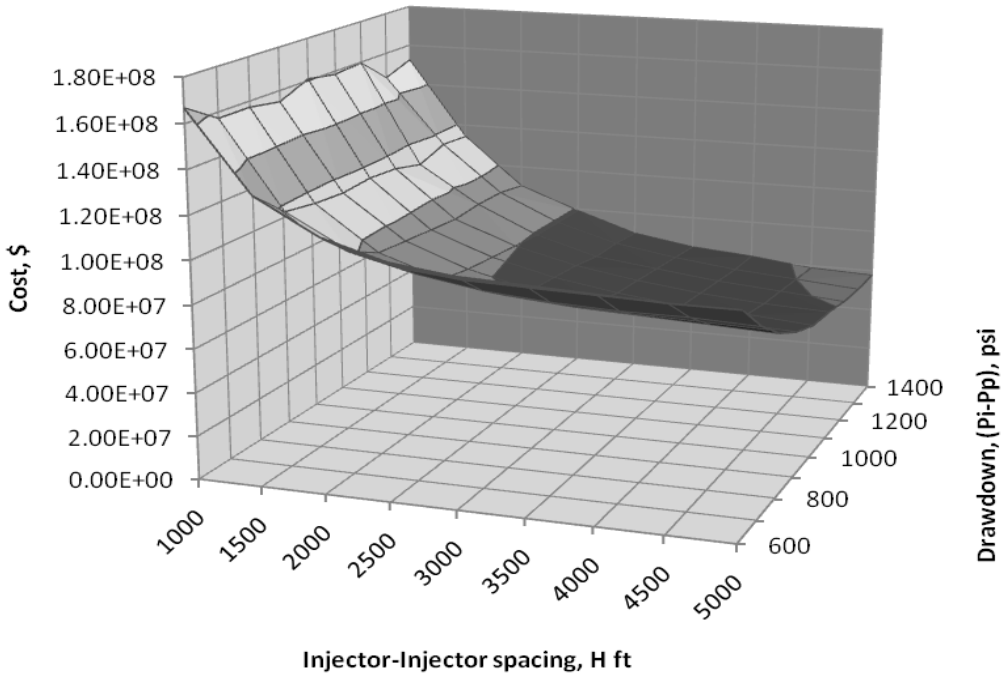

Figure 3-8 Variation of the well cost with respect to to H and drawdown at P_i = 1400 psi and P_b =860 psi.

Figure 3-8 illustrates variation of well costs with respect to drawdown ($P_i - P_p$) and injector-injector spacing (H). As injector-injector spacing increases the well cost decreases; increasing the drawdown has same effect though much less sensitive. This behavior is consistent with the effect of these parameters on the operating point shown in Figure 3-6 and 3-7. There it was shown that with increase in injector-injector spacing (H), the wellpairs required based on flowrate basis constraint does not change but wellpairs required on area basis decrease. This is due to direct dependence of the area basis constraint on injector-injector spacing (H).

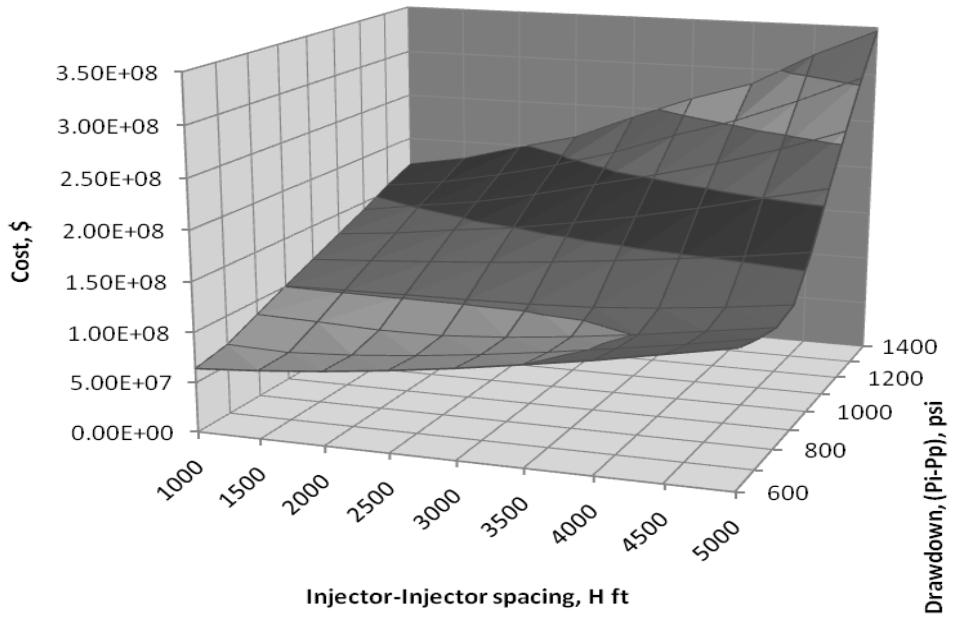

Figure 3-9 Variation of the area cost with respect to H and drawdown at P_i = 1400 psi and P_b =800 psi.

Similarly, Figure 3-9 illustrates variation of area cost, which is proportional to aquifer utilization efficiency. The aquifer utilization efficiency decreases with increase in H/D ratio because higher the H/D ratio, the more elliptical the moving fluid front within the injector/extractor pattern (cf. Figure 3-3a) leading to decrease in sweep efficiency. The area cost increases with drawdown because the producer pressure P_p must be reduced. This reduces the aquifer utilization efficiency because the saturation pressure contour moves towards the injectors.

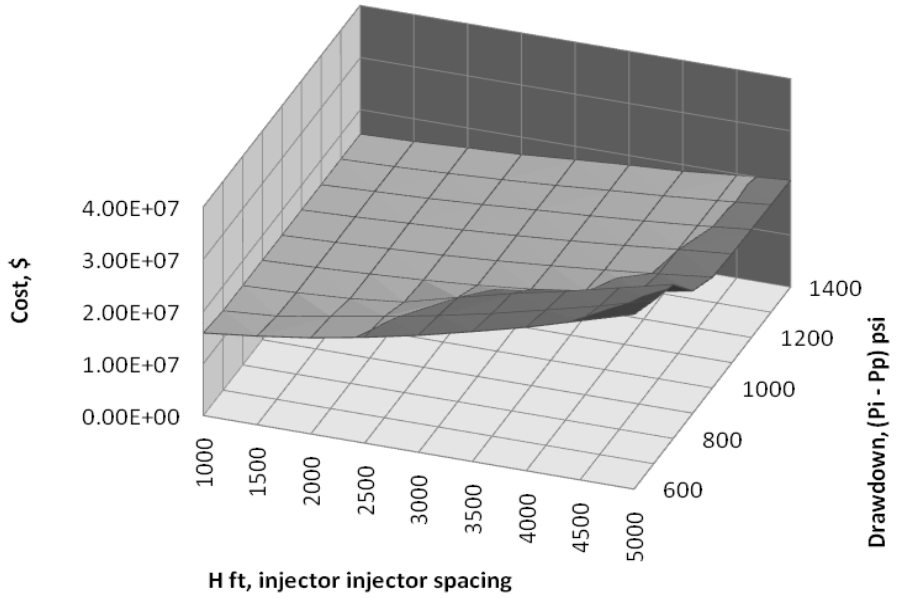

Figure 3-10 Variation of cost of risk of overpressure with respect to H and drawdown at P_i =1400 psi and P_b = 800 psi.

Figure 3-10 illustrates variation of risk cost, which increases with injector-injector spacing because the absolute area within the hydrostatic pressure contour increases. Moreover, an increase in injector-injector spacing moves the operating point toward larger *H/D* (Figure 3-6). Thus at the same drawdown, pressure gradients will be larger (Eq. 3.1). For fixed P_i this means the hydrostatic pressure contour will move toward the producers (Figure 3-3). Risk cost also increases as drawdown decreases. This is because smaller drawdown is achieved by increasing the producer pressure P_p, which moves the hydrostatic pressure contour towards the producers, Figure 3-3. Hence area at risk because of elevated pressure becomes larger.

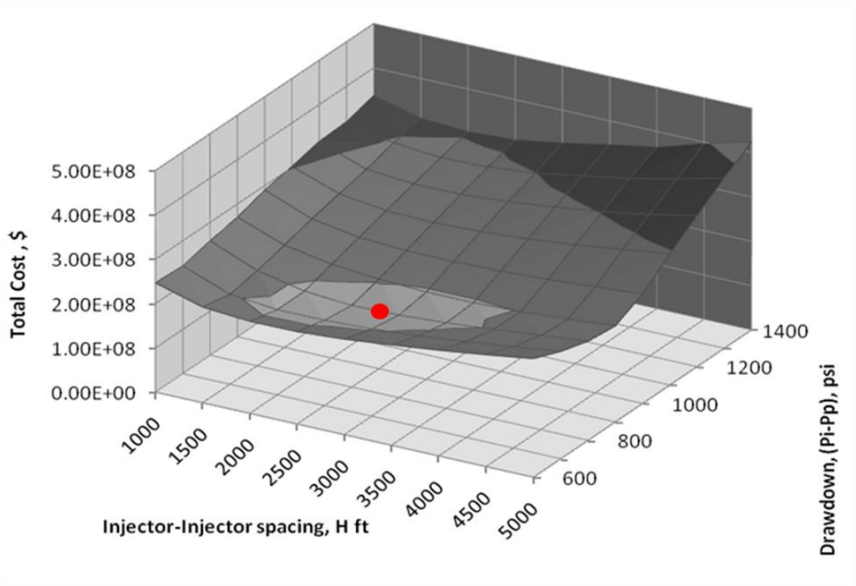

Figure 3-11 Total cost surface based on the cost parameters X = 600$/ft, Y = 4000$/acre and Z = 1000$/acre. The red point shows the point where minimum cost occurs. The combination of all independent parameters at this point defines the optimal choice of H = 2500 ft and P_p = 600 psi given P_i = 1400 psi and P_b = 800 psi.

Combining the costs shown above yields total capital cost surface. The minimum cost point on this surface yields the optimal design for fixed P_i and P_b. The total costs for the pair of values of injection pressure (P_i = 1400 psi) and saturation pressure (P_b = 800 psi) are shown in Figure 3-11. The minimum value on this surface is identified as the optimum. The total cost surface is a bowl shaped surface because the contributing surfaces all slope upwards in different directions. This is the effect of complicated interplay between flow rate and location of the saturation pressure and hydrostatic pressure contours.

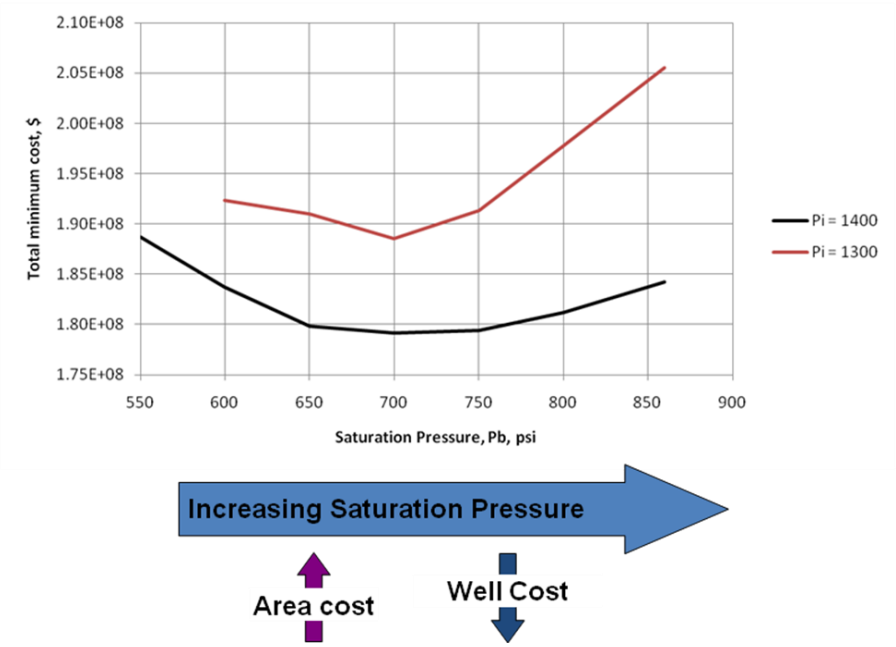

Figure 3-12 Variation of minimum cost point picked from the total cost surface for different bubble point pressures and injection pressures.

To arrive at the global optimum, we have to vary bubble point pressure and injection well bottomhole pressure systematically, determining the local optimum for each pair of values. Thus we repeat the steps that led to Figure 3-11, holding injection pressure fixed and varying saturation pressures. The maximum saturation pressure allowable is the hydrostatic pressure. With increase in saturation pressure, area costs generally increase. This is because the saturation pressure contour moves towards injectors leading to decrease in aquifer utilization efficiency. The well costs, area costs and risk costs all vary in such a fashion that there is a minimum of cost occurring at a saturation pressure less than the hydrostatic, as shown in Figure 3-12 for two different injection pressures. This is a direct result of the location of the saturation pressure contour which affects aquifer utilization efficiency, risk and the number of wells required to meet the sequestration demands.

Finally, we repeat all the above steps for a range of injection pressures. Maximum injection pressure is constrained by the fracture pressure of the aquifer. As illustrated in Figure 3-12, decrease in injection pressure causes increase in costs. The simple reason behind this is that as injection pressure decreases, injection rates decrease, leading to requirement of more well pairs. The aquifer utilization efficiency also decreases because saturation pressure contour moves towards injectors. This leads to less risk costs but the increase in other cost components is much more.

Based on the optimization scheme for surface dissolution design for the aquifer and storage properties given in Table 3-2, the optimum conditions for X = 600 $/ft, Y = 4000 $/acre and Z = 1000 $/acre are injection pressure of 1400 psi (the maximum possible value because of fracture gradient constraints), a saturation pressure of 700 psi (less than the maximum possible value of 860 psi), a producer pressure of 400 psi and an injector/injector spacing of 3000 ft. Storage efficiency at the optimum point is 72% with 52% of the total area under over pressure during injection. 63 well pairs are required at the optimum to maintain the balanced injection. These observations are specific to the cost parameters chosen for the design. In the next section, relative impact of different cost parameters is shown on the optimization scheme.

3.6 SENSITIVITY STUDY TO ANALYZE THE IMPACT OF VARIATION IN DIFFERENT UNDERLYING PARAMETERS (AQUIFER PROPERTIES AND COST PARAMETERS)

Properties	**Range of values**		
	Low	**Mid**	**High**
Permeability (md)	10	100	1000
Porosity	0.2	0.3	0.4
Thickness (ft)	100	500	1000
Salinity (ppm)	15000	30000	45000
Cost Parameters			
Well Cost (*X*) in $/ft	200	600	1000
Area Cost (*Y*) in $/acre	2000	4000	10000
Risk Cost (*Z*) in $/acre	100	1000	10000

Table 3-3 Range of values for sensitivity analysis

Analysis for sensitivity of different uncertain parameters was done with rest of parameters kept same as the design base case described in the previous section. The independent and dependent parameters at the optimum design points for all the above cases are provided in Table 3-4 and 3-5.

3.6.1 Permeability:

The impact of variation in aquifer permeability is shown in Figure 3-13. With increase in permeability of the storage formation, the design point for optimal cost moves towards higher saturation pressures. This is because as permeability increases, the flowrate increases which leads to less well pair requirement. To dispose same amount of CO_2 with less well pairs, aquifer utilization should increase. This increase in aquifer

utilization efficiency with increase in permeability is shown in table 3-4 and 3-5. With increase in permeability, the extractor pressure increases. This leads to movement of saturation pressure towards extraction line. The *H*/*D* ratio at the design points also decreases as permeability increases as shown in table 3-4 and 3-5. The decrease in *H*/*D* ratio along with decrease in drawdown causes aquifer utilization efficiency to increase. With decrease in permeability well costs and area costs increase and this is illustrated in Figure 3-13 (notice the difference in cost values on Y-axis).

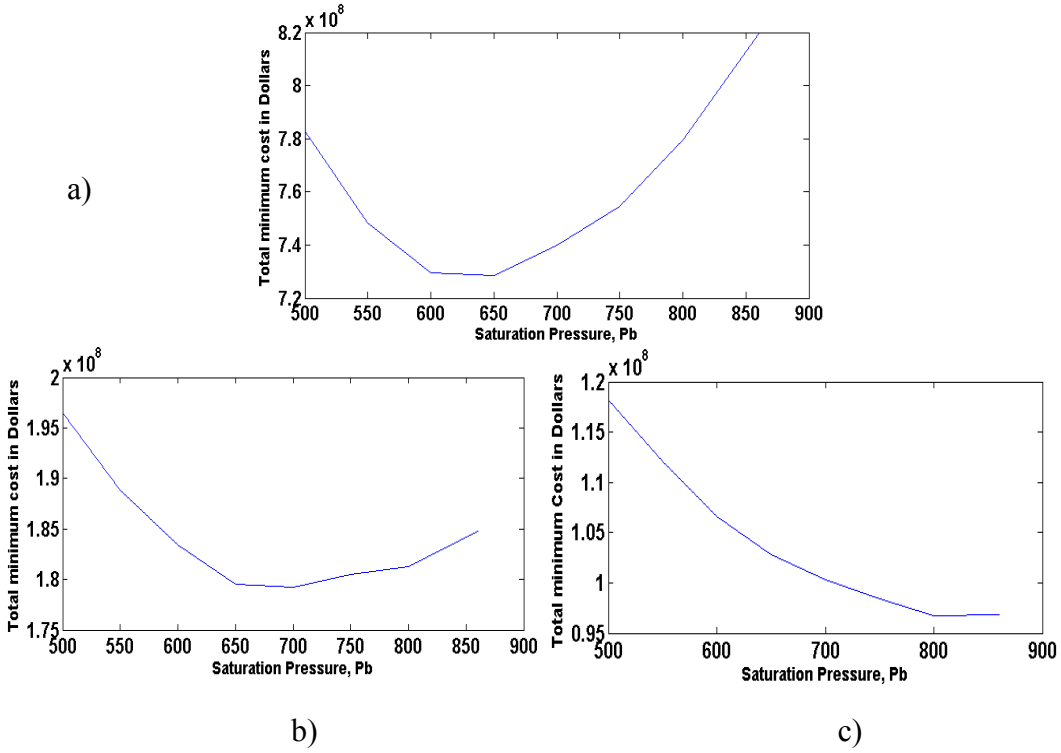

Figure 3-13 Effect of aquifer permeability on cost while other design parameters (same as base case) are kept fixed. a) at k = 10 md, b) k = 100 md and c) k = 1000 md.

3.6.2 Thickness:

The impact of aquifer thickness on the optimal design is illustrated in Figure 3-14. The optimum saturation pressure remains 700 psi regardless of thickness. It remains invariant because well flowrates increase linearly with thickness, while area required for storage decreases linearly with thickness. A larger flowrate leads to fewer well pairs required, according to the flowrate basis constraint (Eq. 3.12). For a given volume to be stored, an increase in thickness leads to decrease in area required. A smaller area also leads to fewer well pairs required, according to the area basis constraint (Eq. 3.11). Both constraints change the number of well pairs by the same factor, namely the ratio of the two values of thickness. Consequently the operating point (cf. Fig. 3-5) moves vertically to a different number of well pairs but without changing the value of H/D. None of the other independent parameters change, either, as shown in Table 3-4. Thus increase in aquifer thickness leads to proportional decrease in the total costs as seen in Figure 3-14 (reflected on Y-axis)

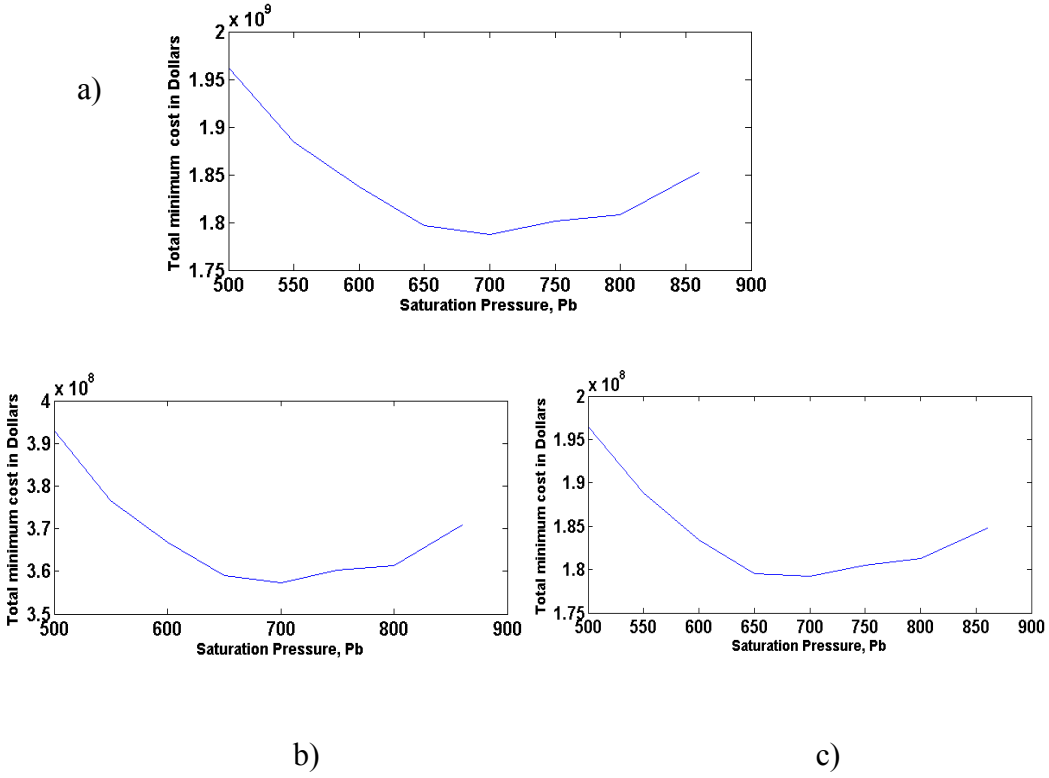

Figure 3-14 Effect of aquifer thickness on cost while other design parameters (same as base case) are kept fixed. a) at h = 100 ft, b) h = 500 ft and c) h = 1000 ft.

3.6.3 Porosity

The impact of variation in aquifer porosity on optimal design point is illustrated in Figure 3-15. With decrease in porosity of the storage formation, the optimal design point moves towards larger saturation pressures. The well flowrates are independent of porosity, so the number of well pairs required on flow rate basis is not affected by a change in porosity. However, a decrease in porosity leads to an increase in the area required to store a given volume. This increase in area cost can be partly counteracted by an increase in saturation pressure, which leads to increase in solubility and thus a smaller volume required for the same mass of CO_2. Similarly, decreasing the drawdown

(increasing extraction well pressure P_p) increases the aquifer utilization efficiency, enabling a smaller area to hold the same mass of CO_2. Table 3-4 shows that the optimum design point moves in this fashion. The overall effect of smaller porosities is to increase total costs due to greater area requirement. This is visible on Y-axis of Figure 3-15.

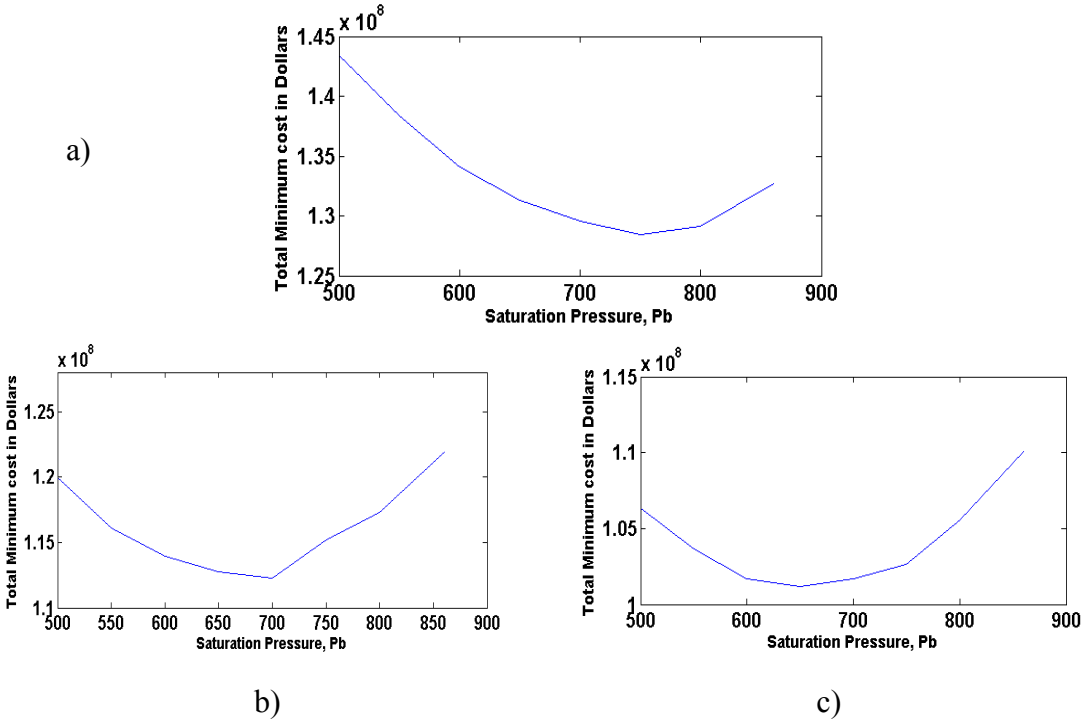

Figure 3-15 Effect of aquifer porosity on cost while other design parameters (same as base case) are kept fixed. a) at Φ= 0.2, b) Φ= 0.3 and c) Φ= 0.4.

3.6.4 Salinity

The impact of salinity variation on the design is illustrated in Figure 3-16. As the salinity of the aquifer brine increases, the solubility of CO_2 decreases. This change in solubility does not affect the flow behavior or pressure field established in the system. It does affect the area required and the total brine flow rate as shown in Eqs 3-9 and 3-10. The area and rate are both proportional to (1-*S*)/*S,* and thus the optimal design point for all the salinity values does not change, Table 3-4. The total costs increase as salinity

increases, as seen on Y-axis of the graphs in Figure 3-16 because the total area and number of wells required increase slightly.

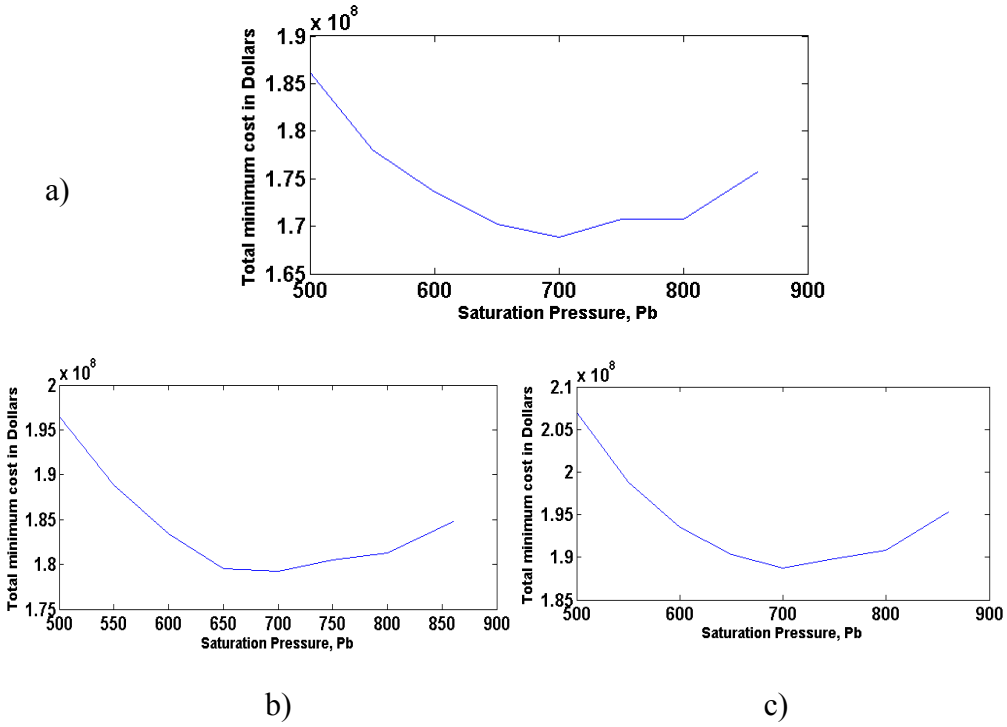

Figure 3-16 Effect of aquifer brine salinity on cost while other design parameters (same as base case) are kept fixed. a) at ppm = 15000, b) ppm = 30000 and c) ppm = 45000.

3.6.5 Relative impact of different cost parameters on the design

a)

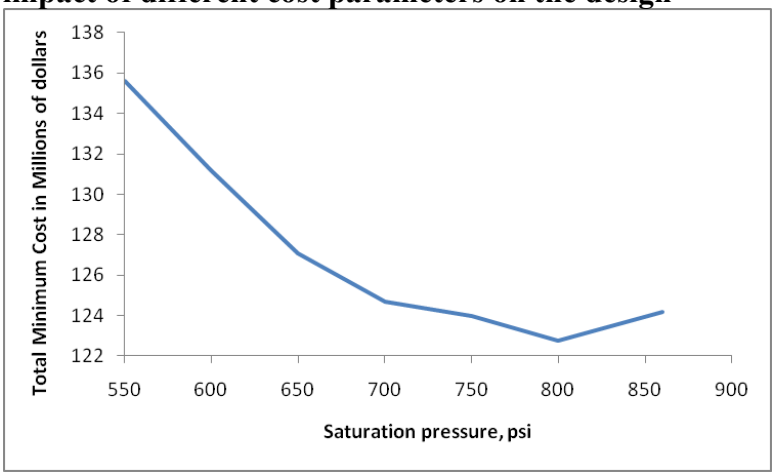

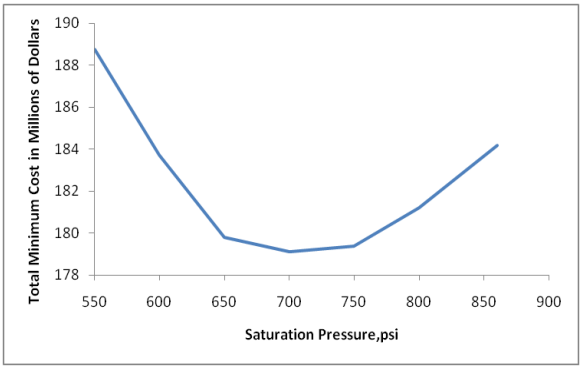

b)

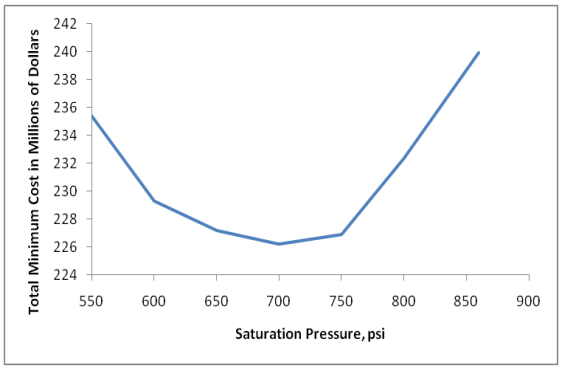

c)

Figure 3-17 Effect of well costs on design while other cost parameters (area and risk) are kept fixed. a) at $X = 200$ \$/ft, b) $X = 600$ \$/ft and c) $X = 1000$ \$/ft where $Y = 4000$ \$/acre and $Z = 1000$ \$/acre.

Increasing the well costs with other cost contributions fixed drives the optimal design point toward the fewer well pairs. Fewer well pairs can still provide the needed injection rate when the drawdown is higher and injector-injector spacing (H) are higher (Figure 3-8). Increase in H and drawdown with increase in well cost is seen in table 3-4 and 3-5. With increase in well costs, H/D ratio at optimal design point also increases. Increase in H/D ratio leads to decrease in aquifer utilization efficiency (Figure 3-4).

Increase in drawdown (achieved by reducing the extraction well pressure) also leads to decrease in aquifer utilization efficiency. This leads to higher area costs. Thus increase in well costs lead to higher absolute costs. This is visible on Y-axis of the curves shown in Figure 3-17

a)

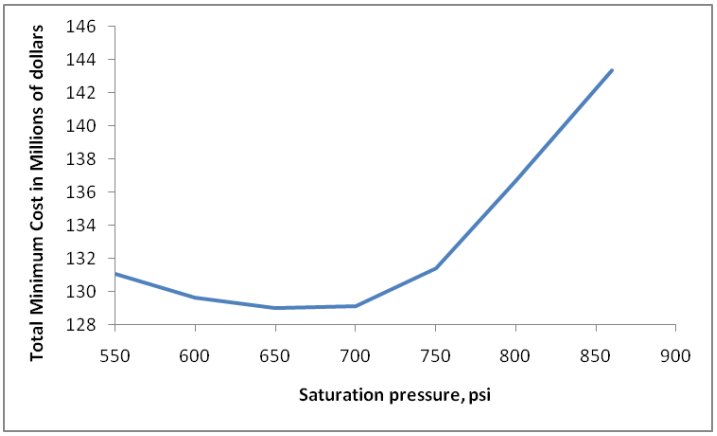

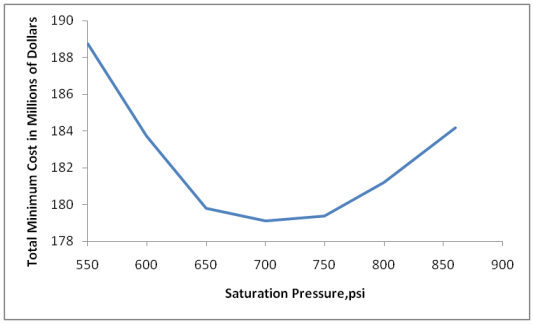

b)

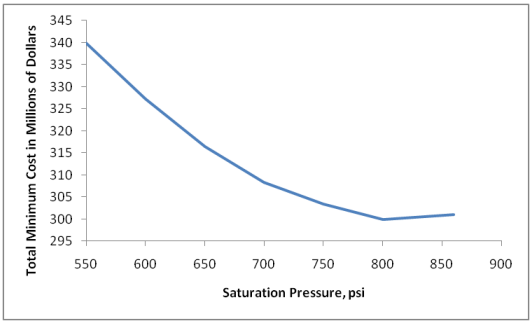

c)

Figure 3-18 Effect of area cost on design while other cost parameters (well and risk) are kept fixed. a) at $Y = 2000$ \$/acre, b) $Y = 4000$ \$/acre and c) $Y = 10000$ \$/acre where $X = 600$ \$/ft and $Z = 1000$ \$/acre.

Figure 3-18 illustrates that as area cost increases with other cost parameters fixed, the optimal design point moves towards higher saturation pressure. At higher area costs, the injector-injector spacing H and required drawdown decreases significantly as shown

in table 3-4 and 3-5. Decrease in H causes the optimal design point to move towards lower H/D ratios (Figure 3-6). At low H/D ratios aquifer utilization efficiency is higher, Figure 3-4. Higher saturation pressure also leads to higher solubility thus more mass of CO_2 could be stored, this also leads to reduction in area required. Thus with increase in area costs, the aquifer utilization efficiency increases (table 3-4 and 3-5). The increase in area costs lead to increase in total costs in absolute terms and is visible on Y-axis in Figure 3-18

a)

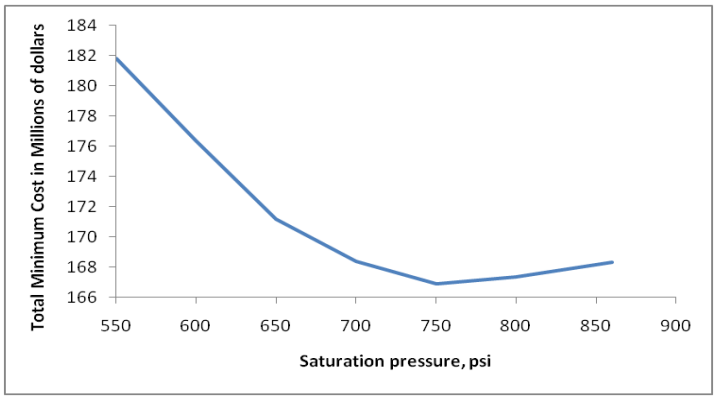

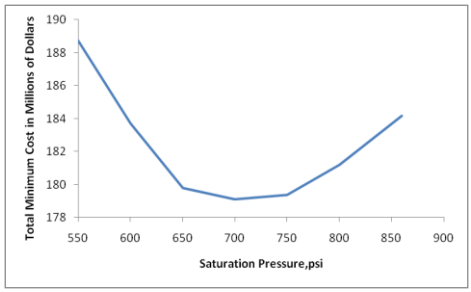

b)

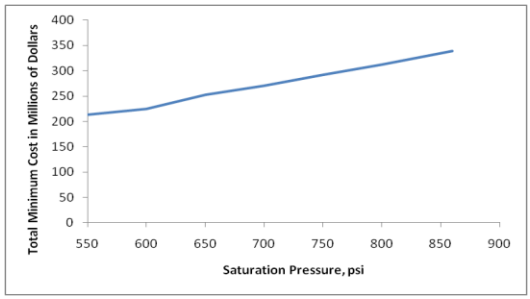

c)

Figure 3-19 Effect of risk costs on design while other cost parameters (well and area) are kept fixed. a) at Z = 100 $/acre, b) Z = 1000 $/acre and c) Z = 10000 $/acre where X = 600 $/ft and Y = 4000 $/acre.

As illustrated in Figure 3-19, as risk costs increase with other cost parameters kept fixed, the optimal design point moves towards smaller saturation pressures. With increase in risk cost, the drawdown at the optimal design point increases as shown in table 3-4 and 3-5. At higher drawdown, with fixed injection pressure less area is over pressured which leads to reduction in risk. But the injector-injector spacing and H/D ratio increase too at optimal design point as risk cost increases. At high H/D ratios aquifer utilization efficiency is low (Figure 3-4). Aquifer utilization efficiency is further reduced due to increase in drawdown as risk cost increases. Thus increase in risk cost leads to decrease in risk and aquifer utilization efficiency. The overall area at risk is also dependent on aquifer utilization efficiency so costs go up significantly as seen in Figure 3-19.

Sensitivity parameters	Independent Parameters			
	H ft	P_b psi	P_i psi	P_p psi
K = 10 md	3000	650	1400	100
K = 100 md	3000	700	1400	400
K = 1000 md	3500	800	1400	700
Porosity = 0.2	2500	750	1400	400
Porosity = 0.3	2500	700	1400	300
Porosity = 0.4	2000	650	1400	200
h = 100 ft	3000	700	1400	400
h = 500 ft	3000	700	1400	400
h = 1000 ft	3000	700	1400	400
X = 200 $/ft	2000	800	1400	600
X = 600 $/ft	3000	700	1400	400
X = 1000 $/ft	3500	700	1400	300
Y = 2000 $/acre	4000	650	1400	200
Y = 4000 $/acre	3000	700	1400	400
Y = 10000 $/acre	2000	800	1400	600
Z = 100 $/acre	2500	750	1400	500
Z = 1000 $/acre	3000	700	1400	400
Z = 10000 $/acre	5000	550	1400	0
Salinity = 15000 ppm	3000	700	1400	400
Salinity = 30000 ppm	3000	700	1400	400
Salinity = 45000 ppm	3000	700	1400	400

Table 3-4 Independent parameters for the sensitivity cases in Table 3-3

Sensitivity parameters	Dependent Parameters							
	***D*ft**	***Q*ft^3/day**	***A*ft^2**	***q*ft3/day**	***a*ft^2**	W_p	***H/D***	***Ea***
***K* = 10 md**	1875	8.33E+06	2.56E+09	3.66E+04	5.63E+06	455	1.6	0.30
***K* = 100 md**	5263	7.93E+06	9.95E+08	2.52E+05	1.58E+07	63	0.57	0.73
***K* = 1000 md**	17500	7.30E+06	8.58E+08	1.04E+06	6.13E+07	14	0.2	0.78
Porosity = 0.2	4032	7.59E+06	5.95E+08	2.57E+05	1.01E+07	59	0.62	0.70
Porosity = 0.3	3472	7.93E+06	4.69E+08	2.94E+05	8.68E+06	54	0.72	0.62
Porosity = 0.4	3390	8.33E+06	3.66E+08	3.08E+05	6.78E+06	54	0.59	0.62
***h* = 100 ft**	5263	7.93E+06	9.88E+09	2.53E+04	1.58E+07	626	0.57	0.73
***h* = 500 ft**	5263	7.93E+06	1.97E+09	1.27E+05	1.58E+07	125	0.57	0.73
***h* = 1000 ft**	5263	7.93E+06	9.95E+08	2.52E+05	1.58E+07	63	0.57	0.73
***X* = 200 $/ft**	5128	7.30E+06	8.21E+08	1.83E+05	1.03E+07	80	0.39	0.81
***X* = 600 $/ft**	5263	7.93E+06	9.95E+08	2.52E+05	1.58E+07	63	0.57	0.73
***X* = 1000 $/ft**	5833	7.93E+06	1.14E+09	2.83E+05	2.04E+07	56	0.6	0.64
***Y* = 2000 $/acre**	5970	8.33E+06	1.27E+09	3.14E+05	2.39E+07	53	0.67	0.69
***Y* = 4000 $/acre**	5263	7.93E+06	9.95E+08	2.52E+05	1.58E+07	63	0.57	0.73
***Y* = 10000 $/acre**	5128	7.30E+06	8.21E+08	1.83E+05	1.03E+07	80	0.39	0.81
***Z* = 100 $/acre**	5208	7.59E+06	8.98E+08	2.20E+05	1.30E+07	69	0.48	0.77
***Z* = 1000 $/acre**	5263	7.93E+06	9.95E+08	2.52E+05	1.58E+07	63	0.57	0.73
***Z* = 10000 $/acre**	6329	9.37E+06	1.58E+09	3.75E+05	3.16E+07	50	0.79	0.54
Salinity = 15000 ppm	5263	7.50E+06	9.32E+08	2.54E+05	1.58E+07	59	0.57	0.73
Salinity = 30000 ppm	5263	7.93E+06	9.95E+08	2.52E+05	1.58E+07	63	0.57	0.73
Salinity = 45000 ppm	5263	8.38E+06	1.04E+09	2.54E+05	1.58E+07	66	0.57	0.73

Table 3-5 Dependent parameters for the sensitivity cases in Table 3-3

3.7 CONCLUSIONS

For surface dissolution sequestration approach, we have developed a pattern design methodology (placement of injection and extraction wells) based on total cost optimization. The pressure field established in the aquifer during injection plays a very important part in governing the safe disposal of CO_2. Injection rates and the pressure field in the aquifer are dependent on the pattern configuration (injector-injector spacing H and injector/extractor spacing D for line drive pattern), injection pressure (P_i) and extraction pressure (P_p). Based on the concentration of dissolved CO_2, the location of saturation pressure contour within the storage formation is identified. The injection front shape when it reaches the saturation pressure (P_b) contour defines the limiting (maximum) areal extent of CO_2-saturated brine and hence the aquifer utilization efficiency. The location of hydrostatic pressure contour defines the area subjected to fluid pressures greater than hydrostatic during injection, and hence the risk. The injection rate per well pattern and the aquifer utilization efficiency provide two independent constraints which are used to determine the operating point, given a set of values for the independent parameters H, P_i, P_p and P_b. The optimization scheme determines the operating points with the least cost, given the properties of the storage formation, the desired storage rate, the project life, and the range of plausible values for the independent parameters.

The solubility of CO_2 in brine in absolute terms is small, so it might be anticipated that the optimal design would call for the maximum achievable dissolution of CO_2. Counter-intuitively the scheme determines the optimum in the example presented here (base case, Table 3-1) to lie at a saturation pressure less than the maximum allowable. This is because a decrease in saturation pressure causes aquifer utilization efficiency to increase if the other independent parameters remain unchanged. Moreover, a decrease in saturation pressure increases the achievable injection rate per well (obtained by reducing

the pressure in extraction wells) if the aquifer utilization efficiency is kept the same. Greater utilization efficiency reduces area costs, and greater injection rates reduce well count and hence well costs. Hence the optimum occurs below the maximum saturation pressure.

Similar tradeoffs emerge for other independent parameters. For example, trying to achieve maximum aquifer utilization efficiency drives the bottomhole pressure of the production wells to increase. This in turn reduces the flowrate, so that more well pairs are required to achieve the same storage rate. Similarly, trying to increase the flowrate per well by allowing the producer bottomhole pressure to fall below saturation pressure leads to larger pore volume requirement. This is because the location of the contour of saturation pressure will move toward the injectors, reducing the aquifer utilization efficiency.

Less surprisingly the optimum appears to be pinned at the maximum injection pressure. This is because as injection pressure (P_i) decreases with fixed extraction well bottomhole pressure (P_p), the drawdown ($P_i - P_p$) decreases and aquifer utilization efficiency also decreases. Aquifer utilization efficiency decreases because the saturation pressure contour moves closer to line of injection wells as injection pressure decreases. Both these effects lead to higher costs, and for the range of parameters studied here, the increase cannot be offset by changing other independent parameters. Thus the optimum injection pressure will be the largest value allowed by restrictions on induced fracturing.

The design is also sensitive to the aquifer properties. An increase in permeability moves the optimum design point towards higher saturation pressures. This is because with increase in permeability, less well pairs are required. To dispose same amount of CO_2, higher aquifer utilization efficiency is required. With increase in permeability, required drawdown decreases at optimal design points and the higher the saturation

pressure the nearer the contour corresponding to that pressure approaches the extraction wells the higher the aquifer utilization efficiency. With increase in injection interval thickness, the optimum saturation pressure does not change. Increase in thickness leads to proportional increase in injection rate (q) per well while leading to decrease in total area required (A). Thus operating point remains invariant. An decrease in porosity moves the optimal design point towards higher saturation pressures. Thus is because change in porosity does not change injection rates. Decrease in porosity though leads to higher area requirement which is partially counterbalanced by increase in saturation pressure which cause increase in solubility. Similarly decrease in drawdown also leads to higher aquifer utilization efficiency. Salinity doesn't affect the location of optimal design point. Increase in salinity only causes decrease in solubility which causes proportional increase in total injection rate and total area required. This leads to over all higher costs but no change in design parameters.

The optimal design is sensitive to the cost parameters and depends on which cost parameter is dominating. With well costs dominating the optimum design point moves towards higher injector-injector spacing H and larger drawdown to enable higher injection rates. Dominant area costs drive the optimum design point towards higher saturation pressures and smaller drawdown which combine to yield higher aquifer utilization efficiency. Similarly dominant risk costs drive the optimal point towards the higher drawdown and higher injector-injector spacing. At higher drawdown the area under over pressure decreases which is where the design point moves when risk costs dominate.

Chapter 4: Time weighted storage capacity of structural traps

4.1 OVERVIEW

Sequestration of CO_2 in geological formations offers a technically feasible way to mitigate greenhouse emissions. Several investigations have tabulated the storage capacity for CO_2 in the regions around the world, and it is widely accepted that sufficient pore volume exists in deep subsurface formations to permit large-scale sequestration of anthropogenic CO_2. Almost all of these investigations correct the bulk pore volume available for storage efficiencies, which are approximations of volumetric sweep efficiency (areal, vertical and gravity override efficiencies) and displacement sweep efficiency. Meaningful mitigation of emissions will require annual storage rates of the order of Gt CO_2 within a few decades. Storage capacity estimates should therefore also incorporate the time required to place CO_2 into the volume.

To account for the above stated time constraint we introduce concept of time weighted storage capacity. We present an approach for weighting capacities in this fashion. We apply it to tabulated properties of 1200 North American oil reservoirs. The distribution of properties is presumed representative of brine-saturated structural traps – anticlines, dipping formations with a fault seal, stratigraphic – that would be preferred targets for CO_2 storage. Such traps are known to have held buoyant fluid phases (hydrocarbons) in place for geologic time. They are therefore expected to play an important role in ensuring the long term security of sequestered CO_2.

For the North American reservoirs, formation injectivity proves to be non-uniformly distributed with formation pore volume: the set of reservoirs with above average injectivity comprises only 10% of the total pore volume. This non-uniformity is a primary reason that time weighted storage capacity for a large set of structural traps is significantly less than ultimate volumetric capacity of those traps. Moreover we find that

the resource requirement (number of structural traps required to achieve a target storage rate) varies non-linearly with storage rate. Hence time-weighted capacities should be used to establish feasibility of large-scale sequestration in structural traps and to optimize deployment of sequestration projects in such traps.

4.2 Relation between Injectivity and Storage Capacity of Structural Traps

The storage capacity estimation for CO_2 sequestration in saline formations has been under study for a long time. The correct estimation of this capacity for saline aquifers is essential because the saline aquifers are viewed as the potential and almost infinite sinks for anthropogenic CO_2. The storage capacity for saline aquifers is based on storage efficiency factors stated in literature. These numbers yields a range of values of available storage capacity. The storage efficiency is the product of areal sweep efficiency (E_a), vertical sweep efficiency (E_i), displacement efficiency (E_d) and gravity override efficiency (E_g) due to density difference between resident brine and CO_2 (Figure 4-1).

$$\text{Volumetric Storage Efficiency} = E_a * E_i * E_d * E_g \qquad (4.1)$$

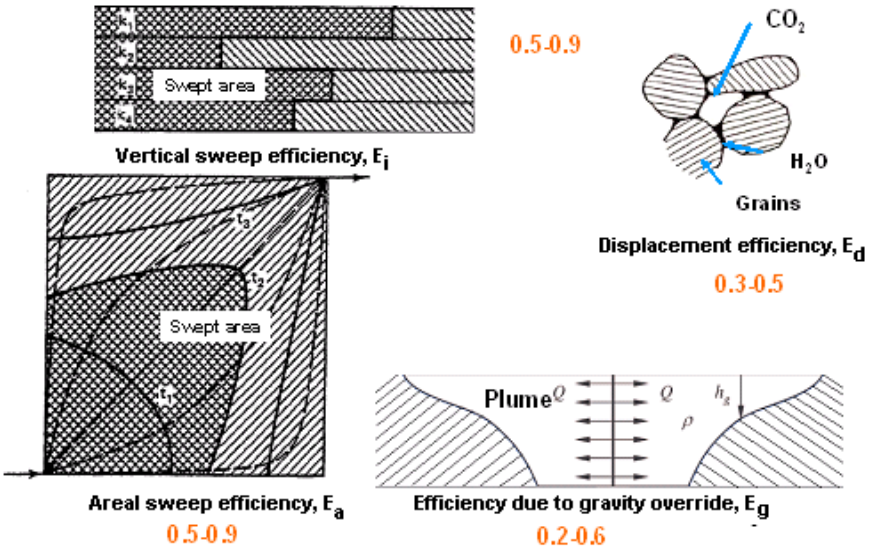

Figure 4-1 Pictorial representation of different factors affecting storage efficiency, with typical ranges of values shown.

For the standard approach to geological storage i.e. the bulk phase CO_2 injection, the storage capacity is usually defined at two stages. The first is at the end of injection period, and the second when CO_2 plume stops moving due to complete trapping (capillary and mineralization) post injection. Analogous to oil reservoirs where oil production depends on well productivity, CO_2 injection into an aquifer similarly depends on well injectivity. Injectivity is defined as the ratio of injection rate and the injection drawdown (injection pressure less average reservoir pressure). This is the text book definition of injectivity which according to Darcy's law is proportional to permeability, net injection interval, and mobility. In this chapter, injectivity is approximated as the product of permeability (k) and injection interval (h). We recognize that this is not the most appropriate way to define injectivity but it is done because effect of mobility is secondary to the product (kh).

Most capacity estimates do not consider the type of boundary to the aquifers under study or the possible use of extraction wells. More importantly, no capacity estimates have allowed for placing the required amount of CO_2 in the structures in a practical time frame, which is measured in decades. Here we describe a method that accounts for these practical constraints to yield a "time weighted storage capacity". In essence this modified capacity integrates the maximum injection rate into a structure with the volumetric storage capacity of the structure, Eq. 4.2. The method also yields a value for the time required to fill a structure, i.e. the time when the time-weighted capacity reaches the volumetric capacity.

$$\text{Time weighted storage capacity} = \frac{\text{Cumulative injected at any time}}{\text{Pore volume available}} \tag{4.2}$$

The injection rate is a function of time, formation properties and boundary conditions. The boundary conditions include maximum allowable injection pressure and

the nature of the storage formation (closed, infinite-acting, or constant far-field pressure). The time-weighted capacity approaches the volumetric storage capacity as time allowed for injection increases (see Figure 4-2). For sufficiently short injection times, time weighted storage capacity may be much less than the volumetric capacity.

We review the parameters which affect storage efficiency, and hence the storage capacity for the bulk phase CO_2 injection and then we describe our method to calculate injection rate for two sets of boundary conditions. We apply the injection rate calculation to a realistic distribution of petrophysical properties and sizes of storage structures, obtained from the Tertiary Oil Recovery Information System (TORIS) database consisting of 1200 North American oil reservoirs. We then make use of this calculation to calculate time weighted storage capacity making certain simplifying assumptions. All the calculations are performed for infinite acting boundary condition and for constant boundary conditions. These conditions correspond to sequestration without and with pressure relief wells, respectively. We then use these concepts to calculate the number of storage structures required to maintain a desired total storage rate.

From the database we observe that the injectivity (the product of average permeability and thickness (kh)) and pore volume (PV) statistic is highly skewed. This skewed statistic has a significant impact on the way the resources should be used for large-scale storage. Assuming this statistic is valid for structural traps in general, regardless of whether they currently contain hydrocarbon, we conclude that the time weighted storage capacity has a significant effect and should be incorporated for planning large-scale sequestration.

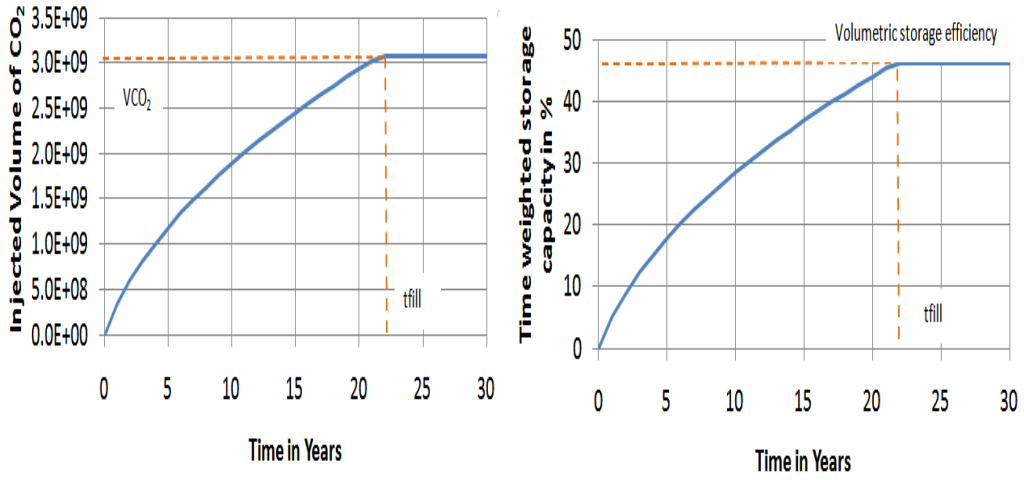

Figure 4-2 (Left) Cumulative injected CO_2 vs time for a single storage structure. The structure is filled (either to a spill point or to capillary seal limit) after 22 years; the amount of CO_2 stored at this time is the volumetric storage capacity V_{CO2} (Right) Dividing the cumulative volume by total pore volume of the structure yields the time weighted storage capacity. The time weighted storage capacity increases with time until it reaches the volumetric capacity of the structure.

4.3 Model Concepts

We are concerned with the time required to place CO_2 into a structural trap that currently contains only brine. For brevity we will refer to such formations as "structures."

4.3.1 Fill Time and Stored Volume

The time taken for CO_2 to fill a storage structure, denoted t_{fill}, is fundamental to this study. This parameter is a function of the size of the structure, the injectivity of the structure and the boundary type. A structure is deemed to be filled when CO_2 reaches the boundary of the structure that defines its volumetric capacity. The "stored volume" for the structure is the amount of CO_2 stored at t_{fill}, denoted VCO_2.

4.3.2 Resource Requirement

The cumulative number of storage formations needed over time to enable a target CO_2 storage rate is the resource requirement. The stored volume and fill time for all the structures in the database are combined to calculate resource requirement. The dependence on time-weighted storage capacity is strong because the flow rate is a non-linear function of time that can increase or decrease depending on boundary conditions. The resource requirement depends on fill time as new structures must be brought on to replace filled structures. In computing resource requirement we assume that no storage project causes pressure interference with any other project. We examine the implications of this assumption in section 4.11

4.3.3 Injectivity and Pore Volume

This study is a result of a very simple observation of the statistics for injectivity (*kh*) and pore volume (PV) for reservoirs in the database. The pore volume of a structure is taken to be the volume originally occupied by oil. This is reasonable assumption for CO_2 storage if oil filled each structure to a spill point or to the limit of a capillary seal. But even if this did not occur for every structure, the observed correlation between *kh* and PV is still likely to apply. The reservoirs with largest injectivity tend to have smallest volume, as shown in Figure 4-3. The non uniform distribution of injectivity leads to wide variations of time-weighted storage capacity and fill times for the structures in the database. This has a profound implication on the quality of the resource in terms of capacity and size (pore volume) and it can be used to infer time weighted capacity at database scale rather than individual structure scale to calculate resource utilization.

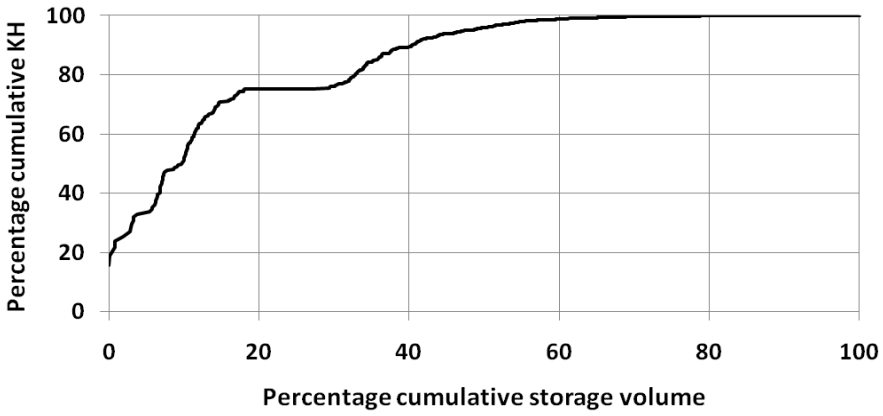

Figure 4-3 Sorting 1200 oil reservoirs in order of decreasing injectivity *kh*, then plotting the cumulative sorted injectivity vs cumulative storage volume PV shows a remarkably non-uniform distribution.

4.4 ASSUMPTIONS

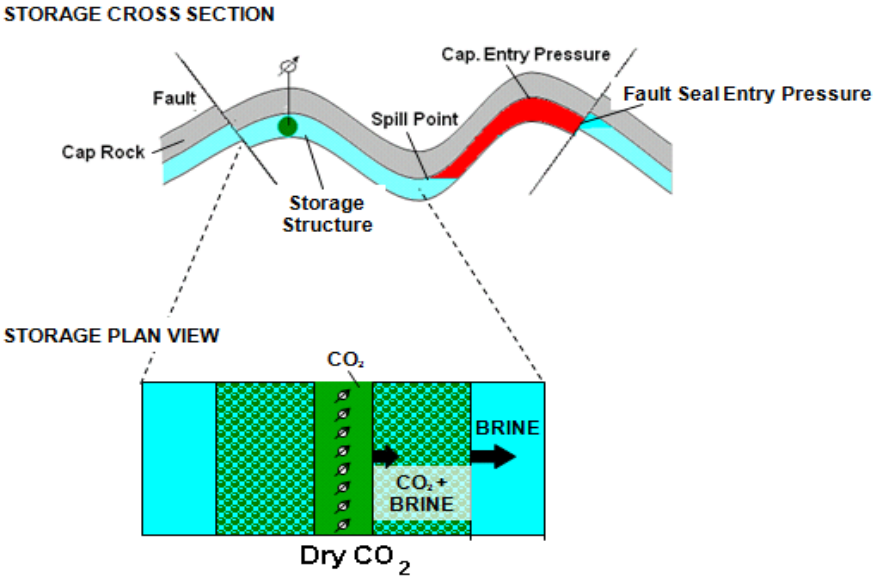

Figure 4-4 Schematic showing the basis behind the assumption of why the *kh* vs *PV* statistic obtained from the oil reservoirs database is applicable to brine filled storage structures along with the plan view of the idealized storage implementation

The *kh* vs PV statistic obtained from the database is assumed representative of all the CO_2 storage structures available. The pore volume data from the database is assumed representative of CO_2 storage structures that rely on structural trapping. This assumption is valid if it is assumed that amount of CO_2 stored will be limited in the storage structures by the top seal entry pressure, fault seal pressure or spill point (Figure 4-4) because these factors also govern the amount of oil trapped in any oil reservoir. This assumption is optimistic though, if the structural traps were filled with oil to the limit governed by top seal capillary entry pressure. If analogous brine-filled structures were filled with CO_2, the column height for CO_2 ($H_{CO2\text{-}brine}$) would usually be less than oil height ($H_{oil\text{-}brine}$) (see Figure 4-4 and 4-7). This is because CO_2 density at the temperature (T) and pressure (P) of the structure is usually less than oil density (Figure 4-5). Thus if capillary entry pressure at the top of the structure is the same for CO_2 as for oil i.e. assuming the same contact angle, then we have.

$$\frac{H_{\text{oil-brine}}}{H_{CO_2\text{-brine}}} = \frac{\sigma_{\text{oil-brine}}}{\sigma_{CO_2\text{-brine}}} * \frac{(\rho_{\text{brine}} - \rho_{CO_2})}{(\rho_{\text{brine}} - \rho_{\text{oil}})} \qquad (4.3)$$

where σ is the interfacial tension, ρ is the density and contact angle with brine is assumed same for oil and for CO_2.

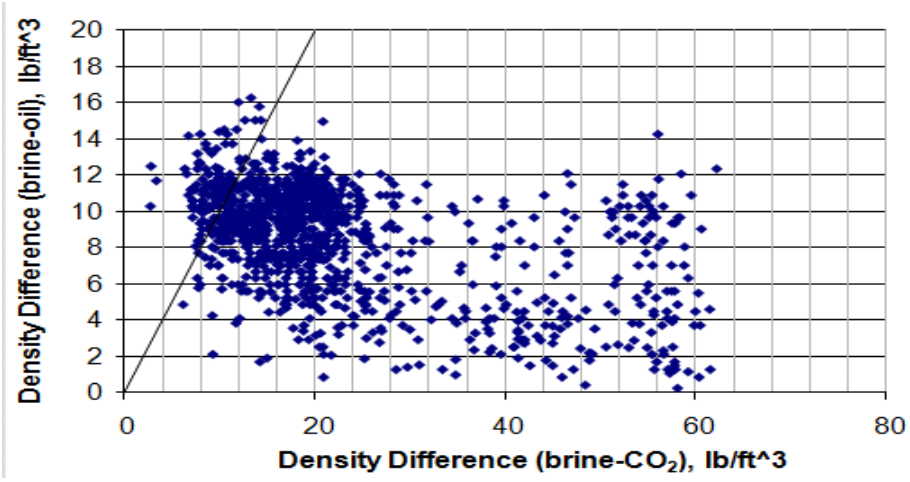

Figure 4-5 For most structures in the database the density of CO_2 at the pressure and temperature of each structure is less than the oil density

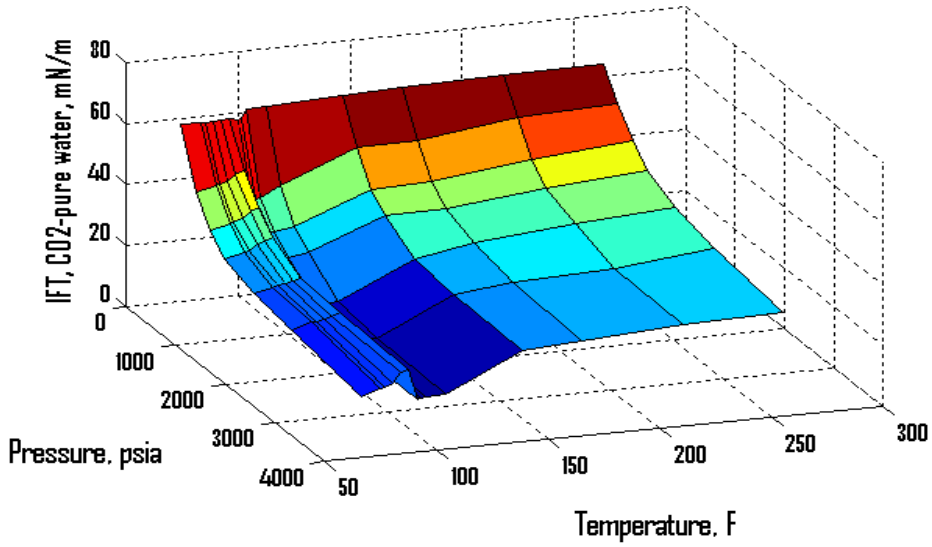

Figure 4-6 Interfacial tension for CO_2-pure water system varying with temperature and pressure (Bachu, 1996)

The prevailing temperature and pressure for each structure is estimated from its depth and typical gradients (0.43 psi/ft for pressure; 16 F/1000 ft for temperature). The density of CO_2 at the structure temperature and pressure was calculated using Peng-Robinson equation of state below critical conditions. For pure component the equation of

state parameters are well known and with pressure and temperature known, the molar volume could be calculated. This molar volume was converted into density of CO_2 at that pressure and temperature condition. The PR-EOS is given as:

$$P = \frac{RT}{V-b} - \frac{a(T)}{V(V+b)+b(V-b)} \tag{4.4}$$

where (b) depends on critical pressure and temperature of CO_2 and $a(T)$ depends on acentric factor, critical pressure and temperature of CO_2. The density of CO_2 in critical region was calculated by the online application provided by Lawrence Berkley National Labs called WebGasEOS.

The interfacial tension between CO_2-brine at the structure conditions was calculated by interpolation applied to the interfacial tension surface shown in Figure 4-6. The interfacial tension values in Figure 4-6 were experimentally measured by Bennion and Bachu (2009). The interfacial tension for oil-water system was assumed to be 30 mN/m because no value was available for each individual structure.

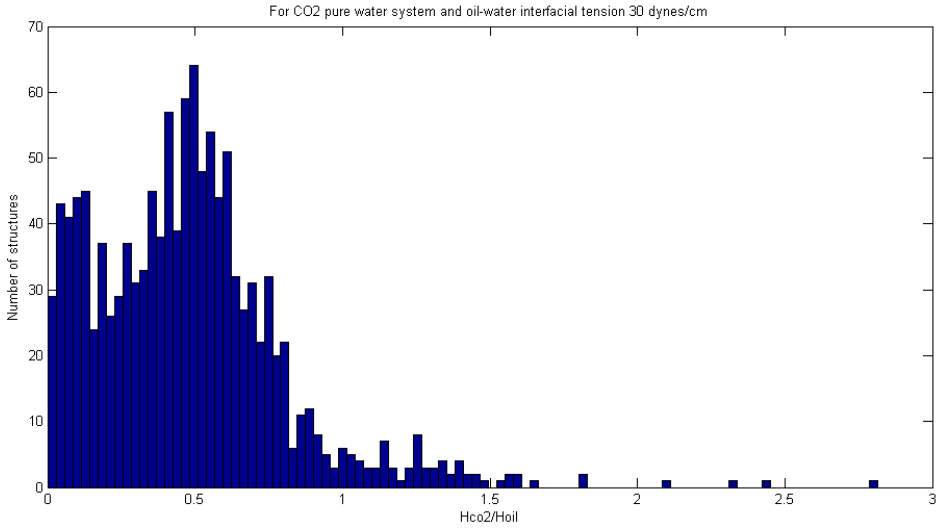

Figure 4-7 Supportable CO_2 column height is less than the oil column height for nearly all structures in the database.

Even if the oil reservoirs were filled to a column height such that the capillary pressure were half the seal entry pressure, the pore volumes would fairly represent available CO_2 storage volume because median for the relative column height lies near 0.5 (Figure 4-7).

The permeability distribution across the database follows log normal distribution (see Figure 4-8). Permeability is distributed log normally in nature which is a direct result of central limit theorem. Thus we expect permeability for storage structures to be distributed log normally. The range of permeability for the aquifers should be similar to what we find in the database (1 md to 10000 md) for the storage structures to be considered viable for storage.

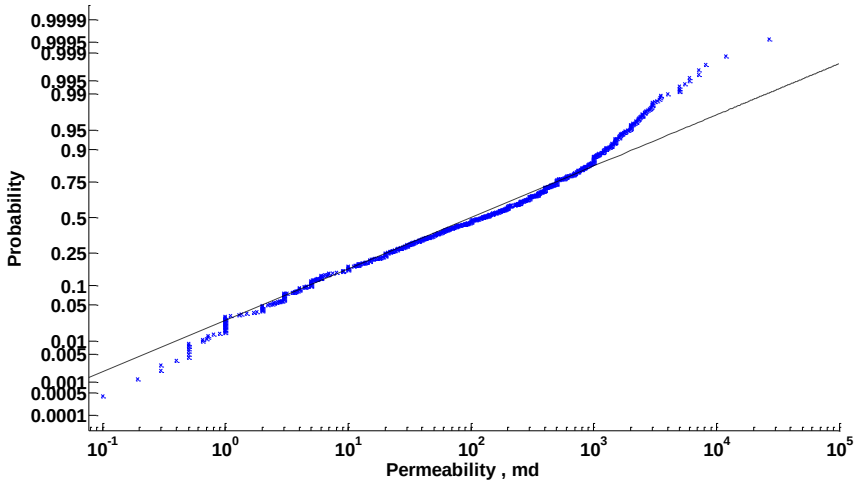

Figure 4-8 Probability plot shows that the permeability of structures in the database is distributed log normally

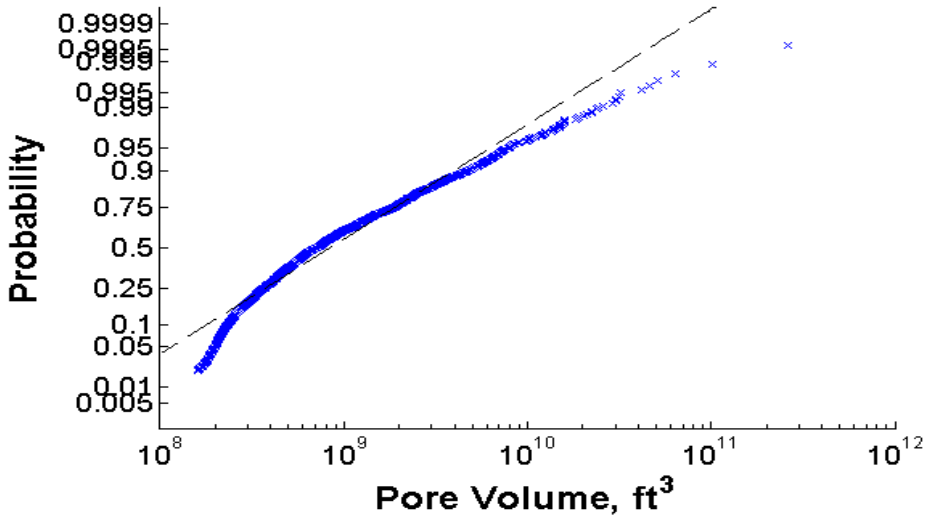

Figure 4-9 Probability plot shows that the pore volume of structures in the data base is very close to log normal distribution

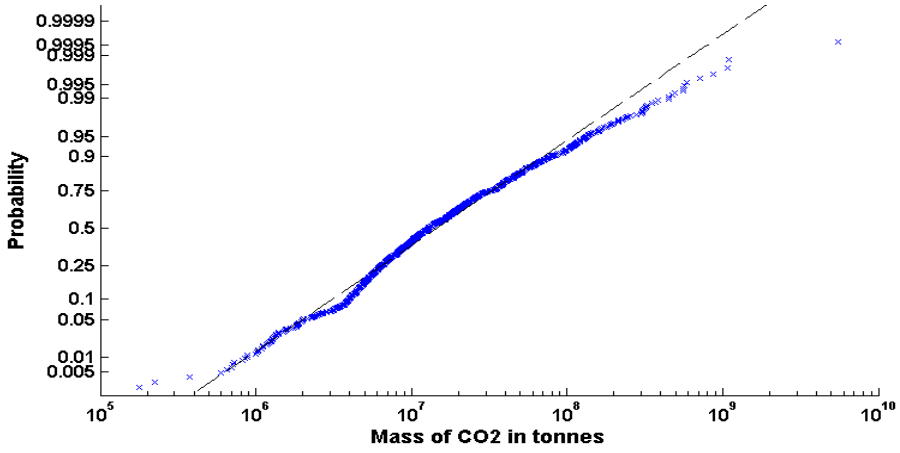

Figure 4-10 Mass of CO_2 that can be stored in each structure is lognormally distributed

The pore volume across the database is very close to log normal distribution (Figure 4-9). The pore volume is a product of areal extent, net thickness and the porosity and the probability distribution of pore volume is the joint distribution for all the three variables. The mass of CO_2 (product of PV and CO_2 density) that theoretically can be

stored in the structures is also log normally distributed (Figure 4-10). The mass of CO_2 has two independent factors, PV and density. According to the central limit theorem, the greater the number of independent multiplicative factors in a variable, the more closely the frequency distribution of that variable approaches log normal. This is evident in Figures 4-9 and 4-10.

4.5 METHODOLOGY FOR CALCULATION OF INJECTION RATES AND FILL TIMES FOR DIFFERENT BOUNDARY CONDITIONS

We assume that all structures are homogeneous. This means areal and vertical sweep efficiencies are unity. We also assume gravity sweep efficiency to be unity. In this respect our calculations of time-weighted storage capacity are optimistic. (We do account for displacement sweep efficiency.) These assumptions remove the effect of flowrate on gravity sweep efficiency, so it is possible to compare the impact of different boundary conditions on resource utilization. These assumptions make our results extremely optimistic but the correct results could be obtained if all the structures are characterised and the properties like porosity, permeability, thickness and areal extent are distributed spatially. The magnitude of the correction for vertical, areal and gravity sweep efficiencies is about 0.1 considering the ranges in Figure 4-1. Thus all VCO_2 reported in this section should be reduced by an order of magnitude.

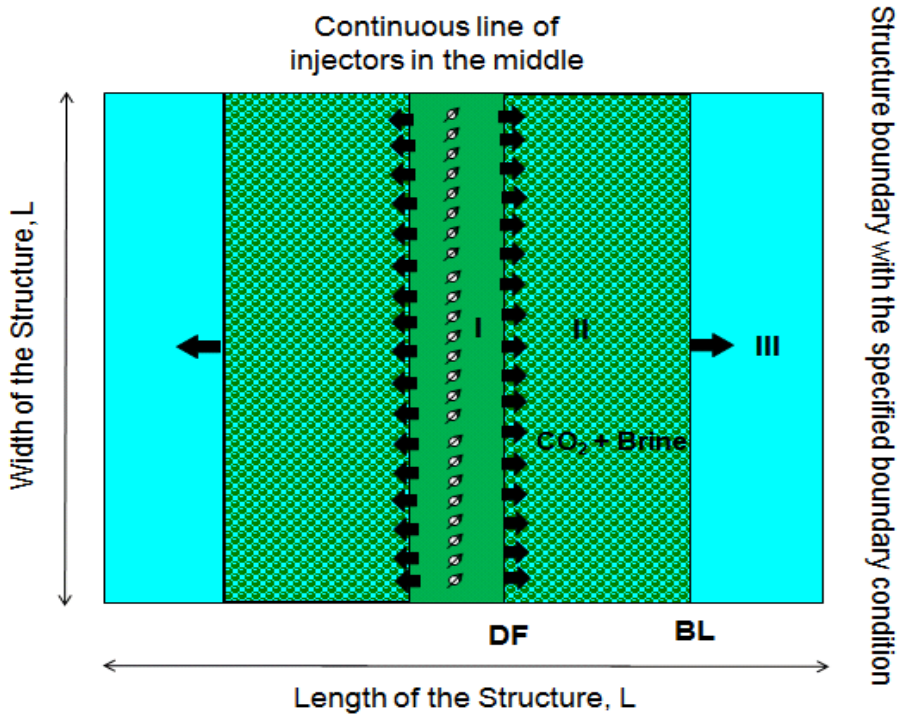

Figure 4-11 Each reservoir in the database is assigned a square shape having same area as the actual structure. A line of injectors is placed in the middle of the structure. CO_2 injection rates are computed using the three-region model (Burton et al., 2008) extended to linear horizontal flow and appropriate boundary condition (constant P or infinite-acting aquifer). The structure is deemed to be filled when the CO_2/brine displacement front BL reaches the boundary a distance $L/2$ from the injector line.

4.5.1 Required data and assumptions as shown in Figure 4-11:

- Each formation in the database is assumed to be a square having the same area as the actual structure.
- Boundary conditions and well placement
  - Infinite acting: Continuous line of injectors in the middle, open boundaries left and right, closed boundaries north and south.

- Constant pressure boundary: Continuous line of injectors in the middle and a continuous line of extractors at the left and right boundaries, closed boundaries north and south.

- The injected CO_2 is assumed to be incompressible at the temperature and pressure conditions of storage structure. This is a reasonable approximation for flowrate calculation because the CO_2 is in supercritical phase at usual storage conditions.
- For infinite acting boundary, we assume that the pressure disturbance reaches the defined boundary instantaneously. This increases the calculated fill time slightly but in comparison to total fill times this increase is very small. The pressure transients travel very fast in the linear flow system so this time to reach the boundary would be very small.
- All the calculations are done for a relative permeability curve of "Cooking Lake" carbonate sample (Bennion and Bachu, 2005).
- All the reservoirs in the database are assumed suitable structures for storage.

4.5.2 Semi analytical injection rate calculation

- Initial pressure distribution is assumed hydrostatic
- Constant injection pressure is applied at the line of injection wells, Figure 4-11. In calculations presented below we assume it to be 500 psi above hydrostatic. We assume this to be the limit specified by regulators so as not to compromise the integrity of the structure.
- Since a different mobility fluid is being injected into the structure, we make the injection rate calculations semi analytically.
- The injection rates at each time step are calculated using 3-region model for CO_2 injection developed by (Burton et al, 2008). This model is described in the

Appendix C. This model predicts three flow regions in the structure during injection.

  - Region I: Single phase CO_2 flow near injection line.
  - Region II: Two phase flow (simultaneous flow of brine and CO_2)
  - Region III: Single phase brine flow

- The sharp boundaries demarcating these regions are called:
  - Drying front (DF): separates Region I and Region II.
  - Buckley Leverret (BL) front: separates Region II and Region III.
- These fronts travel at specific velocities determined by application of fractional flow theory (Noh et. al. 2007, Burton et. al 2009). All the regions have flowing fluids of different mobilities.
- For constant pressure boundary:
  - For this case the boundary pressure and injection pressure are fixed and injection rate changes only due to the movement of DF and BL fronts and consequent change in effective mobility of the system
- For infinite acting boundary:
  - The pressure at the boundary is updated with time. The pressure at the boundary will increase because of net injection into the bounding aquifer. The pressure change at the boundary is calculated using the analytical aquifer model described for linear aquifers in Appendix C. In this case the injection rate changes with time due to change in effective mobility of the system as well as increase in the boundary pressure.
- The injection rate calculations end after 100 y or when CO_2 reaches the boundary, whichever comes first. If the latter, the BL front is located at the boundary of the structure, and the injection time when this occurs is called fill time (t_{fill}). The

amount of CO_2 injected after 100 y or when BL front reaches the boundary is the stored volume VCO_2.

4.6 Distribution of Fill Times and Volumetric Capacity

The fill time is directly proportional to the size of the structure and inversely proportional to the injectivity for any boundary condition. Because large injectivity (kh) tends to be associated with small pore volume, Figure 4-3, most of the structures have large fill times of at least a century, Figure 4-12. Fill time distribution is also a function of boundary type chosen. This is evident from the fill time histogram (Figure 4-12) where for constant pressure boundary, the number of structures with smaller fill times is considerably larger in comparison to infinite acting boundary condition. This difference is also evident on the right side of the histogram where for infinite acting boundary the number of structures with large fill times is almost twice that of constant pressure boundary. The reason for this variation in fill time distribution is that average reservoir pressure increases with injection when the system is infinite acting. Because the injection wells operate at fixed bottomhole pressure, this restricts the flow rates over time, whereas the constant pressure boundary eliminates pressure build up and thus permits continued injection at large rates.

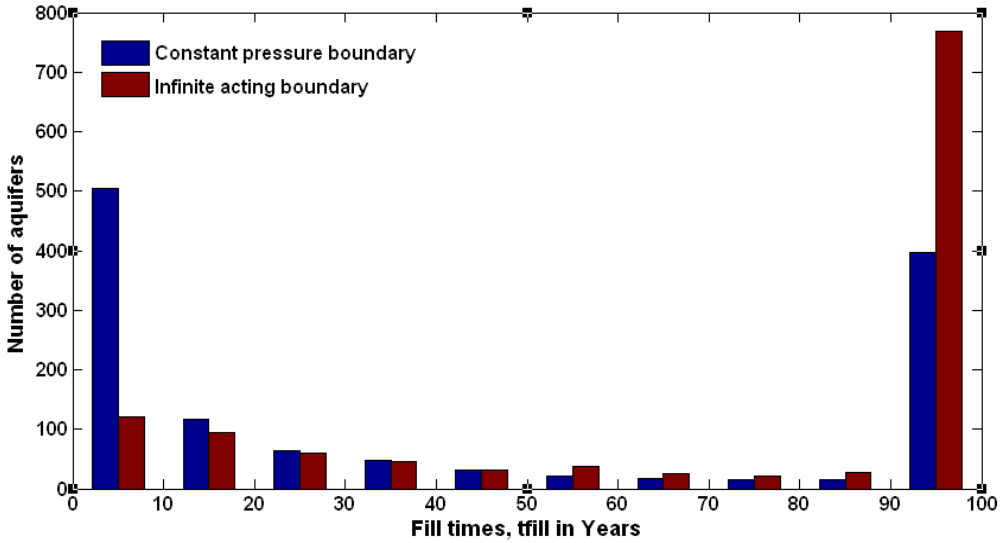

Figure 4-12 Distribution of t_{fill} across the database for different boundary conditions is bimodal and shows the impact of correlation between injectivity and pore volume, Figure 4-3.

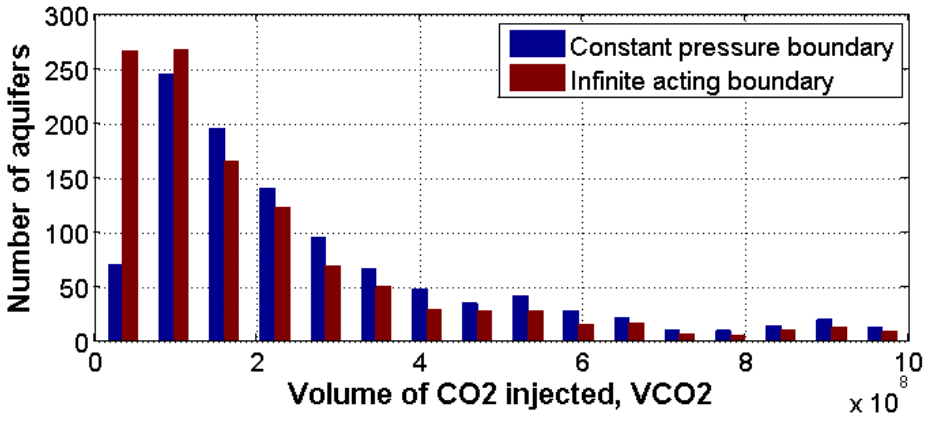

a)

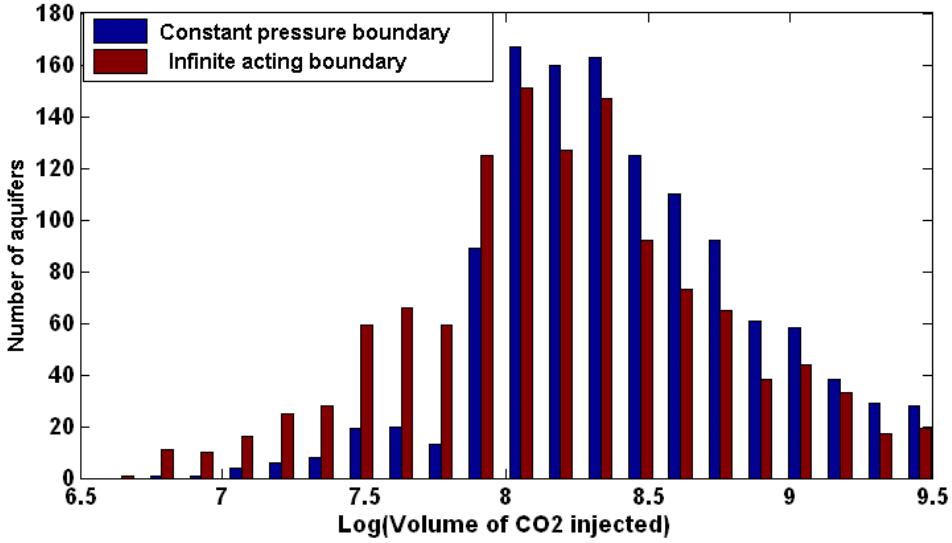

b)

Figure 4-13 Histogram showing the volume of CO_2 injected for different boundary conditions (a) linear scale, volume in units of ft^3; (b) log scale, which suggests a log normal distribution for infinite acting boundary conditions.

The companion histogram to the fill times of Figure 4-12 is Figure 4-13, which shows the distribution of VCO_2 for different boundary conditions. The amount of CO_2 that can be stored is directly proportional to the size of the storage aquifers. Pore volume histogram (Figure 4-14 and 4-15) shows most pore volumes are smaller than 10^9 ft^3, (see

also Figure 4-9). Thus the distribution of stored volumes in Figure 4-13 is skewed because the pore volume distribution is skewed. The values of VCO_2 are an order of magnitude smaller than the pore volumes but nevertheless are optimistic because the volumetric sweep is assumed unity for all the structures. The displacement efficiency on average was 0.56. Each structure is at different depth and thus viscosities of CO_2 and brine vary between structures. This leads to small variation in the displacement efficiency, even though the relative permeability curve is taken to be the same for all structures. (The relative permeability curves in reality would be different for different structures. This would lead to different displacement efficiency for different structures.)

If vertical, areal and gravity sweep efficiency were accounted for then the amount of CO_2 injected would be less by around a factor of 10 (considering the values in Figure 4-1) than shown here. Thus the time weighted capacities would also be less than shown here.

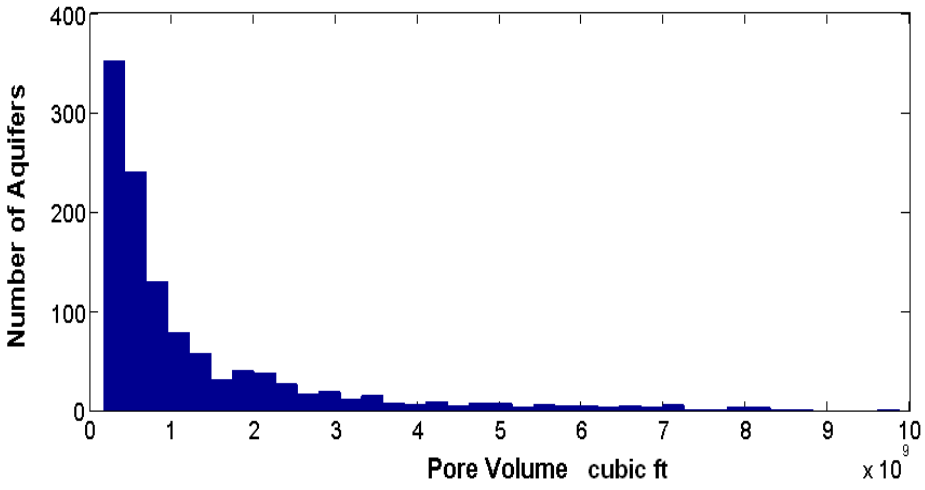

Figure 4-14 Pore volume distribution of structures in the database

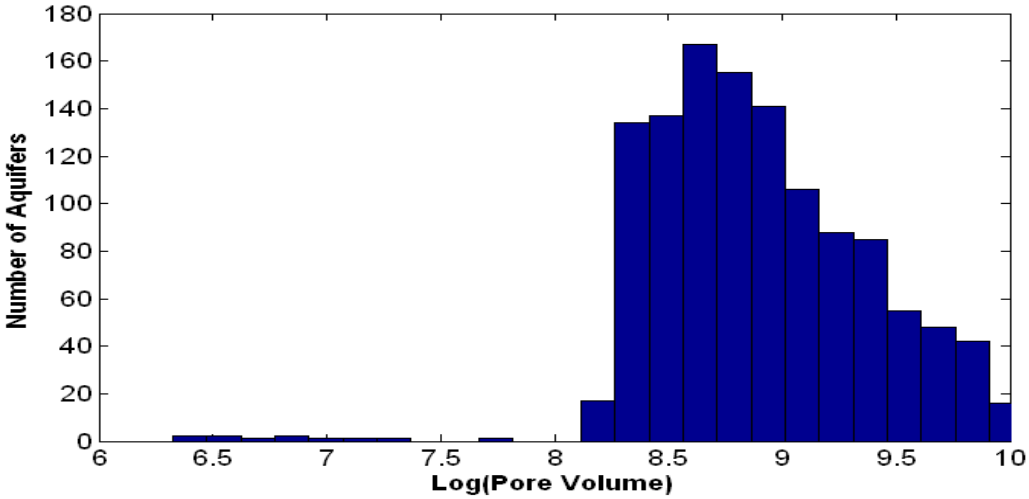

Figure 4-15 Distribution of pore volume in ft^3 of structures in the database (log scale)

The stored volume distribution differs for the two boundary conditions because we stop the injection rate calculation at 100 years. From the fill time distribution of Figure 4-12, more structures have fill times over 100 years for infinite acting boundary. Thus for infinite acting boundary condition, more structures lie in the range of small cumulative injected on the histogram.

The distribution of time weighted storage capacity for individual storage structures varies with time, as shown in Figure 4-16.

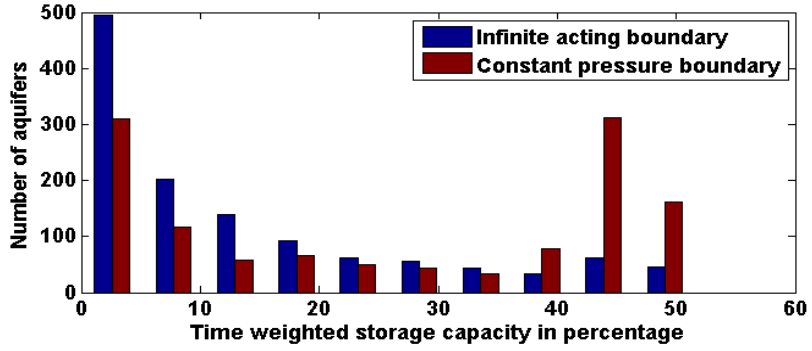

a)

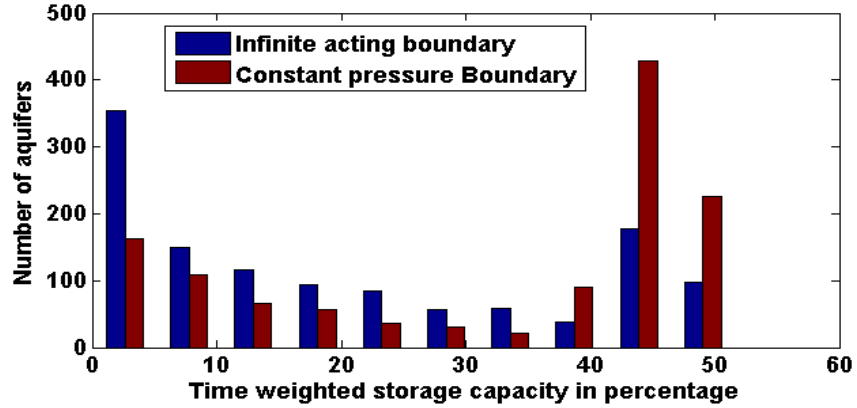

b)

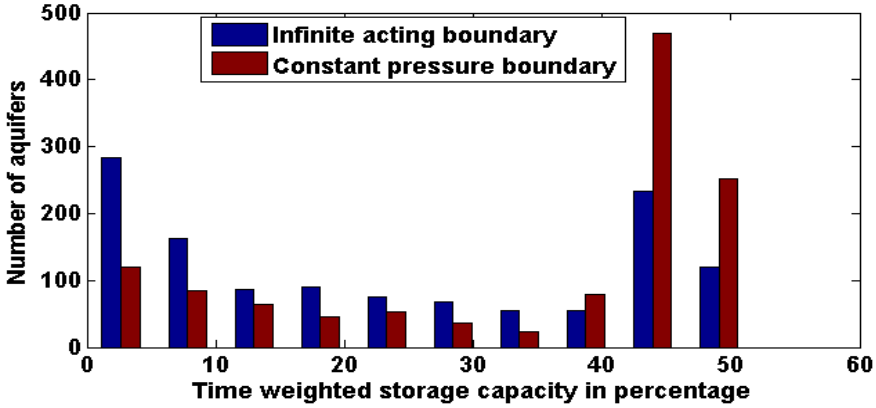

c)

Figure 4-16 Histograms showing the distribution of time weighted storage capacity for all the structures in the database for several injection times. a) t = 10 years b) t = 30 years and c) t = 50 years.

For infinite acting boundary a larger number of structures has time weighted capacities in the lower range of values in comparison to constant pressure boundary. This is the result of slower filling of structures with infinite acting boundary condition. With increase in time, structures start to get filled up and as time weighted capacity approaches volumetric capacity more structures appear on the right side of the histograms shown in Figure 4-16 for both boundary conditions.

The impact of skew in the distribution of *kh* vs PV (Figure 4-3) is manifested as non uniformities in fill times, Figure 4-12 and time weighted storage capacity Figure 4-16. The impact of boundary conditions is also pronounced. Considering these factors together on a broader scale, some interesting conclusions can be made which should prove very important to CO_2 sequestration on large scale. The next section describes the method adopted to further analyze the results and quantify resource requirement.

4.7 Resource Requirement Evaluation

The number of storage structures available to us is limited. The structures suitable for storage will be a fraction of these available storage structures. There will be incentive to make the most efficient use of the structures, as this could greatly reduce the cost of large-scale implementation of sequestration. The efficient use depends upon the following factors:

- Location of aquifers with respect to point sources such as power plants or infrastructure
- CO_2 target disposal rate to keep anthropogenic emissions under limit
- Injectivity distribution with pore volume
- Time weighted storage capacity for all the storage structures
- Boundary conditions

- Fill times
- Pore volume and storage efficiency of the storage structures

Location of storage structures with respect to CO_2 sources is a very important parameter governing optimal resource utilization. This parameter is under human control because depending on the availability of storage structure, infrastructure could be laid out to transport CO_2. Thus for this analyses we assume that this parameter does not affect the resource utilization. We assume that all the available storage structures would not be brought onstream at the same time. Simultaneously deployment would enable the largest possible sequestration rate, but it would also require the largest capital investment. As demonstrated below, this maximum sequestration rate could not be sustained in any case.

Based on the observations above, any scheme for resource utilization should account for the injectivity as well as the size of the structures. Here we use fill time to define the sequence in which structures are used to achieve a sustained total storage rate. An interesting limiting case is ascending fill time (structures with shortest fill time used first, even though they are usually smaller, because they tend to have larger injectivity). The other limiting case is descending fill time (longest lived, largest structures brought on first).

With these two limiting cases of utilization schemes, we can evaluate the resource usage for a fixed CO_2 disposal rate in terms of cumulative number of storage structure used with time and number of storage structures in operation at any given time. All 1200 structures in the TORIS database analyzed in previous sections are assumed available. The target disposal rate is an important parameter for resource estimation because the injection rate for individual structure is nonlinear with time due to multiphase flow effects, the assumption of constant injection pressure and boundary conditions. The cumulative CO_2 injected thus increases non-linearly with time for every individual

structure and so does time weighted storage capacity. The maximum number of available storage structures and the target disposal rate also governs the time scale for which the target sequestration rate could be maintained.

Figure 4-17 shows the storage structures usage (expressed as total number of structures in operation or already filled) with time for a target disposal rate of 0.1 $GtCO_2$/year CO_2. The usage is shown for two utilization schemes and two different boundary conditions.

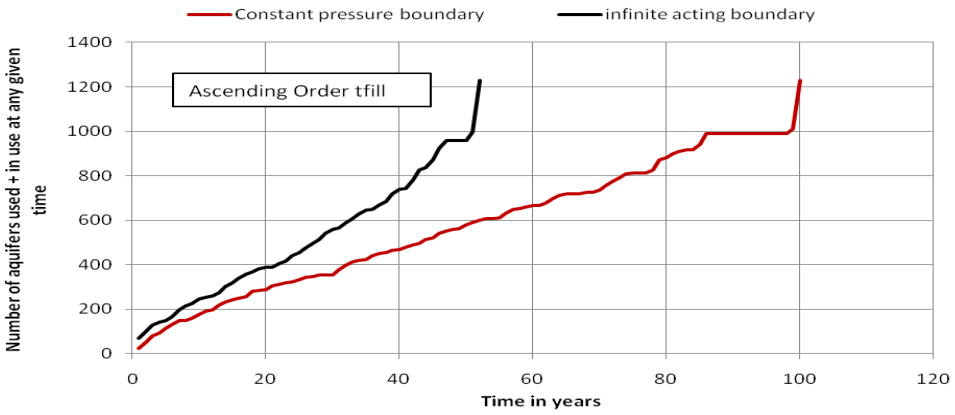

a)

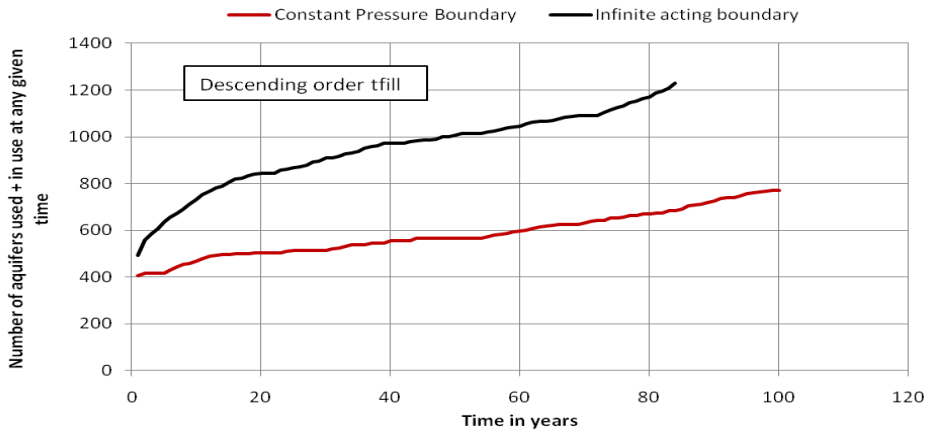

b)

Figure 4-17 Resource requirement for a storage rate of 0.1 Gt CO_2 per annum, assuming 1200 structures available with properties of those in the database. Cumulative number of structures used i.e. filled or being filled, is larger at all times for infinite acting boundary condition. Curves end at 100 years or when 0.1 Gt/y storage rate can no longer be maintained. (a) Structures with shortest fill times used first. (b) Structures with longest fill times used first. Descending order fill time scenario (b) requires more resource in the beginning but allows disposal rate to be maintained longer, ultimately using fewer resources than ascending fill time scenario.

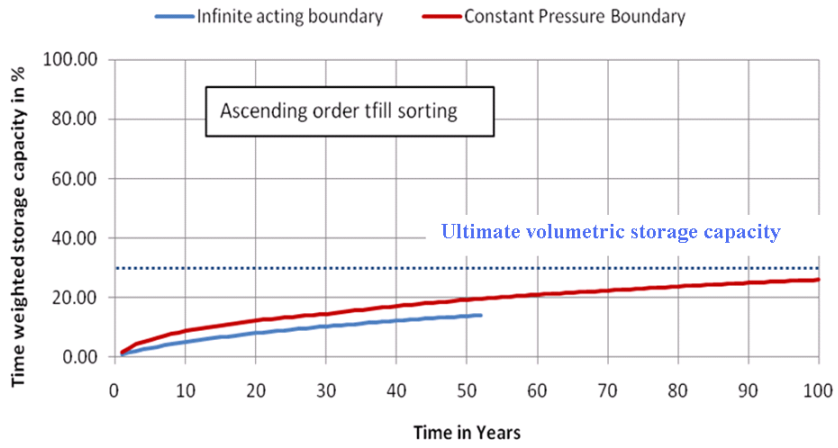

a)

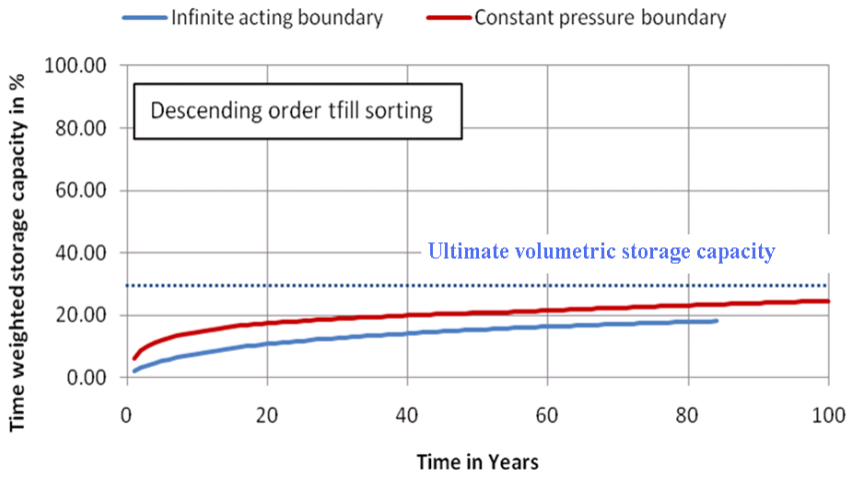

b)

Figure 4-18 The overall time weighted storage capacity for two utilization scenarios (ordered by fill time) and different boundary condition. (a) Time weighted capacity with shortest fill time structures used first (b) Time weighted capacity with longest fill time structures first. Curves end at 100 years or when 0.1 Gt/y storage rate can no longer be maintained.

We assume that 1200 brine-filled structures with properties identical to those in the oil reservoir database are available for storage. The resource usage curves in Figure 4-17 and 4-18 terminate at 100 y or when the target rate of 0.1 Gt/year could be maintained no longer. The target injection rate could be maintained for a longer period of time and

the number of storage structures used at early times is greater, if structures are used in descending order of fill time, Figure 4-17(b). On the other hand, for descending order fill time case, significantly more structures are needed at early time because they tend to have smaller injectivity. This is again a result of correlation between *kh* and PV. Though more structures must be brought on initially, the fact that the poorest injectivity structures tend to have large pore volumes means that new structures are not needed as rapidly as in the ascending order scenario. Thus injection could be maintained at a target rate for a longer period of time in descending fill time scenario. In all cases, when the target storage rate cannot be sustained, some of the resources are only partially filled. Thus the time weighted storage capacity is a fraction of the volumetric capacity, Figure 4-18. For ascending order scenario, infinite acting boundary condition gives half the volumetric capacity.

Both the scenarios have advantages and disadvantages. Consider the curves for infinite-acting boundary. In ascending order fill time scenario, the target rate could be maintained only for 50 y, while in descending order fill time scenario, many more structures are in operation from the beginning which implies higher operating costs. Thus an optimum resource usage scenario may lie between the two limiting cases. Resource usage is more efficient for constant pressure boundary condition: 100 y at the target rate for the ascending order fill time scenario, and half the resource utilization in the descending order scenario. This is the consequence of pressure relief which allows injection rates to stay large over time. Both the boundary conditions have their own limitations. Constant pressure boundary means relief wells which leads to brine disposal problem. Infinite acting boundary scenario leads to faster resource usage. The combined time weighted storage capacity for all the available structures and both utilization schemes is shown in Figure 4-19. The constant pressure boundary case required 100

years to approach volumetric capacity. The infinite acting boundary case only approaches 1/2 to 2/3 of the volumetric capacity depending on utilization scheme. The slope of the time weighted storage capacity for infinite acting case also shows that it would be a long time before the volumetric capacity curve could be reached at any overall storage rate (see Figure 4-17 and Figure 4-18). This is the direct result of the injection rate limitations due to pressure build up in the storage structures. It is critical to recall that these calculations assume 100 % sweep efficiency. For typical field sweep efficiencies, the values of VCO_2 would be ten times smaller. The fill times would also be smaller for heterogeneous formations so ultimate as well as time weighted storage efficiency would decrease by a factor of ten.

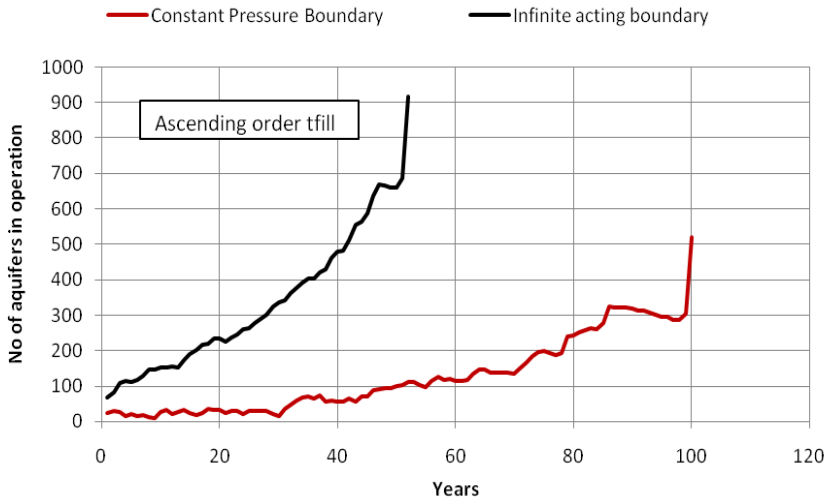

a)

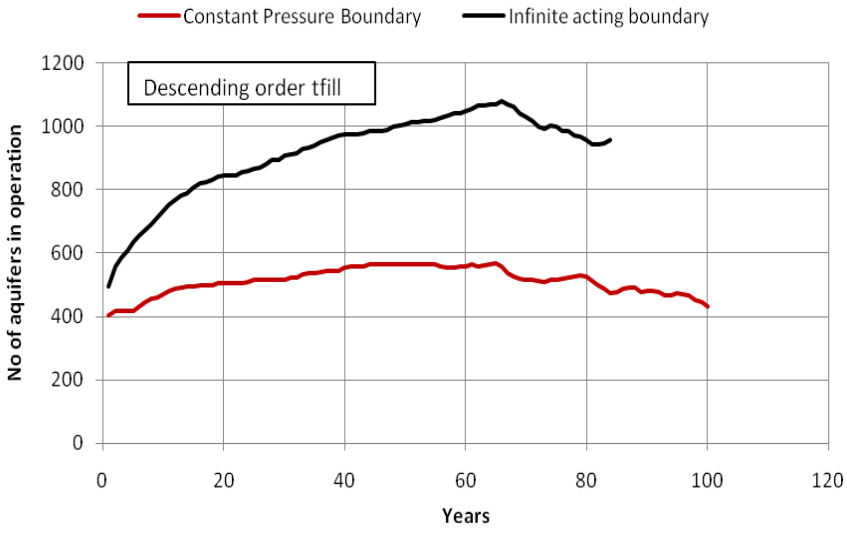

b)

Figure 4-19 The number of structures in operation (being filled) at any given time remains higher for descending order fill time scheme (b) in comparison to ascending order fill time scheme (a). The number of structures in operation for ascending order fill time scheme increases very quickly at large time because structures with largest injectivity have already been used and filled.

The information on number of structures in operation at any given time confirms that correlation between *kh* and PV plays a major role in determining the resource usage

(see Figures 4-19). The number of structures in operation at any time for ascending order fill time scheme is a lot less than the descending order fill time scheme. This is due to the fact that with ascending order fill time scheme structures with best injectivity tend to be brought on first. With time the numbers of structures in operation increases due to the worst ones in terms of injectivity are left for use. The numbers of structures in operation at any given time for constant pressure boundary are less than for infinite acting boundary due to the back pressure mentioned previously. The number of structures in operation also controls the operating cost. Thus operating costs would be higher for descending fill time scenario in comparison to ascending fill time scenario.

4.8 EFFECT OF DISPOSAL RATE ON RESOURCE UTILIZATION

Disposal rate affects the resource utilization in a non-linear fashion. Consider the time for which the target disposal rate could be maintained and the rate at which new structures are brought on to maintain the disposal rate, Figure 4-20.

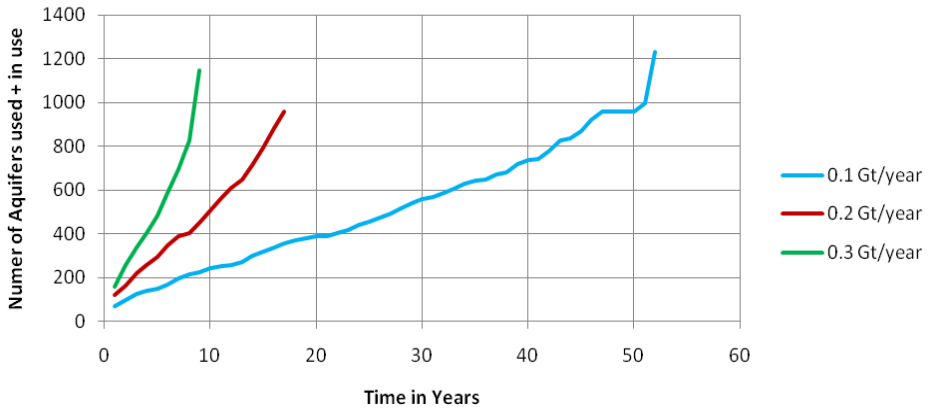

a)

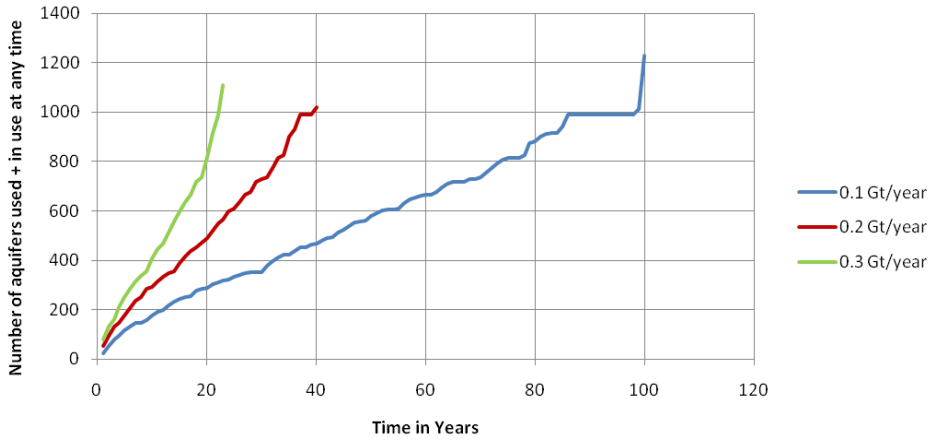

b)

Figure 4-20 Resource utilization is non-linear with disposal rate due to skewed distribution of fill times and injectivity for the storage structures. Results in the figure were obtained with the ascending order fill time scheme. Curves end when target rate cannot be maintained with available structures. (a) Infinite-acting aquifer boundary (b) Constant pressure boundary, note change in x-axis scale.

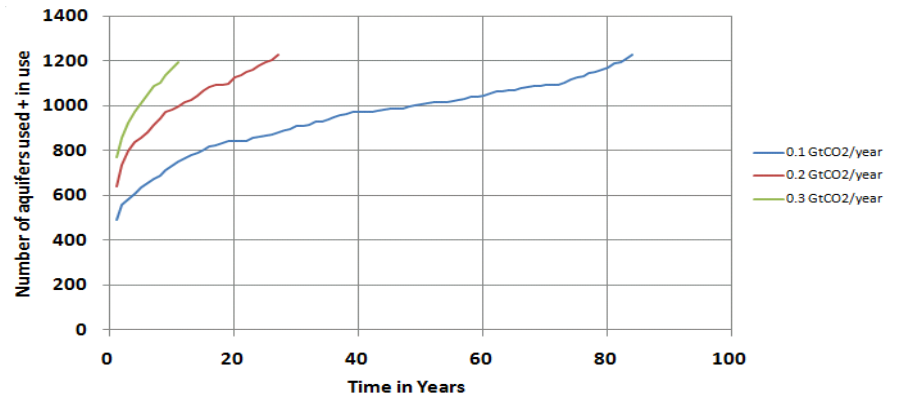

a)

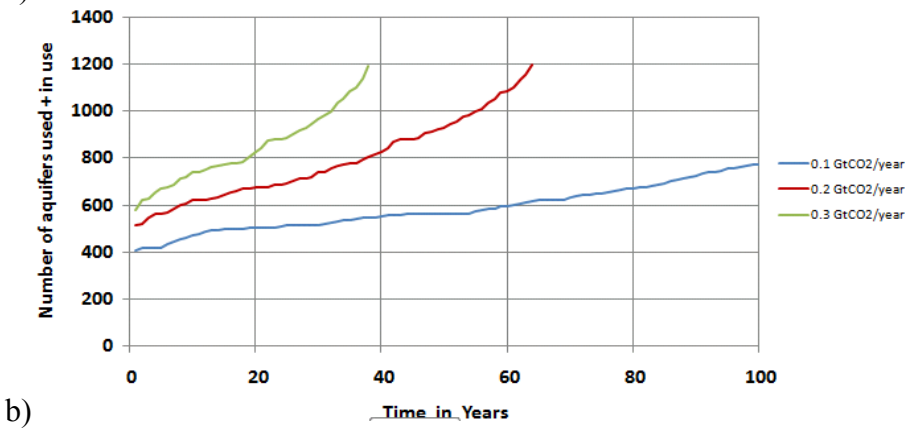

b)

Figure 4-21 Resource utilization for descending order fill time scheme. Curves end when target rate cannot be maintained with available structures. (a) Infinite acting boundary (b) Constant pressure boundary

In Figure 4-20, as the target disposal rate increases, the rate at which new structures must come into operation increases regardless of boundary condition. The resource utilization is calculated assuming structures are brought onstream in order of ascending fill time. The increase in slope of the resource utilization curve is greater than the increase in disposal rate, however. This is another manifestation of the correlation

between injectivity and pore volume. The number of structures required for a target disposal rate is obtained by summing up the injection rates into available structures until the total is equal to disposal rate. But because the distribution of injection rates into structures is skewed in the same way as the injectivity distribution, Figure 4-3, a disproportionately larger number of additional structures is needed for a given increase in disposal rate. These additional structures generally have smaller average injection rates because the structures are being used in ascending order of fill time. Thus the increment in number of structures required is more than the increment in the disposal rate.

When the structures are used in descending order of fill time (Figure 4-21), we see similar behavior as the ascending order case. This is true for infinite acting boundary condition because the flow rate into any structure decreases as the injection continues due to continued pressure elevation in the structure. Thus a greater number of structures is required to maintain the target disposal rate as storage continues. For constant pressure boundary case the rate at which new structures are needed increases only slightly faster than the increase in storage rate. This is because of the effect of relative permeability on injectivity. The Cooking Lake carbonate relative permeability curves are such that as CO_2 injection continues the mobility in the two phase flow region decreases (Burton and Kumar, 2008). This mobility reduction has a smaller effect on injection rate than the increase in reservoir pressure that happens for infinite-acting boundary. Thus its effect on resource utilization is qualitatively similar – it requires disproportionately more resources to accommodate continued storage as storage proceeds – but is not as dramatic. It happens for all the cases shown in Figures 4-20 and 4-21.

4.9 EFFECT OF HETEROGENEITY ON RESOURCE UTILIZATION:

The semi-analytical method used to calculate injection rates assumed that the flow was one dimensional and the storage structures were homogeneous. This method does not account for the heterogeneity in flow units of the storage structures. The effect of gravity was also neglected to make the calculations analytically tractable. To demonstrate the effect of heterogeneity on storage efficiency and fill times we develop a simple analytical approach based on Koval's theory (Koval, 1963)) and compare the results for storage efficiency and fill time calculations in a homogeneous system.

To investigate the effect of permeability heterogeneity, consider a simple 2-D system with permeability layers stacked from top to bottom in descending order of (k/ϕ). This ordering is convenient because the interstitial velocities are controlled by the ratio of permeability to porosity. This is shown below in Figure 4-22.

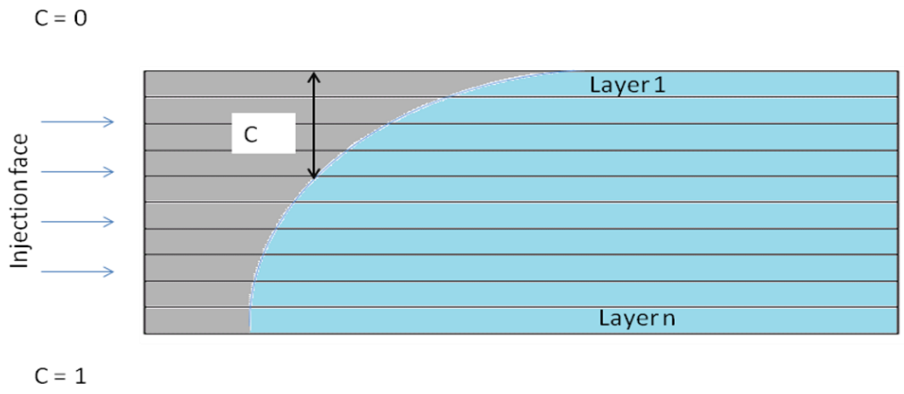

Figure 4-22 Depiction of the plume development in a heterogeneous aquifer during CO_2 injection from the left, with layer 1 being the highest permeability ($C = 0$) and layer n being the lowest permeability layer ($C = 1$)

Based on the definition of C (Eq. 4.6), $C = 0$ refers to the layer with the highest permeability and $C = 1$ refers to the layer with lowest permeability. This comes from

Koval theory which relates flow to the permeability heterogeneity explicitly. For a layered formation with *n* layers, we define

$$F_j = \frac{\sum_{i=1}^{j} k_i h_i}{\sum_{i=1}^{n} k_i h_i} \quad \text{for } 1<j<n \tag{4.5}$$

$$C_j = \frac{\sum_{i=1}^{j} \phi_i h_i}{\sum_{i=1}^{n} \phi_i h_i} \quad \text{for } 1<j<n \tag{4.6}$$

where F_j represents the fraction of j highest permeability layers of the total injectivity available and similarly C_j represents the fraction of pore volume of the j highest permeability layers. The relationship between F and C is used to define the degree of heterogeneity (for example Lorentz coefficient). Koval theory relates the flow part F_j to storage part C_j by a factor called heterogeneity factor H_k (Koval, 1963). It is as follows:

$$F_j = \frac{1}{1+\frac{1-C_j}{H_k . C_j}} \tag{4.7}$$

To define above problem, certain assumptions are made:

- Horizontal flow

- Vertical equilibrium (pressure gradient in the direction of flow is the same at every point along a vertical line anywhere)
- In grey zone of Figure 4-22, only CO_2 flows and in blue zone of Figure 4-22, only brine flows, i.e. sharp boundary between CO_2 and brine region.
- All the brine is displaced by injected CO_2 i.e. CO_2 saturation in grey zone and brine saturation in blue zone of Figure 4-22 are unity.
- Incompressible flow at the formation conditions.

With these assumptions in place, material balance on CO_2 (or brine) gives,

$$\frac{\mathbf{q}}{\mathbf{A}\bar{\phi}\mathbf{H_t}}\frac{\partial \mathbf{f}}{\partial \mathbf{x}} + \frac{\partial \mathbf{C}}{\partial \mathbf{t}} = \mathbf{0} \tag{4.8}$$

Here q is the total injection rate, A is the cross sectional area, $\Phi$is the average porosity and H_t is the total system thickness. f is the fraction of the total flow in the region marked as C on Figure 4-22, given by

$$\mathbf{f} = \frac{1}{1+\frac{1-\mathbf{C}}{\mathbf{M}.\mathbf{H_k}.\mathbf{C}}} \tag{4.9}$$

where M is the mobility ratio defined as

$$\mathbf{M} = \frac{\lambda_{\mathbf{CO_2}}}{\lambda_{\mathbf{H_2O}}} \tag{4.10}$$

where $\lambda$is the mobility k_r / μ of subscripted fluid.

The dimensionless form of equation 4-8 is:

$$\frac{\partial \mathbf{f}}{\partial \mathbf{x_D}} + \frac{\partial \mathbf{C}}{\partial \mathbf{t_D}} = 0 \tag{4.11}$$

where x_D is the dimensionless distance from injection face defined as (x/L) and t_D is the dimensionless time defined as the ratio of cumulative CO_2 injected per unit pore volume contained in the distance L from the injection face. According to method of characteristics, the velocity with which any vertical section with C fraction occupied by CO_2 would travel is given by,

$$\frac{\mathbf{x_D}}{\mathbf{t_D}} = \left.\frac{\partial \mathbf{f}}{\partial \mathbf{C}}\right|_{C} \tag{4.12}$$

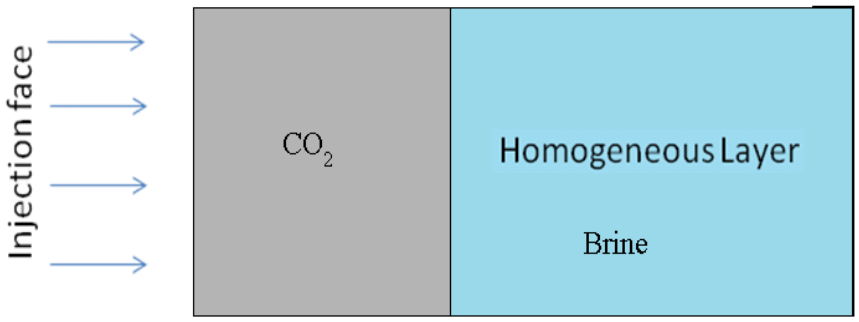

Figure 4-23 Depiction of brine displacement by CO_2 in a homogeneous one dimensional aquifer

Consider now injection into a homogeneous formation, as assumed in the computation of t_{fill} and V_{CO2} above. Suppose that the fraction of flowing brine and brine saturation in blue region are both unity. The corresponding values in grey region where CO_2 flows are zero for brine. Then all the brine is displaced by injected CO_2, and for the homogeneous aquifer the velocity with which the shock travels is unity:

$$\frac{\mathbf{x_D}}{\mathbf{t_D}} = 1 \tag{4.13}$$

The function *f* for heterogeneous case (equation 4-9) is easily differentiable, and an explicit expression for the velocity can be obtained:

Heterogeneous case

$$\mathbf{V_C} = \frac{\mathbf{M.H_k}}{1 + (\mathbf{M.H_k} - 1).\mathbf{C}^{\,2}} \tag{4.14}$$

Homogeneous case

$$\mathbf{V_C} = 1 \tag{4.15}$$

From Figure 4-22, we see that the leading tip of the plume is at *C*=0. The velocity of the tip thus follows from evaluating Eq. 4.14 at *C* = 0. The ratio of the plume tip velocity to the homogeneous displacement velocity is given by,

$$\frac{\mathbf{V_{tip,Heterogeneous}}}{\mathbf{V_{tip,Homogeneous}}} = \mathbf{M} * \mathbf{H_k} \tag{4.16}$$

The heterogeneity factor H_k is always greater than 1 (range of typical values is 2 to 5) and mobility ratio is also greater than one (CO_2 is less viscous and therefore more mobile than brine at typical aquifer storage conditions; typical ratio is 5). Thus this simple model yields tip velocity in the heterogeneous structure that is always larger than in the homogeneous structure by a factor of 10 to 20. In other words the CO_2 plume will always reach the boundary of a heterogeneous structure before it reaches the boundary of an otherwise equivalent homogeneous structure. Thus we can see that fill time, which is the time required for the plume tip to reach the specified boundary, for heterogeneous case is 10 to 20 times smaller than the homogeneous case. This heterogeneity factor also

stretches the plume and thus storage efficiency is also less by a factor of M*H_k for heterogeneous case compared to the homogeneous case.

This analysis is limited to modeling of vertical heterogeneity. If areal heterogeneity is accounted for then the storage capacity would further reduce by a factor of 1.2 to 2 (Figure 4-1). The fill times would also be reduced by another factor of 1.1 to 1.5.

Thus if heterogeneity was included in the analysis, the fill times would have been smaller for all the formations by a factor of 10 to 30, and storage efficiency would also be smaller by a factor of 10 to 30. Thus the resource utilization trends in Figures 4-20 and 4-21 are very optimistic. In reality resources requirement would be 10 to 20 times higher to maintain target injection rate for a given amount of time.

4.10 WHAT IF KH VS PV STATISTIC WAS VALID FOR 12000 STORAGE STRUCTURES INSTEAD OF 1200?

The resource evaluation scheme shown above was for the *kh* vs PV statistic we obtained from the TORIS database. There were 1200 storage structures in the database. The database spanned structures with permeability ranging from milli darcy to darcy formations. We have assumed earlier that the pore volumes are representative of actual saline-water-filled structural traps available for CO_2 storage. Assume that there are *n* storage structures available for storage (*n* greater than 1200) and the *kh* vs PV statistic of Figure 4-3 holds.

- If the target injection rate is also scaled up by a factor of *n*/1200, then resource utilization as a fraction of available structures shown in Figures 4-18 would not change at all. The total time for which target storage rate could be maintained would remain the same. The presumed persistence of the *kh* vs PV correlation

means the increase in storage rate could be proportionally distributed amongst the larger number of structures that have the same distribution of injectivity.

- If the target injection rate is not increased in proportion to the increase in number of available structures, then resource utilization changes as if the number of structures is fixed and the target rate changes. This effect was demonstrated in the section 4.8, where the impact of change in target sequestration rates and its impact on resource utilization was analyzed. For fixed resources smaller target disposal rates can be sustained longer the rate at which new structures have to come into operation is smaller.

4.11 PRESSURE LIMITATIONS DUE TO MULTIPLE PROJECTS

For large scale sequestration multiple projects will operate simultaneously. According to IPCC US alone would have to sequester 3 $GtCO_2$/year until cleaner technologies are proven for use. Development of cleaner fuels or energy sources is going to take time and sequestration can only work as an interim solution to the climate problem. Thus sequestration projects would have to be designed to last for a few decades.

The total area under influence for any sequestration project includes actual CO_2 footprint and the larger area where pressure has increased. Injection for a few decades in multiple projects without pressure relief wells may cause pressure interference. In this section some simple calculations are presented to estimate the percentage of total United States land area under pressure influence for injection of 3 $GtCO_2$/year for 50 years distributed across multiple projects. The objective is to determine how much area would be needed, if it were desired that individual storage projects do not interfere. In other words, is it possible to locate enough projects to eliminate substantial GHG emissions without causing injectivity reduction by pressure build up? As shown in Figure 4-19,

pressure build up within a storage structure reduces time weighted storage capacity. Pressure build up outside the structure will compound this problem.

For this calculation it is assumed that all the storage formations are in communication with each other which is to say that all the formations are infinite acting but none are close enough to cause pressure interference. It is also assumed that the injection is possible throughout the depth interval from 2500-10000 ft. With typical pressure and temperature gradients CO_2 would be in supercritical phase in the storage formations in this depth range The area under pressure influence is very large in comparison to the CO_2 footprint during injection because brine is nearly incompressible and pressure transients would travel very quickly through it.

Based on this assumption, the single-phase-flow well test equation determines the area under pressure influence at the end of 50 years. The distance travelled by the pressure transient does not depend on the injection rate. It only depends on the physical properties of the medium: porosity, permeability, total compressibility and the viscosity of the fluid through which the transients travel. Figure 4-24 shows the arrangement of several injection projects (small boxes) within regions (large boxes) whose pressure is influenced by the injection project. The goal is determine the size of the larger boxes so that the pressure elevation at the boundary of each box is small. The pressure elevation is taken to be small at a distance equal to the theoretical extent of the pressure transient. For a single structure the radius (r) of pressure influence would be given by:

$$r^2 = \frac{kt}{\phi \mu c_t} \tag{4.17}$$

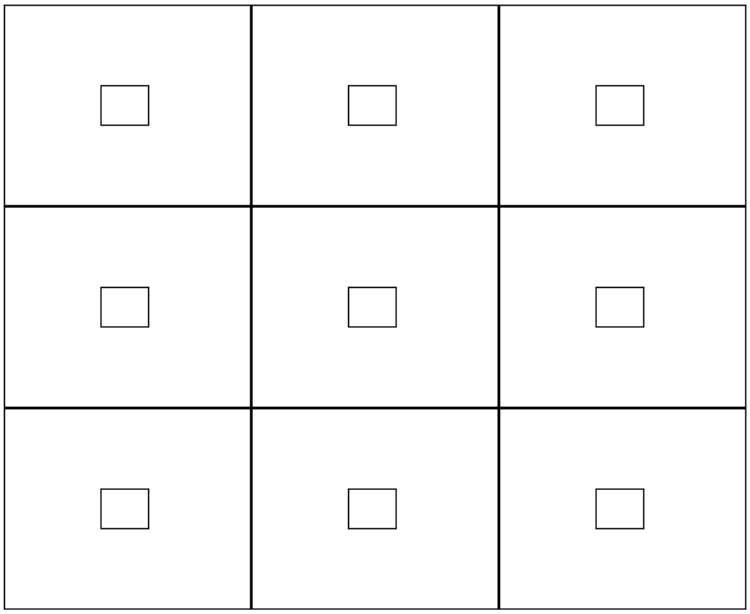

Figure 4-24 Small boxes represent storage structures with bigger boxes representing extent of pressure influence

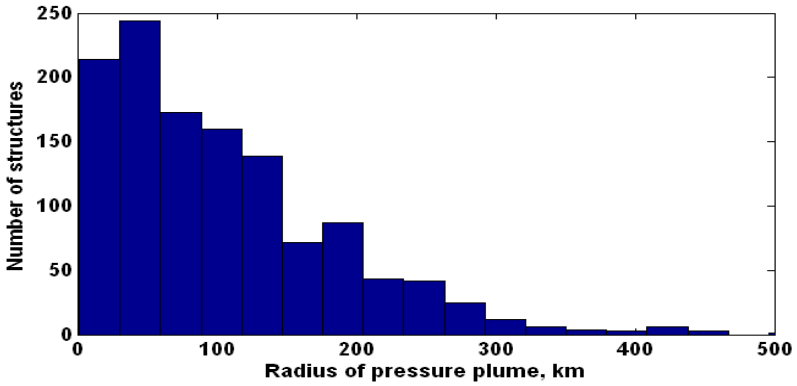

Figure 4-25 Distribution of radius of pressure plume in 50 years for all the structures in the database.

We assume the *kh* vs PV statistic from the TORIS database applies to the structures in Figure 4-24. Thus we can scale up resource utilization calculations for the ascending order fill time, infinite acting boundary case (Figure 4-18) to find the number

of structures required to enable injection of 3 $GtCO_2$/year for 50 years. As shown in Figure 4-18, the 0.1 Gt/year of CO_2 disposal rate was maintained for 50 years when 1200 structures were available. Thus storage of 3 $GtCO_2$/year for 50 years would require 1200 × 3 / 0.1 = 36000 structures.

Aquifer Properties	
Porosity, Φ	**0.2**
Compressibility, c_t	**1E-6 psi^{-1}**
Permeability, k	**100 md**
Viscosity, μ	**1 cp**

Table 4-1 Aquifer properties for calculation of radius of pressure influence

In 50 years the areal extent (r) of the pressure plume based on equation 4-19 and the values in Table 4-1 is 76 km. The median value of radius of pressure plume is also very close to this number from the distribution shown in Figure 4-25. If the compressibility is increased by a factor of 5 the radius (r) of pressure plume would be 30 km.

The average net thickness of structures from the database is 100 ft. In the depth range of 2500-10000 ft twenty five such layers were assumed to be available for storage. The overall net to gross ratio then becomes 0.33 which is a typical value for sedimentary basins.

No. of structures required for 50 year injection at 3 Gt/year	**36000**
Average structure thickness from the database	**100 ft**
No. of structures assumed present between 2500-10000 ft	**25**
Overall net to gross ratio	**0.33**
Radius of influence based on pressure plume (Eq. 4.19)	**76 km**
Percentage of US land area(10^7 km^2) under pressure influence	**336 %**

Table 4-2 Results for the percentage of US land area required for 3 $GtCO_2$/year injection rate for 50 years

For a radius of pressure influence of 76 km, a square array of storage projects will require an area of $4\times76\times76 = 23100$ km^2 surrounding each injection site. (A triangular array would require slightly less: $\pi \times 76^2 = 18000$ km^2.) With 25 structures stacked within the depth interval between 2500 ft and 10000 ft, a total of 36,000/25 = 1440 structures would be in pressure communication within each notional 300 ft thick layer of the Earth's crust. The area of elevated pressure surrounding these 1440 structures is 1440×23100 km^2 which is over 300% of the total US land area. If the radius of pressure influence is 30 km then about 50% of the US land area would be under pressure influence. Recall that the estimate of 36000 structures is derived from Figure 4-17, which was computed assuming that areal and vertical sweep efficiencies are 100%. Accounting for typical values means that perhaps ten times more structures (about 360000) would be necessary and the land area needed to avoid pressure interference between projects would be correspondingly ten times greater.

This calculation suggests that large-scale storage in structural traps in the US will require projects to be placed close enough together to cause pressure interference. Once

these pressure plumes interfere, the infinite acting boundary condition assumed for this calculation will no longer be applicable. Instead the system would behave more like a hydraulically closed system. In the limiting case the amount of storage available is determined by the compressibility of the system, which is small (~ 10^{-6} psi^{-1}) for aquifers. Clearly the rate at which CO_2 could be injected would be smaller than rates computed in analysis of Figure 4-17 and 4-18. Thus the time weighted storage capacity would be even smaller.

Because of political and economic challenges, allocating 10% of the US land area for the purpose of geologic sequestration would be a significant achievement. Thus it is instructive to consider what storage rate could be sustained if 10% of the US land area, or 10^6 km^2, were available for storage. Conservatively supposing a radius of pressure influence to be 30 km, the area of elevated pressure for a single structure would be equal to 4*30*30 = 3600 km^2. A total of $10^6/3600$ = 280 structures could be distributed areally within a single communicating layer of the subsurface without suffering pressure interference. Assuming 25 such layers exist within the 2500-10000 ft depth interval, a total of 280×25 = 7000 structures would be available. From Figure 4-17, the storage rate that could be sustained for 50 years would be approximately 0.5 $GtCO_2$/year. This again is based on the assumption that vertical and areal sweep efficiencies are 100%. If the typical efficiencies are used, then a storage rate perhaps ten times smaller, or 0.05 $GtCO_2$/y, would be sustainable.

These considerations indicate that pressure management, in particular avoiding the reduction in injection rate caused by buildup of pressure in the storage structure, is a major impediment to achieving large-scale emissions reductions (> 1 $GtCO_2$/y) in the US by means of geologic sequestration in brine filled structural traps. One solution to this could lie in surface dissolution (Chapter 3). Surface dissolution is a process whereby CO_2

is dissolved into the brine extracted from an aquifer and the CO_2 saturated brine is then re-injected back into the aquifer. The extraction wells confine the region of pressure influence to essentially the same region as that occupied by CO_2. This eliminates the very large inefficiency implicit in the project spacing of Figure 4-24.

Whereas the storage efficiency in the standard approach of injecting supercritical CO_2 includes the product of areal and vertical sweep efficiencies and displacement efficiency, the displacement of resident brine by CO_2 saturated brine occurs at unit mobility and within a single phase. Thus the corresponding efficiencies are much larger. If we assume a conservative value of 20% for the total volumetric efficiency of injecting CO_2-saturated brine and a typical value of CO_2 solubility of 0.01 mole fraction, we find that only 2% of US land area is required to store CO_2 at a target rate of 3 $GtCO_2$/year for 50 years.

4.12 CONCLUSIONS

Along with ultimate volumetric storage capacity for geological sequestration, the time required to access the available storage structures is important. Estimating the storage capacity accessible over a given interval of time requires accounting for injectivities of the storage structures. We present an approach for doing this, assuming that the statistics of relevant properties of 1200 North American oil reservoirs (obtained from the TORIS database) are the same as for the brine filled structural traps suitable for CO_2 storage. The injectivities (permeability-thickness product) and the pore volume (inferred from original oil in place) of these reservoirs are found to be strongly correlated, with large injectivity associated with small pore volume.

We propose an idealized model of CO_2 injection which places all structures on a common basis. The model yields the amount of CO_2 injected as a function of time (this

governs time weighted storage capacity), the time required to fill each structure and the volume of CO_2 in the structure when filled or after 100 years of injection, whichever comes first. The volumes thus calculated are an order of magnitude smaller than the pore volume. Consequently the time weighted storage capacity is about 20 to 30 % in 100 years.

The skewed distribution of fill times and stored volumes makes the problem of allocating structures to achieve a target overall rate of storage nontrivial. Organizing the available structures on basis of fill time strongly affects the capital costs schedule (number of structures brought on line per year) of large-scale sequestration. Using the structures with best injectivity first leads to faster resource usage but less resources are needed initially. On the other hand, using the structures with smallest injectivity first leads to more resource usage from the beginning but the resource usage rate (number of new structures needed per year) is less. For example, the 1200 structures described above would enable storage of 0.2 $GtCO_2/y$ for 20 to 40 years depending on utilization scheme; this corresponds to 10 to 30 % of the volumetric storage capacity of those structures.

If a fixed set of structures is available, the number of structures needed to satisfy an overall target storage rate increases non-linearly with storage rate. This is because the injection rate distribution is skewed in the similar manner as injectivity distribution. This leads to disproportionate increase in resource usage with increase in storage rate. The effect of boundary condition (infinite acting boundaries vs constant pressure boundaries) is that resource usage is faster for infinite acting boundaries in comparison to constant pressure boundary. This is a result of pressure build up in the formations during injection with infinite acting boundaries. Thus a fixed set of structures will be used more efficiently at smaller storage rates. An increase in number of available storage structures

enables a proportionate increase in sustainable sequestration rate, and the trend of resource utilization as a function of time would be the same.

The injected volumes computed above are optimistic because areal, vertical and gravity efficiencies are assumed to be 100%. If permeability heterogeneity in the form of vertical layering is considered, then the injected CO_2 reaches the structure boundary 10 to 20 times faster. Consequently the fill times are 10 to 20 times smaller, as is the cumulative amount of CO_2 injected in a structure. Considering this calculation and typical values of areal and gravity efficiencies indicates that the volume of CO_2 injected could be 20 to 30 times smaller for each structure. Thus resource utilization is even more challenging than described above, i.e. a factor of 20 more resources would be required for a target disposal rate.

For material disposal rates for the US, e.g. 3 $GtCO_2$/year, over a significant time scale, e.g. for 50 years, storage that avoids pressure interference between projects would require pore space beneath an area comparable to the entire US land area. The impracticality of implementing projects in that way indicates the importance of pressure relief wells for sequestration in structural traps. Installation of relief wells makes the resource utilization more efficient and reduces the areal extent of pressure interference by one to two orders of magnitude. Thus the land area needed for storing 3 $GtCO_2$/year for 50 y via surface dissolution is around 2%. This is significantly less than for standard approach of injecting supercritical CO_2. Introduced originally as a means of ensuring safe and permanent disposal of CO_2, surface dissolution may also prove to be useful for achieving material rates of GHG mitigation.

Chapter 5: Conclusions and Future Work

5.1 SURFACE DISSOLUTION

5.1.1 Conclusions

For surface dissolution sequestration approach, we have developed a pattern design methodology (placement of injection and extraction wells) based on total cost optimization. The pressure field established in the aquifer during injection plays a very important part in governing the safe disposal of CO_2. Injection rates and the pressure field in the aquifer are dependent on the pattern configuration (injector-injector spacing H and injector/extractor spacing D for line drive pattern), injection pressure (P_i) and extraction pressure (P_p). Based on the concentration of dissolved CO_2, the location of saturation pressure contour within the storage formation is identified. The injection front shape when it reaches the saturation pressure (P_b) contour defines the limiting (maximum) areal extent of CO_2-saturated brine and hence the aquifer utilization efficiency. The location of hydrostatic pressure contour defines the area subjected to fluid pressures greater than hydrostatic during injection, and hence the risk. The injection rate per well pattern and the aquifer utilization efficiency provide two independent constraints which are used to determine the operating point, given a set of values for the independent parameters H, P_i, P_p and P_b. The optimization scheme determines the operating points with the least cost, given the properties of the storage formation, the desired storage rate, the project life, and the range of plausible values for the independent parameters. Counter-intuitively the scheme determines the optimum in the example presented here to lie at a saturation pressure less than the maximum allowable. This is because decrease in saturation pressure increases aquifer utilization efficiency if everything else is kept the same. Similarly, decrease in saturation pressure increases the flow rate if the aquifer utilization

efficiency is kept the same. Less surprisingly the optimum exists at the maximum injection pressure. The impact of saturation pressure thus brings in complex interplay between all the independent parameters.

5.1.2 Future work

There are several issues with surface dissolution design modeling which could be improved upon by future research:

- The simple design procedure could be extended to include properties of a real aquifer like Mt. Simon formation or Frio formation and reservoir modeling could be done including heterogeneity using a reservoir simulator. Effect of dispersion could be studied better on the aquifer utilization efficiency.
- Phase behavior of flue gases from power plant with brine (without scrubbing CO_2) could be studied and the solubility trend could be studied with pressure and temperature. Then the same design analysis could be done and the sensitivity to various factors could be analyzed. Since presence of H_2S increases solubility of CO_2 in brine this could increase storage capacity and decrease in total costs.
- The hydrodynamic regime of the aquifer system may result in movement of CO_2 saturated brine post injection. This has to be studied in detail to understand the total area under influence as this might lead to higher area and monitoring costs.
- It was observed that the number of wells required for surface dissolution to work for a reasonably sized power plant would be in hundreds. This has a big social implication in terms of the surface area acquisition and the

public perception. Laying down surface facilities is going to be expensive so a proper design analysis for surface facilities has to be done in detail.

- The assumptions underlying the flow calculations assume an infinite series of alternating lines of injectors and extractors, so that the flow rate within the pattern element associated with a single injector/extractor pair is $q/2$, where q is the injection rate per well. If the number of well pairs is a few hundred or less, it is possible that the wells along the outer edge of the pattern may be a significant fraction of the total. Deviations from the assumed flow rate per pattern could then alter the optimum design. An extension of the method to account for this problem would be useful.
- The solubility if CO_2 in brine is very low in absolute terms. For a reasonably sized power plant, the size of mixing tanks and the number of stages of mixing required to achieve the target solubility would be crucial for practical implementation. Measurement of the time required for CO_2 to dissolve into brine would therefore be useful.
- Surface dissolution involves extraction, surface dissolution and reinjection of brine. The costs of surface equipment for dissolution could be substantial. If dissolution can be achieved downhole, it could reduce the costs dramatically. This might be called sub-surface dissolution.

5.2 TIME WEIGHTED STORAGE CAPACITY

5.2.1 Conclusions

Along with the ultimate volumetric storage capacity for geological sequestration, the time required to access the available storage structures is also important. Estimating the storage capacity accessible over a given interval of time requires accounting for

injectivities of the storage structures. We present an approach for doing this, assuming that the statistics of relevant properties of 1200 North American oil reservoirs are the same as for brine-filled structures suitable for CO_2 storage. The injectivities (permeability-thickness product) and pore volumes (inferred from original oil in place) of these reservoirs are strongly correlated, with large injectivity associated with small pore volume. We developed an idealized model of CO_2 injection which places all structures on a common basis, from which we compute the time required to fill each structure and the volume of CO_2 in the structure when filled or after 100 y injection, whichever comes first. The volumes thus calculated are an order of magnitude smaller than the pore volume, and this estimate is optimistic since volumetric storage efficiencies are assumed to be 100%. The skewed distribution of fill times and stored volumes makes the problem of allocating structures to achieve a target overall rate of storage nontrivial. We show that organizing the available structures on the basis of fill time strongly affects the capital costs (cumulative number of structures brought on line) of large-scale sequestration. If a fixed set of structures is available, the number of structures needed to satisfy an overall target storage rate increases nonlinearly with storage rate.

If storage projects are sited with sufficient separation to eliminate pressure interference, and if the projects are implemented in structural traps with the same statistics as those examined here, then achieving material rates of sequestration (of order 1 $GtCO_2/y$) would require more land area than is available in the US. One way to circumvent this limitation would be to apply the surface dissolution method described in Chapter 3, which greatly reduces the pressure plume of each project. Large storage rates could be sustained for 50 y using the pore volume beneath about 2% of the US land area. On the other hand, since the limitation derives from the presumption that CO_2 should be stored in structures suitable for holding a buoyant fluid (anticlines, fault-seals,

stratigraphic traps), another option would be to implement storage in structures that are not traps but are more widely available.

5.2.2 Future work

- We used the TORIS database for the resource evaluation. Our conclusions depend on the assumption that the *kh* vs PV statistic derived from the TORIS structures is applicable to all the saline aquifers that have structural traps (anticlines, fault seals, stratigraphic traps, etc.). This assumption needs to be validated. It could be improved upon by collecting the regional data from all the basins within the US and the correct resource estimation can be performed. This is a research in itself but this is being done for the storage formations in UK.
- It was assumed that the location of point sources of CO_2 with respect to the storage formations is not a factor in the resource usage analysis. For the optimal resource usage, however, the expense of setting up the infrastructure for CO_2 transport is likely to reduce the number of available target structures for any particular storage project. This is likely to lead to less efficient overall resource utilization, and this possibility should be investigated further.
- We assumed that the storage formations are homogeneous. A more accurate estimate of time weighted storage capacities and the subsequent evaluation of optimal resource utilization would require geological models that represent permeability heterogeneity and realistic boundary conditions.

- The model presented for the effect of layered heterogeneity upon storage efficiency can be improved by incorporating the effect of gravity and the effect of gravity number on the storage efficiency. If gravity forces are important then the effect of layer heterogeneity on storage efficiency would also depend on the order in which the permeable layers are stacked. The interaction between this ordering and gravity could be evaluated by certain simple improvements to the model described in the thesis. The post injection movement of the CO_2 plume could also be analyzed in the similar manner as was done by Juanes and MacMinn (2008) for the homogeneous saline formations.
- The interference of the pressure plumes while injecting in several different projects at the same time and its effect on storage capacity could be evaluated more accurately with proper reservoir modeling at the regional and basin scale throughout US.

Appendix A

A.1 Derivation of injectivity equation 3.1 for balanced line drive injection pattern

To derive injectivity equation for a line drive pattern of Fig. A-1, we assume that near the wells the flow regime is radial flow, and away from the wells a linear flow regime exists. Under these assumptions the radial flow would extend in a semi circle of radius (H/2) near wellbores (see Fig. A-1). In Fig. A-1 the imposed extent of the linear flow region overlaps with the radial flow region on both sides. The reason for the overlap lies in a geometric expression of conservation of total mass. We calculate the equivalent length (L) for linear flow from the balance equation

$$\frac{\pi H^2 \phi h \rho}{4} + LH\phi h\rho = HD\phi h\rho \tag{A.1}$$

where L is the length in which linear flow takes place. The first term on left hand side is mass of fluid in the radial flow regime, and the second term is the mass of fluid in the linear regime. The right hand side is the mass of fluid in the section of the line-drive pattern influenced by the injector/extractor pair. The equation is valid for incompressible fluids with displacement mobility ratio of unity, which is the case for the surface dissolution process. From equation A.1 we get,

$$L = D - \frac{\pi H}{4} \tag{A.2}$$

Radial flow near injectors and producers and linear flow away from them is the premise for the derivation of the injectivity equation. We define pressure between radial and linear flow boundary close to injector as P_{r1} and pressure between radial and linear flow boundary close to producer as P_{r2}. The flow takes place in series for successive regions of flow so we can write,

$$P_i - P_p = (P_i - P_{r1}) + (P_{r1} - P_{r2}) + (P_{r2} - P_p) \tag{A.3}$$

The flow between one injector/producer pair is half the injection rate for each injector. This knowledge will help us express the pressure difference terms in equation A.3 as function of flow rate, permeability and viscosity.

$$P_i - P_{r1} = \frac{q\mu}{2\pi kh} \ln\left(\frac{H}{2r_w}\right) \tag{A.4}$$

$$P_{r1} - P_{r2} = \frac{q\mu}{2kh} \frac{L}{H} \tag{A.5}$$

$$P_{r1} - P_p = \frac{q\mu}{2\pi kh} \ln\left(\frac{H}{2r_w}\right) \tag{A.6}$$

Wellbore radius of injectors and producers is assumed to be equal with zero skin. Substituting the values of the pressure differences in equation (A.3) yields

$$P_i - P_p = \frac{q\mu}{2kh}\left[\frac{2}{\pi} \ln\left(\frac{H}{2r_w}\right) + \frac{L}{H}\right] \tag{A.7}$$

We know L in terms of H and D from equation A.2. Substitution of L in the equation A.7 gives the final injectivity equation for line drive pattern.

$$P_i - P_p = \frac{q\mu}{2kh}\left[\frac{2}{\pi} \ln\left(\frac{H}{2r_w}\right) + \frac{D}{H} - \frac{\pi}{4}\right]$$

This is same as Eq. 3.1.

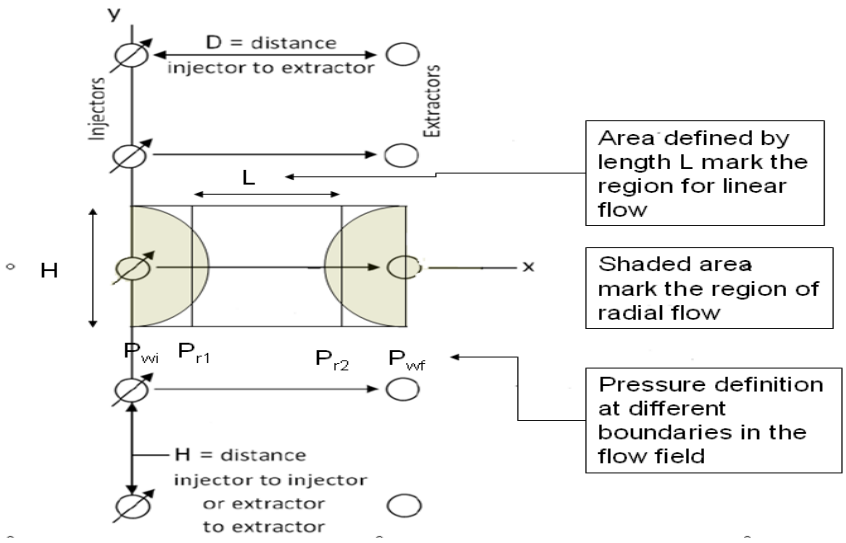

Fig. A-1 Schematic shows the basis behind derivation of injectivity equation. It also shows pressures at different flow regime boundaries. The overlap of linear flow region with radial flow region on both sides comes about because of mass balance, Eq A-2.

The method described above is limited to the cases where (*H/D*) is less equal to unity. At the values higher than 1 the regions of radial flow near the wells start to interact and thus the assumptions above are not valid. To avoid this we use a method based on streamlines which is outlined in Appendix B. Method outlined in Appendix B is used for flowrate calculations in Chapter 3.

Appendix B

B.1 METHOD SHOWING CALCULATION OF AQUIFER UTILIZATION EFFICIENCY AND TO RELATE DRAWDOWN WITH FLOWRATE

The line/sink source solution with application of Darcy's law and material balance for steady state flow in radial coordinates is given by:

$$\frac{\partial}{\partial r}\left(\frac{r\partial\Phi}{\partial r}\right)=0 \tag{B.1}$$

where r is the radius and Φ is the potential.

Assuming homogeneous medium, constant properties of the fluid and the rock, equation B.1 can be integrated to obtain,

$$\Phi = C_1 \ln(r) + C_2 \tag{B.2}$$

The constants in the above equation can be evaluated if the value of potential is known at two locations. Assume that the value of potential is known at r_1 and r_2 then,

$$C_1 = \frac{\Phi_2 - \Phi_1}{\ln\frac{r_2}{r_1}} \tag{B.3}$$

Application of Darcy's law in radial coordinates for steady state single-phase flow results in

$$\frac{\Phi_2 - \Phi_1}{\ln\frac{r_2}{r_1}} = \frac{-q\mu}{2\pi kh} \tag{B.4}$$

Thus from equations B.3 and B.4 we obtain value of C_1 which is then substituted in equation B.2 to yield,

$$\Phi = \frac{-q\mu}{2\pi kh}\ln(r) + C_2 \tag{B.5}$$

Changing the coordinates to Cartesian yields the following,

$$\Phi = \frac{-q\mu}{4\pi kh}\ln(x^2 + y^2) + C_2 \tag{B.6}$$

If the well is flowing at the rate of q and located at a location (x_o, y_o) then the above equation can be written

$$\Phi = \frac{-q\mu}{4\pi kh}\ln\ (x - x_0)^2 + (y - y_0)^2\ + C_2 \tag{B.7}$$

With the above equation defining potential (up to a constant C_2) at any location in the flow field, velocity of streamline in x-direction is derived from the following equation.

$$v_x = \frac{u_x}{\phi} = \frac{-k}{\mu\phi}\frac{\partial\Phi}{\partial x} \tag{B.8}$$

Because the Laplace equation is a linear partial differential equation, the principle of superposition for number of wells in the flow field located at (x_i, y_i) locations flowing at rate q_i applies to the solution:

$$\Phi = \frac{-\mu}{4\pi kh}\sum q_i \ln\ (x - x_i)^2 + (y - y_i)^2\ + C_2 \tag{B.9}$$

For line-drive configuration envisioned in Fig. 3-3, the injectors are separated from each other by a distance H, and a line of injectors is separated from a line of extractors by distance D. With all the wells flowing at a rate q (positive for injectors, negative for extractors), the potential equation for the field between line of injectors and a line of extractors is

$$\Phi = \Phi_1 + \Phi_2 \tag{B.10}$$

$$\Phi_1 = \frac{-q\mu}{4\pi kh}\left[\ln\ x^2 + y^2\ - \ln\ (x-D)^2 + y^2\ \right] + C_2 \tag{B.11}$$

$$\Phi_2 = \frac{-q\mu}{4\pi kh}\left[\sum_{i=1}^{n} \ln\ x^2 + (y-iH)^2\ - \ln\ (x-D)^2 + (y-iH)^2\ + \ln\ x^2 + (y+iH)^2\ - \ln\ (x-D)^2 + (y+iH)^2\ \right] \tag{B.12}$$

where *n* is the total number of injector-extractor pairs influencing the flow field.

The potential in a horizontal aquifer is equal to the pressure. Thus the potential gradient is shown below by Eq. B.13 could be used to get the value of potential at each point along the line joining injector and extractor. With boundary conditions known i.e. bottomhole pressures at injectors and extractors, the flowrate could then be related to the drawdown by Eq. B.16

$$\frac{\partial \Phi}{\partial x} = \frac{\partial \Phi_1}{\partial x} + \frac{\partial \Phi_2}{\partial x} \tag{B.13}$$

$$\frac{\partial \Phi_1}{\partial x} = \frac{-q\mu}{4\pi kh}\left[\frac{2x}{x^2 + y^2} - \frac{2(x-D)}{(x-D)^2 + y^2}\right]$$

$$\frac{\partial \Phi_2}{\partial x} = \frac{-q\mu}{4\pi kh}\left[\sum_{i=1}^{n}\left(\frac{2x}{x^2 + (y-iH)^2} - \frac{2(x-D)}{(x-D)^2 + (y-iH)^2} + \frac{2x}{x^2 + (y+iH)^2} - \frac{2(x-D)}{(x-D)^2 + (y+iH)^2}\right)\right] \tag{B.14}$$

(B.15)

$$\Phi_{\mathbf{i}} - \Phi_{\mathbf{p}} = \int_{\mathbf{x}=0}^{\mathbf{x}=\mathbf{D}} \frac{\partial \Phi}{\partial \mathbf{x}} \mathbf{dx} \tag{B.16}$$

A streamline is defined as the path traced by the fluid particle in a flow field. In a line drive pattern a fluid particle traveling along the line joining injector and producer has the least distance to cover to reach the producer. This particle has no velocity component in a direction perpendicular to this line joining injector and producer. All the other fluid particles leaving injectors at other angles have to travel more distance and have velocity component in the perpendicular direction. This causes them to cover less distance in x direction per unit time. Thus the fastest streamline travels along the line joining injectors and producers.

Using the equation B.8 and B.13 the velocity of the fastest streamline is calculated. This velocity then gives the time required for fluid particle to reach a distance x from injector as,

$$t = \int_0^x \frac{\partial x}{v_x(x)} \tag{B.17}$$

For a streamline traveling along $y = 0$, the time and distance can be written in a dimensionless form

$$td = \frac{qt}{2HDh\phi} = \text{dimensionless time} \tag{B.18}$$

$$X_d = \frac{x}{D} = \text{dimensionless distance from the injector} \tag{B.19}$$

The aquifer utilization efficiency when the CO_2 saturated brine has reached a particular distance from the line of injection wells is the dimensionless time at that stage of injection.

The saturation pressure would exist between injector at $x = 0$ and extractor at $x = D$. The boundary conditions are also known i.e. $\Phi = P_i$ at $x = 0$. The potential gradient Eq B.20 can be solved for x if pressure $\Phi = P_b$.

$$\Phi_{\mathbf{x}} = \int_{\mathbf{x}=0}^{\mathbf{x}} \frac{\partial \Phi}{\partial \mathbf{x}} \mathbf{dx} + \Phi_{\mathbf{i}} \tag{B.20}$$

Then aquifer utilization efficiency follows by setting x to the value obtained from above in Eq. B.17 to find t, and the E_a is the value of t_D from substituting t into Eq. B.18.

Appendix C

C.1 3-REGION INJECTIVITY MODEL FLOW CO_2 FLOW IN LINEAR AQUIFERS

Injection of CO_2 into a saline aquifer creates three flow regions. Region I is close to injection well where continual injection of CO_2 vaporizes all the brine. The mass transfer dries this region and thus only CO_2 flows in this region. In Region II, which is downstream of Region I, CO_2 and brine flow simultaneously. In Region III which is farthest from the injector, only brine flows. The front separating Regions I and II is called drying front (DF), and the front separating Regions II and III is called Buckley Leverett front (BL). Application of fractional flow theory and mass balance on CO_2 determines the velocities of these fronts. The dimensionless form of these velocities in linear flow is defined as:

$$\frac{\mathbf{x_D}}{\mathbf{t_D}} = \mathbf{V_{D,dry}} = \frac{\mathbf{f_{g,dry}} - \mathbf{D_{BL\rightarrow dry}}}{\mathbf{S_{g,dry}} - \mathbf{D_{BL\rightarrow dry}}} = \left.\frac{\partial \mathbf{f_g}}{\partial \mathbf{S_g}}\right|_{\mathbf{S_{g,dry}}} \tag{C.1}$$

$$\frac{\mathbf{x_D}}{\mathbf{t_D}} = \mathbf{V_{D,BL}} = \frac{\mathbf{f_{g,BL}} - \mathbf{D_{brine\rightarrow BL}}}{\mathbf{S_{g,BL}} - \mathbf{D_{brine\rightarrow BL}}} = \left.\frac{\partial \mathbf{f_g}}{\partial \mathbf{S_g}}\right|_{\mathbf{S_{g,BL}}} \tag{C.2}$$

where $f_{g,dry}$ is the fractional flow just downstream of the drying front and $f_{g,BL}$ is the fractional flow just upstream of the BL front (Burton et al, 2008). Similarly, $S_{g,dry}$ is the gas saturation just downstream of the drying front and $S_{g,BL}$ is the gas saturation just upstream of the BL front, cf Fig. C-1 Since it is also assumed that the mass transfer between CO_2 and brine does not change the flow properties of CO_2 and brine, these velocities would be equal to the tangent to the CO_2-brine fractional flow curve according to fractional flow theory. The construction of the relevant tangents is shown in the Figure

C-1. The *D* terms in the above equations are dependent on the CO_2 solubility in the brine and brine vaporization into CO_2 phase, Eq. C-3 and C-4.

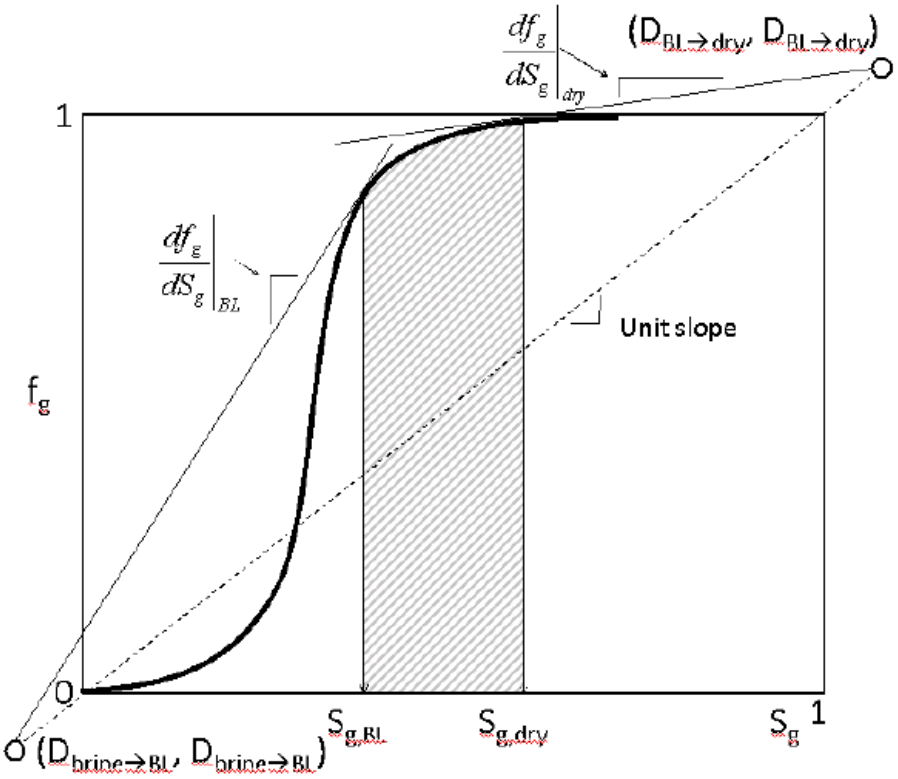

Figure C-1 This fractional flow curve is evaluated for the velocities of drying front and Buckley-Leverett front by drawing the tangents from the *D* terms shown to account for the effects of dissolution of CO_2 into the water phase and water into the gas phase. The shaded region is the spreading wave in the Region II.(Burton, 2008)

$$\mathbf{D_{brine\to BL}} = \frac{\mathbf{C^{BL}_{CO_2,a}}}{\mathbf{C^{BL}_{CO_2,a} - C^{BL}_{CO_2,g}}} \tag{C.3}$$

$$\mathbf{D_{BL\to dry}} = \frac{\mathbf{C^{dry}_{CO_2,g} - C^{BL}_{CO_2,a}}}{\mathbf{C^{BL}_{CO_2,g} - C^{BL}_{CO_2,a}}} \tag{C.4}$$

where the concentrations C have units of moles/volume and have a superscript which defines the region and a subscript which defines the phase (i.e. "CO_2,g" is CO_2 in gaseous phase and "CO_2,a" is CO_2 in aqueous phase).

To make the injection calculations convenient, we average the saturation in the Region II. It does not make a difference to our calculations because the range of saturation defined by DF and BL fronts is narrow for many relative permeability curves. The concentration of CO_2 in different phases is dependent on pressure, temperature and salinity of the brine. Any storage structure is assumed to be isothermal and the pressure in Region I is assumed to be equal to injection pressure (500 psi over hydrostatic for the calculations in Chapter 4), pressure in Region II is assumed to be 200 psi less than the pressure in Region I for the purpose of computing concentrations. Changing pressure, temperature or salinity values has very small impact on the front velocities (Burton et. al, 2008) and thus small errors arising due to these assumptions do not cause significant errors to the flow rate calculations.

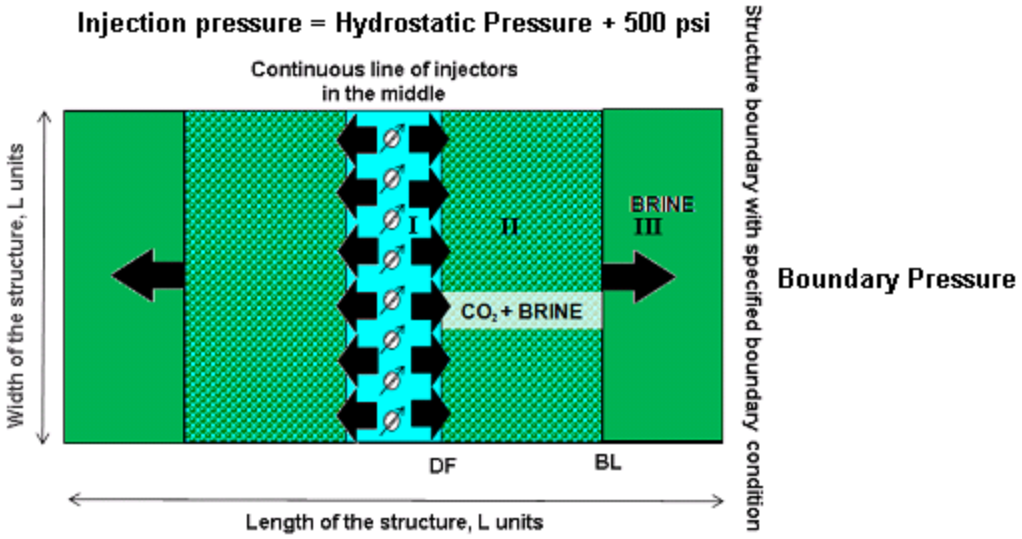

Figure C-2 Figure shows the three flow regions in the aquifer with the boundary conditions used. For infinite acting boundary condition pressure varies with time. For the constant pressure boundary condition, the boundary pressure is set to hydrostatic pressure.

The flow through the three regions in the aquifer is in series. The total flow rate across any cross section is assumed to be the same at any given time because at aquifer temperature and pressure conditions CO_2 and brine are assumed to be incompressible. The injectivity equation for this linear flow system is given by summing the contributions to the pressure drop across each of the three regions:

$$P_i - P_b = \frac{q}{2khL}\left[\frac{\mu_g}{k_{rg,S_g=1}}x_{DF} + \left(\frac{k_{rg}}{\mu_g}+\frac{k_{rw}}{\mu_w}\right)^{-1}\Bigg|_{S_{g,avg}}(x_{BL}-x_{DF}) + \mu_w(L-x_{BL})\right] \quad (C.5)$$

where P_i is the injection pressure, P_b is the pressure at the boundary (which differs depending on choice of boundary condition). q is the total injection rate at any given time, k is the permeability of the formation, h is the thickness and L is the width of the

structure. μ is the viscosity with the subscript (g) referring to the gas phase and (w) referring to brine phase. k_{rg} and k_{rw} are the relative permeabilities to gas and brine phases respectively. In Region I there is only CO_2 i.e only gas phase flowing so the relative permeability to the flowing phase in Region I is taken at S_g of unity. This value is rarely reported in experiments; in this work we use $k_{rg}(S_g = 1) = 1$. In Region II the mobilities of brine and gas phases are taken at the average gas saturation. In Region III only brine flows and brine relative permeability at gas saturation of zero is unity. x_{DF} and x_{BL} are the positions of the drying and Buckley Leverett front at any time. There valued are calculated from the fractional flow theory described above.

At any time x_{DF} and x_{BL} are given by:

$$\mathbf{x_{DF}} = \frac{\int_0^t \mathbf{qdt}}{\mathbf{2Lh\phi}} \mathbf{V_{DF}} \qquad \text{(C.6)}$$

$$\mathbf{x_{BL}} = \frac{\int_0^t \mathbf{qdt}}{\mathbf{2Lh\phi}} \mathbf{V_{BL}} \qquad \text{(C.7)}$$

The factor of two appearing in equations C-5, C-6 and C-7 reflects the fact that the flow goes in both the directions as shown in Figure C-1 and q is the injection rate in a single well.

The next step is to calculate the injection rates. We assume that injection occurs at maximum allowed bottomhole pressure (P_i) at the injectors. Thus we fix one of the boundary conditions by setting the injection pressure P_i as a constant. The other boundary

condition is set at the boundary of the storage structure (the left and right edges of the domain in Figure C-2.

For a constant pressure boundary, we suppose a line of hypothetical extraction wells placed at each edge of the domain, and we set the bottomhole pressure (P_b) of each of these wells to be at hydrostatic pressure. Even with injection and boundary pressures fixed, the injection rate will change with time because the effective mobility of the fluid phases will change with time as the CO_2 advances. Thus we discretize the problem with small time steps; during each step we assume that the drying and BuckleyLeverett fronts remain at fixed position x_{DF} and x_{BL} and calculate the instantaneous injection rates (q) from Eq. C-5. We calculate the amount of CO_2 injected during each time step by taking the product of injection rate and size of time step. The sum of volume of CO_2 injected over all the time steps gives the cumulative volume of CO_2 injected. . The cumulative injected CO_2 determines the position of DF and BL fronts. At this point the iteration over time steps begins, and the calculations advance until the BL front reaches the boundary or total injection time reaches 100 years, whichever comes first. Thus this calculation yields the fill time, cumulative CO_2 injected and the amount of CO_2 injected over time for a structure.

For an infinite acting boundary of the storage structure, the boundary pressure P_b changes with time. Initially P_b is equal to hydrostatic. We assume that when injection starts the corresponding pressure disturbance reaches the boundary instantaneously. For linear flow the change in the boundary pressure depends on the amount of brine which crosses the boundary. It also depends on the compressibility of the bounding aquifer, porosity of the structure , viscosity of brine, thickness of structure and width (L) of the formation (Nabor, 1961). Since the injection rate changes with time, pressure change at the boundary has to be calculated by application of superposition.

The pressure change at the boundary for linear aquifer at constant flux is given by (Nabor, 1961):

$$\Delta p = \frac{q\mu}{kLh}\left[2\sqrt{\left(\frac{7kt}{22\phi\mu c_t}\right)}\right] \tag{C.8}$$

Since flowrate changes with time, superposition gives:

$$\Delta p = \frac{\mu}{kh}\left[q_0 F(t_d) + (q_1 - q_0)F(t_d - t_{d_1}) + ...\right] \tag{C.9}$$

where q_0 and q_1 are injection rates at time step 1 and 2. The dimensionless function $F(t_d)$ is defined as:

$$F(t_d) = 2.\sqrt{\frac{7t_d}{22}} \tag{C.10}$$

And t_d is defined as:

$$t_d = \frac{kt}{\phi\mu c_t L^2} \tag{C.11}$$

Thus at every time step for infinite acting system, we calculate the position of DF and BL fronts based on the cumulative injected CO_2 until that time step and the change in pressure at the boundary. The injection rate at the next time step is based on the change in system mobility due to movement of DF and BL fronts as well as the change is total drawdown. The calculations continue until the BL front reaches the boundary or total time is 100 years, whichever comes first. This again allows us to calculate fill times, cumulative CO_2 injected as well as the amount of CO_2 injected with time.

References

Allinson, W.G. 2003, The economics of geological storage of CO_2 in Australia, APPEA Journal, 623.

Bachu, S. 2000, Sequestration of CO_2in Geological Media: Criteria and Approach for Site Selection. Energy Conservation and Management, 41(9), 953-970.

Bachu, S. 2003, Screening and Ranking of Sedimentary Basins for Sequestration of CO_2 in Geological Media. Environmental Geology, 44(3), 277-289

Bryant, S.L., Lakshminarasimhan, S., and Pope, G.A. 2006, Buoyancy Dominated Multiphase Flow and Its Impact on Geological Sequestration of CO_2. SPE 99938, proceedings of 2006 SPE/DOE Symposium on Improved Oil Recovery, Tulsa, OK, 22-26 April, 2006

Bennion, D.B. and Bachu, S. 2008, Drainage and Imbibition Relative Permeability Relationships for Supercritical CO_2/Brine and H_2S/Brine Systems in Intergranular Sandstone, Carbonate, Shale, and Anhydrite Rocks. SPEREE 11:487-496.

Burton, M., Kumar, N., and Bryant, S.L. 2008, Time Dependent Injectivity During CO_2 Storage in Aquifers. SPE/DOE Symposium on IOR .

Burton, M. 2008. Surface Dissolution: Addressing Technical Challenges of CO_2 Injection and Storage in Brine Aquifers. M.S. Thesis, University of Texas at Austin

Burton, M. and Bryant, S.L. 2009, Eliminating Buoyant Migration of Sequestered CO_2 Through Surface Dissolution: Implementation Costs and Technical Challenges. SPEREE, 12:399-407.

Burruss, R.C. 2009, CO_2 Storage Resources, Reserves, and Reserve Growth: Toward a Methodology for Integrated Assessment of the Storage Capacity of Oil and Gas Reservoirs and Saline Formations. Energy Procedia, 1:2679-2683.

Cook, P.J. 1999, Sustainability and Nonrenewable Resources. Environmental Geosciences, 6(4), 185-190

Dunsmore, H.E. 1992, A geological Perspective on Global Warming and the Possibility of CO_2 removal as Calcium Carbonate Mineral. Energy Conversion and Management, 33(5-8), pp. 565-572.

Doughty, C., Pruess, K., Benson, S.M., Hovorka, S.D., Knox, P.R. and Green, C.T. 2001, Capacity Investigation of Brine-bearing Sands of the Frio Formation for Geologic Sequestration of CO_2. Proceedings of First national Conference on Carbon Sequestration, 14-17 May 2001, Washington, D.C., United States DOE, NETL.

Ennis-King, J.P. and Paterson, L. 2003, Role of Convective Mixing in the Long-term Storage of CO_2 in Deep Saline Formations. Presented at Society of Petroleum Engineers Annual Technical Conference and Exhibition, Denver, Colorado, 5-8 October 2003, SPE 84344.

Fisher, K., Beitler, C., Rueter, C.,Searcy, K.,Rochelle,G. and Jassim, M. 2005, Integrating MEA Regeneration with CO2 Compression and Peaking to Reduce CO_2 Capture Costs. Final Report, Contract No. FG02-04ER84111, DOE

Flett, M.A, Gurton R.M. and Taggart I.J. 2005. Heterogeneous Saline Formations: Long-term Benefits for Geo-sequestration of Greenhouse Gases. Proceedings of the 7th International Conference on Greenhouse Gas Control Technologies, September 5-9, 2004Vancouver, Canada, v.I, 510-510

Gunter, W.D., Perkins, E.H. and McCann, T.J. 1993, Aquifer Disposal of CO_2 rich gases: Reaction Design for Added Capacity. Energy Conversion and Management, 34, 941-948.

Georgescu, S., Lindeberg, E., and Holt, T. 2006, Co-Injection of CO_2 and Water in Non-sealed Saline Aquifers. Proceedings, 8th International Conference on Greenhouse Gas Control Technologies, Trondheim, Norway, 19-22 June, 2006

Holdren, J. and Baldwin, S. 2001, The PCAST energy studies: Toward a National Consensus on Energy Research, Development, Demonstration, and Deployment Policy. Annual Reviews of Energy and Environment 26:391-434

IEA(International Energy Agency): "Key World Energy Statistics", Downloaded from http://www.iea.org on October12, 2009

IPCC (Intergovernmental Pane on Climate Change): Climate Change 2007: The Physical Science Basis. Cambridge University Press, Cambridge

Imbus, S. and Orr, F.M. 2006. Critical Issues in CO_2 Capture and Storage: Findings of the SPE Advanced Technology Workshop (ATW) on Carbon Sequestration: SPE 102968, proceedings of Annual Technical Conference and Exhibition, San Antonio, TX, 24-27.

Juanes, R. and MacMinn, C.W. 2009, A Mathematical Model of the Footprint of the CO_2 Plume During and After Injection in Deep Saline Aquifer Systems. Energy Procedia, 1:3429-3436.

Kaya, Y. 1995, The Role of CO_2 Removal and Disposal. Energy Conversion and Management, 36(6-9) pp. 375-380.

Kheshgi, H.S. 2003, Evasion of CO_2 injected into the Ocean in the Context of CO_2 Stabilization. Proceedings of the 6th International Conference on Greenhouse Gas Control Technologies, J.Gale, and Y. Kaya (eds), Elsevier Science Ltd, Amsterdam, pp. 811-816

Kumar, A., Noh, M., Pope, G.A., Sepehnoori, K., Bryant, S.L., and Lake, L.W. 2004, Reservoir Simulation of CO_2 Storage in Deep Saline Aquifers, SPE Journal, 10:336-348.

Kuijper. M. 2010, Public Acceptance Challenges for Onshore CO_2 Storage in Barendrecht. Proceedings of the 10th International Conference on Greenhouse Gas Control Technologies (GHGT-10), September 20-23, 2010, Amsterdam, Netherlands

Loken, K.P. and Austvik, T. 1993, Ocean Disposal of CO_2: Feasibility, Economics and Effects. Energy Conversion and Management. 34:967-976

Lindeberg, E. and Bergmo, P. 2003, The Long-term fate of CO_2 Injected into an Aquifer. Proceedings of the 6th International Conference on Greenhouse Gas Control Technologies (GHGT-6), J.Gale and Y.Kaya (eds), 1-4 October 2002, Kyoto, Japan, Pergamon, v.I,489-494

Morel-Seytoux, H.J. 1966, Unit Mobility Ratio Displacement Calculation for Pattern Floods in Homogeneous Medium. SPE Journal, 6:217-227.

Marchetti, C. 1977, On Geo-engineering and the CO_2 Problem. Climate Change, 1, pp. 59-68

Magoon, L.B. and Dow, W.G. 1994, The Petroleum System. American Association of Petroleum Geologists, Memoir 60, 3-24.

Nabor, G.W. and Barham, R.H. 1964, Linear Aquifer Behavior. JPT 16:561-563.

Nordbotten, J.M. and Celia, M.A. 2005, Semi-analytical Solution for CO_2 Leakage Through an Abandoned Well. Environmental Science and Technology, 39(2), 602-611

Noh, M., Lake, L., Bryant, S., and Araque-Martinez, A. 2007, Implications of Coupling Fractional Flow Theory and Geochemistry for CO_2 Injection in Aquifers. SPE 89341, SPE Reservoir Evaluation and Engineering, August 2007, p. 406-414

Perkins, E. 2005. Long Term Predictions of CO_2 Storage by Minerals and Solubility Trapping in the Weyburn Midale Reservoir. Proceedings of 7th International Conference on Greenhouse Gas Control Technologies (GHGT-7), September 5-9, 2004, Vancouver, Canada, v.II, 2093-2096

Perry, K.F. 2005, Natural Gas Storage Industry Experience and Technology: Potential Application to CO_2 Geological Storage, Carbon Dioxide Capture for Storage in Deep Geologic Formations-Results from the CO_2 Capture Project,v.2: Geologic Storage of Carbon Dioxide with Monitoring and Verification, S.M. Benson (ed), Elsevier Science, London, pp. 815-826.

Rutqvist, J. and Tsang, C-F. 2002, A Study of Caprock Hydromechanical Changes Associated With CO_2 Injection into a Brine Formation. Environmental Geology,42, 296-305.

Seifritz, W. 1990, CO_2 Disposal by Means of Silicates. Nature, 345, pp. 486.

Salvi, S., Quattrocchi, F., Angelone, M., Brunori, C.A. 2000, A Multidisciplinary Approach to Earthquake Research: Implementation of a Geochemical Geographic Information System for the Gargano Site, Southern Italy, Natural Hazard, 20(1), 255-278

Streit, J., Siggins, A. and Evans, B. 2005, Predicting and Monitoring Geomechanical effects of CO_2 Injection, CO_2 Capture for Storage in Deep Geologic Formations – Results from the CO_2 Capture Project, v.2: Geological Storage of CO_2 with Monitoring and Verification, S.M. Benson (ed.), Elsevier Science, London, pp. 751-766

Van der Meer, L.G.H. 1995, The CO_2 Storage Efficiency of Aquifers. Energy Conservation and Management, 36(6-9), 513-518

Wilkinson, E.R. 1971, California Offshore Oil and Seeps. California Summary of Operations Vol. 57 No. 1

Walton, F.C. 2005, Geological Storage of CO_2: A Statistical Approach to Assessing Performance and Risk. Proceedings of the 7^{th} International Conference on Greenhouse Gas Control Technologies (GHGT-7), September 5-9, 2004, Vancouver, Canada, v.I, 693-700

Vita

Lokendra Jain was born in Udaipur, Rajasthan, India in the year 1984. After finishing his high school education from Alok Senior Secondary School, Udaipur, India, he entered Indian School of Mines (ISM), Dhanbad, India in August 2002. During winter 2003 and summer 2004 he worked as summer trainee for Oil and Natural Gas Corporation Ltd, India. In summer 2005, he worked as summer intern in Reliance Oil and Gas Ltd, India. he received the degree of Bachelor of Technology in Petroleum Engineering from Indian School of Mines, Dhanbad in May 2006. Starting July 2006, he worked as Reservoir Engineer for Reliance Industry Ltd. (E&P) in Mumbai, India. in August 2008, he entered the Graduate School at The University of Texas at Austin.

Email: Lokendra1984@gmail.com

This thesis was typed by the author